MOF materials as therapeutic agents, drug carriers, imaging agents and biosensors in cancer biomedicine

DOI:
10.1016/j.pmatsci.2020.100743

ARTICLE IN PRESS

Progress in Materials Science xxx (xxxx) xxxx

Contents lists available at ScienceDirect

Progress in Materials Science

journal homepage: www.elsevier.com/locate/pmatsci

MOF materials as therapeutic agents, drug carriers, imaging agents and biosensors in cancer biomedicine: Recent advances and perspectives

Adam Bieniek[a], Artur P. Terzyk[a,*], Marek Wiśniewski[a], Katarzyna Roszek[b], Piotr Kowalczyk[c], Lev Sarkisov[d], Seda Keskin[e], Katsumi Kaneko[f,*]

[a] Faculty of Chemistry, Physicochemistry of Carbon Materials Research Group, Nicolaus Copernicus University in Toruń, Gagarin Street 7, 87-100 Toruń, Poland
[b] Department of Biochemistry, Faculty of Biological and Veterinary Sciences, Lwowska 1, 87-100 Toruń, Poland
[c] School of Engineering and Information Technology, Murdoch University, Murdoch 6150 WA, Australia
[d] Institute for Materials and Processes, School of Engineering University of Edinburgh, King's Buildings, Edinburgh EH9 3JL, UK
[e] Department of Chemical and Biological Engineering, Koc University, Rumelifeneri Yolu, Sariyer, 34450 Istanbul, Turkey
[f] Faculty of Engineering, Shinshu University, 4-17-1 Wakasato, Nagano 880-8553, Japan

ARTICLE INFO

Keywords:
MOF
Anticancer therapy
mtvMOF
MOF-based nanothermometers
Biomedicine
Medical appliaction of MOFs
Drug delivery

ABSTRACT

We summarize recent advances in application of MOFs as therapeutic agents, drug carriers, imaging agents and biosensors in cancer biomedicine. A holistic perspective is adopted to produce a comprehensive, critical and readable document useful to a broad community in chemistry, material science, medical fields etc. None of the previous articles adopted a holistic approach focusing on a specific disease or area, such as cancer. MOFs have a tremendous potential in cancer diagnostics and treatment. Although a new field, the amount of literature and data accumulated in this area is vast, quickly growing and requires some systematization and processing. We propose a broad overview of MOF-related literature in the treatment and diagnosis of cancer. In our study, we set: (i) to consolidate the most important and up to date information from the field of MOFs applications in medicine, particularly in anticancer therapy; and to reflect these developments in one, comprehensive study, (ii) to highlight new and emerging topics in the field, (iii) to tabulate the large number of the application examples and case studies to make the information more accessible and easy to follow, (iv) and finally, to broadly reflect on the potential of MOFs in application to cancer treatment, including the existing challenges and emerging opportunities.

In the foreseeable future cancer will remain one of the most significant health challenges and causes of death. Although substantial progress has been made in treatment of many cancer types (predominantly due to the improved early diagnostics), in other cases, such as lung or pancreas cancer, the survival rate remains dramatically low. For many types of cancer effective methods of early detection remain elusive, while the existing methods of treatment suffer from low specificity and adverse side effects. This is why new strategies for cancer treatment are being intensely explored, particularly based on drug delivery concepts, which aim to make therapies more targeted and effective, with lower side effects. At the heart of drug delivery technologies are drug carriers, which can be porous materials, nanoparticles, lyposomes or some other vehicles, capable of carrying and releasing the drug at the

* Corresponding authors.
E-mail addresses: aterzyk@chem.umk.pl (A.P. Terzyk), kkaneko@shinshu-u.ac.jp (K. Kaneko).

https://doi.org/10.1016/j.pmatsci.2020.100743
Received 8 February 2018; Received in revised form 7 September 2020; Accepted 28 September 2020

Nomenclature

Abbreviations

(DACH)Pt(BP) R,R-diaminocyclohexane oxaliplatine biphosphonate
1,2,4-BTC Tris(methylammonium)-benzene-1,2,4-tricarboxylate
1D One dimensional
2,2′-BPY 2,2′- Bipyridine
2D Two dimensional
2-MIM 2-methylimidazole
3D Three dimensional
4,4′-BPY 4,4′-Bipyridine
4T1 Murine mammary carcinoma cell line
5-FU 5-fluorouracil
A2780 Human ovarian cancer cells
A2780cis Human ovarian cancer cells resistant to cisplatin
A498 Human renal cancer cell line
A549 Adenocarcinoma human alveolar basal epithelial cells
AA Anisamide
AD Adenine
ADME Absorption, Distribution, Metabolism, and Excretion
AL Alendronate
AlPcS4 Al(III) phthalo-cyanine chloride tetrasulfonic acid
ALT Alanine transaminase enzyme
Amino-TPDC Amino-triphenyldicarboxylic acid
AMOF Amorphous Metal-Organic Framework
AMP Adenosine 5′-monophosphate
anti-PSA TCNQ Anti biomarker in prostate and breast cancer tetracyanoquinodimethane
APC Antigen-presenting cell
API Active pharmaceutical ingredient
APTES 3-Triethoxysilylpropylamine
ARS Artemisinin
ART Artesunate
AsPC-1 Human pancreas adenocarcinoma ascites metastasis
AST Aspartate transaminase enzyme
AuNC Gold nano clusters
AzBTS 2,2′-azinobis-(3-ethylbenzthiazoline-6-sulphonate)
AZT Azidothymidine
AZT-MP Azidothymidine monophosphate
AZT-TP Azidothymidine triphosphate
B16-F10 Melanoma cell lines
BABL-3T3 Mouse embryonic fibroblast cells
BBI 1,1′-(1,4-butanodiyl)-bis(imidazol)
BHC Benzenehexacarboxylate
BIOMOF Bioactive Metal-Organic Framework
BIT-1 Beijing Institute of Technology
BIX 1,4-bis(imidazol-1-ylmethyl)benzene
BODIPY boron-dipyrromethene
BPDC Biphenyl-4,4′-dicarboxylate
BSB Carboxylate-functionalized binapthyl bis-tridentate Schiff base
BTB 1,3,5-benzenetrisbenzoic acid
BTCA Benzene-1,3,5-tricarboxyl-adenine
BU Busulfan
BUN Blood urea nitrogen
BxPC-3 Pancreatic cancer cells
C(RGDfK) Cyclic (Arginine-Glycine-Aspartic acid-d-Phenylalanine-Lysine)
C57BL/6j Mouse embryonic stem
Ca-AL Calcium 4-ammonium-1-hydroxy-butyl-idene-1,1-bis-phosphonate
Capan-1 Human pancreatic ductal adenocarcinoma cell line
CAT Catalase
CCRF-CEM Human Caucasian acute lymphoblastic leukaemia
CD1 mice Albino mice
CD5 Carboxylato-pillar[5]arene
C-dots Carbon dots
CDV Cidofovir
CHG S-(N-p-chlorophenyl-N-hydroxycarbamoyl) glutathione
CHOL Cholesterol
CI Combination index
CIS Cisplatin
CLSM Confocal laser scanning microscopy
CNS Central nervous system
CNT Carbon nanotubes
COS7 Fibroblast-like cell lines
CpG Immunostimulatory unmethylated cytosine-phosphate-guanine oligonucleotide
CPO Coordination Polymer of Oslo
CPT Camptothecin
Crea Creatinine
cRGD Cyclic arginine-glycine-aspartate peptide
CSD The Cambridge Structural Database
CT Computed Tomography
CT26 Undifferentiated colon carcinoma cell line
CTAB Cetyltrimethylammonium bromide
Cu-CPP Copper coordination polymer particles
CCM Curcumin
CUS Coordinatively unsaturated metal sites
Cy3-labelled Caspase-3 substrate peptide SGDEVDK
dAMP 2′-deoxy-adenosine 5′-monophosphate
DAU Daunomycin
DABCO 1,4-diazabicyclo[2.2.2]octane
DBCO Dibenzylcyclooctyne
DDS Drug delivery system
DEF Diethylformamide
DFT Density functional theory
dG2MP Dimeric 2′-deoxy guanosine 5′-monophosphate
dGMP 2′-Deoxyguanosine 5′-monophosphate
D-H2CAM D-camphoric acid
DHTP 2,5-dihydroxyterephthalic acid
DLC Drug loading capability
DLE Drug loading encapsulation efficiency
DMA N,N'-dimethylacetamide
DMBDC 2,5-dimethoxy-1,4-benzenedicarboxylate
DMF Dimethylformamide
DNA Deoxyribonucleic acid
DOBDC 2,5-dioxido- 1,4-benzenedicarboxylic acid
DOPA 1,2-dioleoyl-*sn*-glycero-3-phosphate sodium salt
DOPC 1,2-dioleoyl-*sn*-glycero-3-phosphocholine
DOPE Dioleoyl L-a-phosphatidylethanolamine
DOTAP Dioleoyl trimethylammonium propane

DOX Doxorubicin
DSCP Disuccinatocisplatin
DSPE-PEG2K 1,2-distearoyl-*sn*-glycero-3-phosphoethanolamine-N-[methoxy(polyethylene glycol)-2000]
DU145 Human prostate cancer cell line
ECl Electrochemiluminescence
ES-2 Ovarian cancer cell line
ESCP Ethoxysuccinato-cisplatin
EtOH Ethanol
FC 1,1′-dicarboxyl ferrocene
FITC Fluorescein isothiocyanate
FITZ-HSA αvβ3-expressing canine endothelial sarcoma cell line
FMN Phosphorylated vitamin B2
FOL Folate
GAL Gallate
GAP-43 Growth Associated Protein 43
GEM Gemcitabine
GEM-MP Gemcitabine monophosphate
GNS Gold nanostar
GPTS 3-glycidyloxypropyl)trimethoxysilane
GRGD-NH2 H-glycine-RGD-serine-NH_2 peptide
GRGDS-NH2 H-glycine-arginine-glycine-aspartate-serine-NH_2
GSH_{red} Glutathione reduced
H1299 Human non-small cell lung carcinoma cell line
H22 Hepatoma-22 cell line
H2BDC Terephthalic acid
H2BDC-F4 2,3,5,6-tetrafluoro-1,4-benzenedicarboxylate
H2BPY-5,5′-DC 2,2′-bipyridine-5,5′-dicarboxylic acid
H2BPY-6,6′-DC 2,2′-bipyridine-6,6′-dicarboxylic acid
H2CMP (Carboxymethyl)iminodi(methylphosphonic acid)
H2DBP 5,15-di(p-benzoato)porphyrin
H2DBP-Pt Pt(II)-5,15-di(p-benzoato)porphyrin
H2DCBP 4,4′-dicarboxy-2,2′-bipyridine
H2DCPPY 2,2′- bipyridine-4,4′-dicarboxylic acid
H2DSTP 2,4-(2,2′:6′,2″-terpyridin-4′-yl)-benzenedisulfonic acid
H2N-PEG-FOL amino-poly(ethylene glycol)-folate
H2PIA 5-(pyridin-4-yl)isophthalic acid
H2QPDC-NH2 Amino-quaterphenyldicarboxylic acid
H2TP 1,1′:4′,1-terphenyl]-4,4″-dicarboxylic acid
H3CPDA 5-(4-carboxyphenyl)-2,6-pyridinedicarboxylic acid
H3IMDC 4,5-imidazole dicarboxylic acid
H3TATAB 4,4′,4″-s-triazine-1,3,5-triyltri-p-aminobenzoic acid
H3TCA Tricarboxytriphenyl amine
H4TBC 5,10,15,20-tetra(p-benzoato)chlorin
H4QPTCA 1,1′:4′,1″:4″,1‴-quaterphenyl-3,3‴,5,5‴-tetracarboxylic acid
HAIP 5-aminoisophthalic acid
HBSS Hank's balanced salt solution
HCT-116 Human colon cancer cells
HEK 293T Human embryonic kidney cells 293
HEK293 Human embryonic kidney cells
HeLa Cells from cancerous cervical tumor
HepG2 Liver hepatocellular cells
HGAL Gallic acid
HIPP 2-(1H-imidazo[5,5-f][1,1-]-phenanthrolin-2-yl) phen
HKUST-1 Hong Kong University of Science and Technology
HL-60 Human promyelocytic leukemia cells
HNSCC135 Cisplatin-sensitive head and neck squamous cell carcinoma
HPB Hollow Prussian Blue
HPLC High performance liquid chromatography
HSC-3 Human oral squamous carcinoma cell line
HT29 Human colorectal adenocarcinoma cell line
HUVEC Human umbilical vein endothelial cells
I4-BDC-H2 2,3,5,6-tetraiodo-1,4-benzenedicarboxylicacid
IBU Ibuprofen
IC50 Half maximal inhibitory concentration
IDOi Indoleamine 2,3-dioxygenase inhibitor
IFMC Institute of Functional Material Chemistry
IRMOF Isoreticular Metal-Organic Framework
IUPAC International Union of Pure and Applied Chemistry
J774 Human murine macrophage-like cell line
JSQ3 Human head and neck squamous cell carcinoma cell line
K(ad)RGDSPEG1900) αvβ3 integrin targeting peptide functionalized polymer Lys(adamantane)-Arg-Gly-Asp-Ser-bi-PEG1900 (bi = benzoic imine bond)
L929 Mouse fibroblast cell line
LPA Ovarian cancer biomarker
Ls301 NIR fluorescent agent
MBioF Metal–Biomolecule Frameworks
MC38 Murine colon adenocarcinoma cells
MCF-7 Human breast carcinoma cell line
MDA-MB-231 Human breast cancer cell line
MDA-MB-468 Human breast cancer cell line
medi-MOF Medical metal–organic framework
MG Mechanically grinded
MiaPaCa-2 Human pancreatic cancer cell line
MIL Materials Institut Lavoisier
miRNA Micro ribonucleic acid
MOF Metal-organic framework
MRI Magnetic resonance imaging
MTD Maximum tolerated dose
MTT 3-(4,5-dimethylthiazol-2-yl)-2,5-diphenyltetrazolium bromide
MTV-MOF Multivariate metal–organic framework
MTX Methotrexate
MTZ Mitoxantrone
MWCNT Multiwalled cabon nanotubes
nBDP_X 4-bis(1H-pyrazol-4-yl)-2-X-benzene (X = H, NO_2, NH_2, OH)
NC Nanoporous carbon
NCI-H292 Human pulmonary mucoepidermoid carcinoma cell line
NCI-H446 Small cell lung cancer cells
NCI-H460 (h460) Human lung cancer cell line
NCP Nanoscale coordination polymer
NH2-BDC 2-aminobenzene-1,4-dicarboxylic acid
NIH3T3 Murine fibroblast cell line
NIM Nimesulid
NIR Near-infrared radiation
NIRF dye Near infrared fluorescent dye
NMOF Nanoscale metal–organic framework
NP Nanoparticle
OA Oxalic acid

specified target. Among the most promising systems, are coordination polymers, and especially Metal-Organic Frameworks (MOFs) built of metal-containing inorganic units and organic polycomplexant linkers.

In general, MOFs are considered to be promising materials for a wide range of relevant applications, including gas purification and storage, in catalysis, sensing etc. Many MOFs structures have truly exceptional properties, such as ultra-high surface areas and porosities, defying our preformed concepts of what is possible in the world of porous crystals. The wide range of possibilities for the choice of building units allows us to develop MOFs that are nontoxic and biocompatible and/or bioactive, and thus applicable as a drug delivery system. Most importantly, the enormous number of possible MOFs and their modifications leads to a concept of *bespoke materials*: that is, materials with functionalities tailored for a specific application, such as anticancer therapy. Theranostics, or thernanostic nanomedicine, is an emerging concept, where the same vector acts as both a therapeutic agent and an imaging (diagnostic) agent; and this is where MOFs are also seen as a promising platform. This exemplifies how simultaneous developments in the material science and nanotechnology can lead to a paradigm shift in treatment strategies and stimulate creation of new therapies. The reasons enumerated above have promoted us to explore and review recent advances in the field of application of MOFs as biomaterials in anticancer therapy and related areas. This is the major purpose of our study, where we set:

- to consolidate the most important and up to date information from the field of MOF materials applications in medicine, particularly in anticancer therapy; and to reflect these developments in one, comprehensive study,
- to highlight new and emerging topics in the field (for example mtvMOF, MOF-based nanothermometers, etc.),
- to tabulate the large number of the application examples and case studies to make the information more accessible and easy to follow,
- and finally, to broadly reflect on the potential of MOFs in application to biomedicine, including the existing challenges and emerging opportunities.

None of the previous review articles adopted a holistic approach focusing on a specific desease or area, such as cancer. Yet, numerous recent studies indicate, that due to a number of unique properties, MOFs have a tremendous potential in cancer diagnostics and treatment. Although a new field, the amount of literature and data accumulated in this area is vast, quickly growing and requires some systematization and processing.

1. Introduction

In the last 20 years metal–organic frameworks, or MOFs, have been a truly explosive area of research. As of 2016 there were 75.600 MOF structures (almost 9% of all compounds) submitted to the *Cambridge Structural Database* (CSD). Pioneering studies on MOF materials first emerged in the 90s of the last century (although similar compounds were reported even earlier but went essentially unnoted [1]), and the breakthrough came in 1999 when Yaghi's group described synthesis of MOF-5 ($[Zn_4O(BDC)_3]_n$), having the surface area around 3000 m^2/g (being at that time the upper limit for all existing porous materials). One may see this point as the inception of the field of MOFs, known also as PCPs (*Porous Coordination Polymers*) [2–8]. It should be mentioned that the discrepancies in the literature exist what is the definition of a MOF [2]. Thus, in this study we use the International Union of Pure and Applied Chemistry (IUPAC) recommendation claiming that [3]: “A Metal–Organic framework, abbreviated to MOF, is a coordination network with organic ligands containing potential voids.” Although MOFs are facing a number of challenges, such as cost and stability, before they find industrial applications in the fundamental material science they became a dominant topic in comparison with other well-known porous materials such as activated carbons, silica or zeolites.

MOFs can be one (1D), two (2D) or three dimensional (3D) structures [9,10], containing nodes formed by inorganic units called PBU (*Primary Building Unit*) or clusters of metal cations called SBU (*Secondary Built Unit*), connected with organic polydentate ligands [10,11]. Since the coordination bonding between a metal and a ligand is relatively strong, well-defined porous crystal structures are formed, being stable even after the removal of the solvent, typically needed at the stage of synthesis [12]. This is, however, not always the case and many MOFs, particularly with high porosity, are very fragile and sensitive to how solvent is removed.

Transition metals such as Zn, Cu, Fe, Cr, Co, Ni, V, Sc, Y are the most commonly used elements in nodes, but also alkaline earth metals (for example Mg, Ca, Sr, Ba, Ra), basic metals of the periodic table main groups (for example, Sn or Al) and/or rare earth metals (such as Lanthanides) have been employed [13,14]. The organic ligand (also called a *linker*) is another required building block of a MOF structure. O- (e.g. phosphonates, carboxylates, sulfonates) or N-donors (e.g. tirazines, pyrididnes, imidazoles) are some of the most commonly used classes of linkers [15] [Fig. 1].

Evolution of MOFs as a new class of materials involved continuous expansion of the arsenal of building blocks (metal clusters and organic linkers) and topologies [16]. This led to practically an infinite number of plausible combinations, and therefore materials, with a wide range of properties, such as porosity (from ultramicroporous to mesoporous), hydrophobicity, pore architecture and surface chemistry. Moreover, post-synthetic modification of MOFs offers additional avenues for the development of new structures [17]. It was estimated that about 6000 new structures are reported each year [18,19]. This is accompanied by substantial developments in the field of synthesis methods, including solvo/hydrothermal, microwave, ultrasound, electro- and mechanochemical methods [20]. With these methods at our disposal we can now perform synthesis of a MOF under mild conditions, and using relatively cheap precursors [21,22]. The majority of these methods use solvents that should be removed to make porous thestructure accessible. This activation process is usually performed at high temperature and lower pressure or using a solvent exchange [23]. Supercritical solvent removal techniques have been also proposed to avoid structural collapse during the activation process of some fragile MOFs [24].

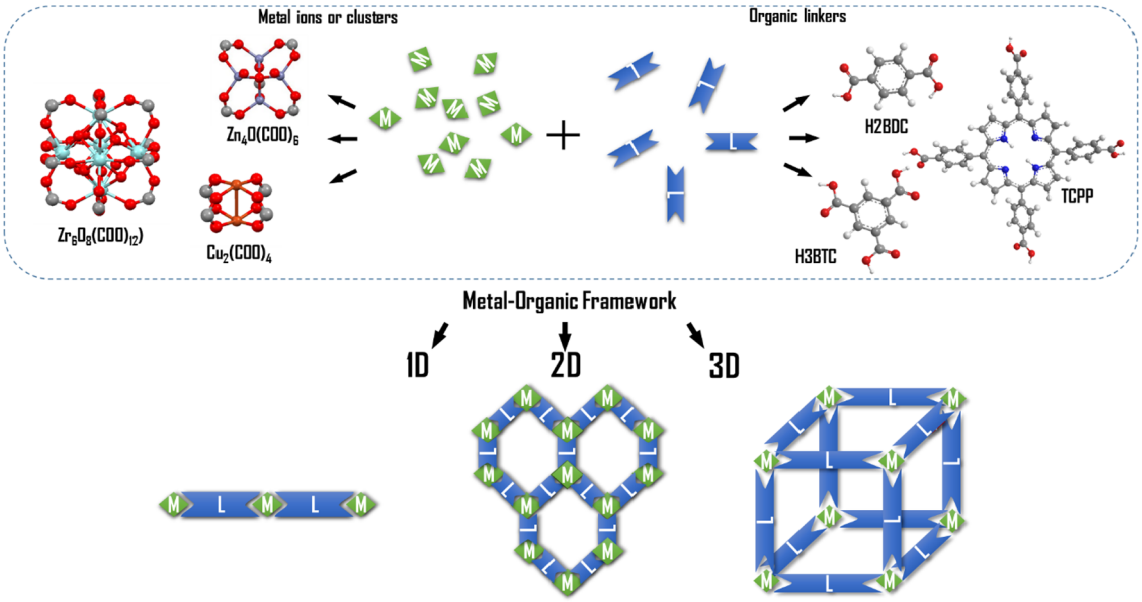

Fig. 1. A generic scheme for the preparation of 1D, 2D and 3D MOF structures, with examples of metallic units called PBU (*Primary Building Unit*) (for example, Cu(II), Zn(II) and Zr(IV)) or clusters of metal cations named SBU (*Secondary Built Unit*) (for example, $Zn_4O(COO)_6$ (MOF-5), $Cu_2(COO)_4$ (HKUST-1), and $Zr_6O_8(COO)_{12}$ (UiO-66), connected with organic ligands (H2BDC – terephthalic acid, H3BTC – 1,3,5-benzene-tricarboxylica acid or trimesic acid, TCPP – 5,10,15,20-tetrakis(4-carboxyphenyl)porphyrin to build various structures. Grey – carbon, blue – nitrogen, red – oxygen, orange – copper, turquoise – zirconium, white – hydrogen, violet – zinc. (For interpretation of the references to colour in this figure legend, the reader is referred to the web version of this article.)

Accurate control of MOF synthesis is expected to lead to the development of even more stable, functional, and structurally sophisticated materials [12,25,26]. In fact, MOFs already defy many of our perceptions of what is possible in the world of crystalline porous materials. For example, many MOFs possess unique properties such as, for example, ultra high surface areas (in the range of 1000–10,000 m^2/g) [12], exceeding the values recorded for any other widely used porous materials such as activated carbons or zeolites; very low density (in the range of 0.13–1.5 g/cm^3), large porosity (higher than 50%), pore sizes in a wide range of 3–100 Å, good thermal (up to 300–500 °C) and chemical stability [12,17,21,23,27]. One particularly interesting and unique property of MOFs is the ability of some of them to undergo reversible structural transformations in response to the external stimuli such as temperature, pressure and adsorption, while remaining crystalline [8,28,29]. Several classes of these transformations have been identified over the years including the so-called *breathing effect* [30], or gating phenomena [10]. A representative example of this novel gating phenomenon is the behaviour of the elastic layered structure of MOF $[Cu(4,4'\text{-bpy})_2(BF_4)_2]$ (ELM-11). This material shows unique gate opening and closing properties upon sorption of CO_2, N_2 and CH_4 through an expansive modulation of the layered structure [31]. Functional materials with this dynamic behaviour can potentially find applications as highly selective sensors, molecular separating materials and catalysts [8].

However, the most important property of MOFs is their modular nature. Using simple variation of the building blocks many different structures can be constructed following the same topology. This implies that novel materials can be accurately designed to have very specific properties (such as porosity, dimensions of the channels, and surface chemistry) and functions. These materials can be further modified in the post-synthetic process to add additional functionalities and properties. This high level of "designability" (for the lack of better word) of materials is indeed unprecedented in the world of porous materials and it opens a unique avenue towards multifunctional, bespoke materials for specific applications [17,20,27].

Naturally, unique properties of MOFs have been attracting attention not only in the chemistry community, but also for chemical engineering applications, in materials engineering, nanotechnology, physics, energy, biology, medicine and environmental engineering [32]. This in turn attracted the attention of industrial companies recognizing the potential, associated with the industrial applications of MOFs. For example, BASF became the first large scale industrial player to look into scaling up of MOF synthesis and to explore their potential industrial applications [33]. Now, there several companies and start-ups working specifically on large scale synthesis of MOFs (NuMat Technologies, MOF Technologies, Immaterial Labs). The most important (in terms of scale and impact) potential industrial application of MOFs is gas adsorption and separation (mainly N_2, CO_2, H_2, CH_4 [20]), although applications of MOFs as materials for energy (batteries, supercapacitors and fuel cells) and gas storage, catalysts, optotronic and luminescence materials, porous magnets, sensors, and biomedical materials (drug delivery systems, diagnostic tests, imaging) should be also mentioned [7,8,10,12,17,20,21,25,34–43]. For the large scale applications, the cost and robustness of a MOF is a dominating factor, however, for niche applications such as sensing and drug delivery this is not as important and the benefits of MOFs may significantly overweight the deficiencies. In our opinion, biomedical applications will be one of the main driving forces for the discovery of new MOFs in the next several years.

The aim of our study is to review the current state-of-the-art and potential of MOFs in application to anticancer therapy from the detection stage to imaging and therapy. We discuss not only the existing ideas and practices but we also explore the emerging concepts and new ways and methods of using MOFs in this context. This review collects and divides literature reports on MOFs used for biomedical purposes, showing that research on cell lines (*in vitro*) as an early stage of verification toxicity (and therapeutic/diagnostic efficiency) of MOFs as biomedical agents are common and in many cases they provide promising results. Thank to this it is possible to move to the next much more advanced stage, i.e. to research on living organisms (*in vivo*). *In vivo* study on animals, taking into account complexity of living organism, also confirms that the selected materials demonstrate the significant application potential, thus positive results from the *in vivo* stage gives possibility to enter to an even more advanced stage of work such as clinical trials, and then to use them widely in life, outside of laboratory conditions. We start from the discussion of the requirements that should be met by a MOF in order to be used *in vivo* as a part of the therapy; following with some important concepts of MOF challenges in medicine, and finally we also discuss in detail the key examples of MOFs in drug delivery, biomedical imaging and and biosensing. Finally, we present some perspectives on the future of this field.

2. MOF materials in medical applications: Summary of major concepts

Biomedical potential of MOF materials stems predominantly from their high porosity, their ability to adsorb and host biologically active compounds, and the existing wide range of functionalization methods. Among the existing MOFs, several classes of MOFs have been identified that are non-toxic, biocompatible and may also have interesting bespoke pH response [44]. The complete design space of MOFs for biomedical application is summarized in Fig. 2. The detailed analysis of the previous reports discussing the application of MOF in biomedicine [18,23,32,45–70], leads us to the conclusion that three general methods to incorporate active (inorganic or organic) compounds into a MOF are commonly used [65]:

(i) an active compound is incorporated onto the internal and/or external surface of a preformed MOF structure by covalent and/or noncovalent (adsorption) bonding;
(ii) an active compound becomes a constitutive part of the material structure using therapeutically active cations and/or ligands – Bioactive MOF (so-called BIOMOF);
(iii) a combination of methods (i) and (ii) as in the case of, for example, a porous BIOMOF material.

By using of (i-iii) it is possible to employ MOF materials in biomedical applications as:

- drug delivery systems, using either drug-loaded MOFs or BioMOFs as pro-drugs
- contrast agents and/or theranostic agents
- sensors.

Fig. 3 schematically summarizes these ideas. What is important to emphasize however, is that for the design of MOFs in biomedical applications, additional specific requirements such as biocompatibility and non-toxicity of the components must be adhered from the onset, regardless the route (host MOF, or BIOMOF) or application (drug delivery, imaging, or a combination of both). We will return to this issue in more detail later in the review.

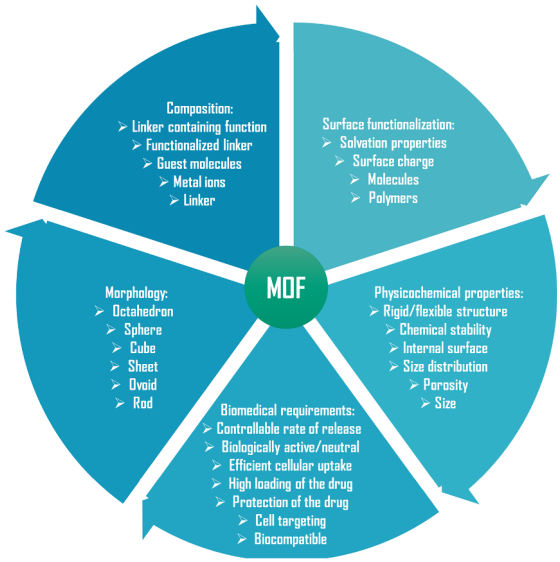

Fig. 2. Overview of the most important design parameters for the synthesis of a MOF for bioapplications.

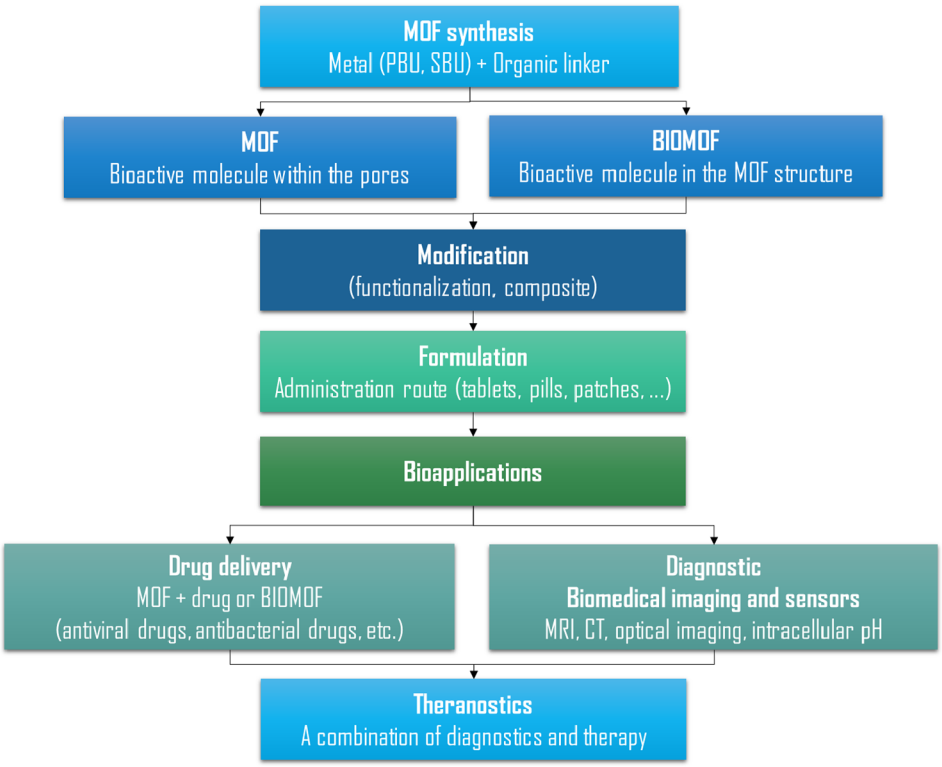

Fig. 3. A general scheme for designing MOFs for biomedical applications.

The final MOF structure can be further functionalized to improve its properties or to extend its features (for example, for targeted therapy, or stealth capability).

2.1. Drug delivery system (DDS)

Many of the well-known drugs are not very effective, because the active pharmaceutical ingredient (API) is hardly soluble, or unstable, rapidly and extensively metabolized, and/or its biodistribution in the body is nonselective. Typically, it leads to the lower efficacy and higher cost of the therapy, while in the worst case scenario it may also lead to the damage of healthy cells and tissues and severe adverse side effects. Thus, the objective of a drug delivery system, in general, is to circumvent these problems. In the simplest implementation of this idea, the API would be protected by being incorporated inside a porous material host (zeolites, silica and carbon materials), or by being inside some other structure, such as dendrimers, lyposomes etc. [71,72]. In case of porous materials, such as zeolites or silica, their structure remains unchanged throughout the active substance release, limiting their bioelimination, which is frequently associated with toxic effects. On the other hand, the second group of hosts, such as certain polymers and liposomes, releases API by degrading their own structure. Typically, non-degradable porous materials of the first group have a much higher specific loading capacity for API, compared to the degradable structures of the second group [72]. There is a clear need for a new class of materials which would combine high loading capacity of inert porous materials with controlled biodegradability of polymers, lyposomes and related structures. Further, the drug release kinetics is obviously one of the major design parameter of the DDS. In this process, chemical structure of both the DDS and the drug, together with the drug – DDS interactions are the major factors influencing drug diffusion and DDS stability [67,73]. The major significant drawbacks of materials previously considered for DDS (for example, inorganic materials such zeolites or porous silica) are: inadequate adsorption capacity, and still not sufficiently delayed or controlled release of drugs (observed mainly for some organic materials such as liposomes, dendrimers, micelles and polymers) leading to the so-called “burst effect” [74].

Thus, the new DDSs are being explored [75], emerging MOFs, among some of the more promising candidates, filling the gap between organic and inorganic materials [67], the interactions between the linkers and metals favouring the gradual degradation of the MOF and API release [65]. In more recent approaches, the DDS structure performs also a number of additional functions, such as releasing the cargo only under certain conditions or in a specific environment (pH, temperature, osmolality, or via an enzymatic activity), binding to specific cells (via recognition ligands e.g., folic acids, peptides, etc.), DDS can be targeted to specific cells; specific targeting can be also reached by using magnetic fields; etc. [72].

Moreover, the following properties make MOF materials particularly suitable for internalization of drugs, and for controlled drug delivery [52]:

- the possibility of application of nontoxic metals or metals with low toxicity (for example Fe, Zn, Ca, Mg, Bi) [52,76] and ligands (such as, for example, amino acids) for porous structure forming,
- biodegradability in aqueous solutions and/or in physiological conditions,
- MOF surface properties can be adjusted in such a way, that the accumulation of a range of biologically active molecules is possible,
- the rate of delivery can be further modulated by incorporation of different polar or nonpolar surface groups onto the ligand structure,
- MOF structure can be flexible and responsive to some selected external factors.

The combination of factors described above is responsible for a significant surge of interest in using MOFs for drug delivery applications.

Historically, the first method of therapeutics incorporation into a MOF was via adsorption [38]. This post-synthetic approach requires two stages. In the first stage a MOF, with specified properties, is synthesized and activated. In the second stage, a biologically active compound is incorporated into the pores of a MOF by chemical (covalent bonding to the structure) or physical adsorption (noncovalent bonding) [Fig. 4]. Additionally according to He et al. [56], it should be noted that in the case of nano-sized-MOF (NMOF, or MOF nanoparticles), lower loadings are achieved, compared to the bulk MOF materials. Among the major drawbacks of this approach are heterogeneous distribution of the active compound throughout the MOF structure. This heterogeneity makes delivery kinetics hard to control, which in its turn diminishes utilization and efficacy of the drug [56].

In the case of chemisorption, API actually forms chemical bonds with the host structure. As upon the process API looses its chemical identity, one should ensure that there is no loss of biological activity of the API as a result. Furthermore, the adsorbed molecules should dissociate under required conditions, to make the delivery of an API possible. Systems that regain their biological activity upon some dissociation process once their reach their specified target are commonly called prodrugs and an API covalently bonded to a MOF is an example of this approach. The major drawback of the covalent bonding is (similarly to the physical adsorption case) the heterogeneous drug distribution. In this case, drug molecules often tend to concentrate on the external surface of a MOF [56].

First application of a MOF as a drug carrier was reported in 2006 by Horcajada et al. [38,67]. Ibuprofen was adsorbed in the mesoporous chromium(III) carboxylates MIL-100(Cr) (0.35 g/g) and MIL-101(Cr) (1.38 g/g) structures. The non-covalent bonding method was used (but leaset a fraction of Ibuprofen coordinates to the metal site, so it could be considered as chemisorption also). The authors reported the complete delivery of the drug from the MIL-100(Cr) after 3 days while for the MIL-101(Cr) was delivered after 6 days, being constant in the first 8 h [38,67].

Similar approach was reported by Horcajada et al. [77] for the flexible microporous chromium(III) and iron(III) terephtalates MIL-53(Cr) and MIL-53 (Fe), able to reversibly modulate their pore size as a function of different stimuli (temperature, pressure, adsorbate). The very long (3 weeks) and unusual zero-order kinetics drug release from both solids is a consequence of the flexibility of the framework which adapts its pore size to the dimensions of the drug to optimize drug-matrix interactions (creation of hydrogen bonds between carboxylic ibuprofen groups and hydroxyl groups of the host material). Similar drug loadings (ca 0.2 g/g) were observed in both MOFs (Cr and Fe) . Modest values of available pore volume were the primary reason for the low drug loading.

The adsorption approach discussed above is the most commonly applied approach for encapsulation and delivery of anticancer drugs, as well as for antiviral drugs ((azidothimidine triphosphate (AZT-Tp), cidofovir (CDV), busulfan (BU), and doxorubicin (DOX))

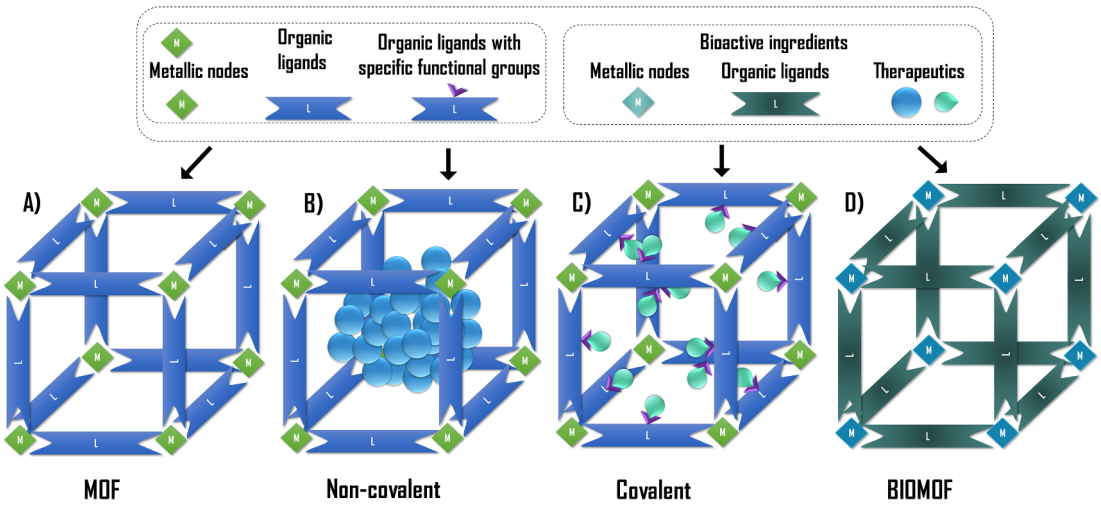

Fig. 4. A generic scheme representing different strategies to incorporate biomedically relevant agents into a MOF. Building a MOF structure (A), noncovalent cargo loading (B), covalent cargo loading (C). In some cases a metal ion or bridging a ligand can be biologically active and can be introduced into the structure at the stage A – BIOMOF (D).

[59] and gasotransmitters such as NO and H_2S [52,78,79].

As an example of covalent bonding, the study of Taylor-Pashow et al. [80] can be considered. The authors performed the synthesis of nanometric iron(III) aminoterephthalate MIL-101-Fe (~200 nm). Next, BODIPY (fluorescent derivative of anticancer drug vinblastine) was covalently, postsynthetically bonded to the amine group of the nanoMOF. The loading was in the range of 11% (w/w). In the same study the drug c,c,t-[$PtCl_2(NH_3)_2(Oet)O_2CCH_2CH_2CO_2H$] (ethoxysuccinato-cisplatin), was attached to the amine group of the ligand of the nanoamino-MIL-101 with the loading equal to 12.8% (w/w) [9,80]. Comparing to noncovalent bonding approach, the covalent bonding prevents premature drug delivery because the drug is usually delivered after degradation of the whole structure [63].

As limitation, sometimes the kinetic diameter of the active molecule is too large to penetrate the pores of the host material. In this case, the concept of *ship-in-a-bottle* proposed by Zhuang et al. [81] can be advantageously employed. In this method, an active compound is introduced into the internal MOF structure at the stage of synthesis. The authors encapsulated fluoresceine (fluorescent dye) and camptothecine (anticancer drug) inside the microporouos zinc imidazolate ZIF-8 structure. Although this concept is very interesting, the majority of APIs are unstable at the conditions of MOF synthesis, being the main limitation of this *ship-in-a-bottle* approach [81].

2.2. BIOMOF materials as pro-drugs

As has been already discussed, a typical and simplest procedure for drug encapsulation in a porous material is a via physisorption, which is based on non-covalent interactions with the host, and therefore both the loading and the kinetics of delivery depends on the strength of these interactions, among other factors. If the delivery is accompanied by a MOF degradation [23] the problem of toxicity of nodes and ligands forming a MOF must be addressed. Several concepts have been proposed to avoid this problem. One approach would be to use endogenous metals and various biomolecules as ligands, such as for example amino acids, peptides, nitrogenous bases etc. An example of this approach is provided by Imaz et al. [47] who developed a so-called MBioF (Metal-Biomolecule Framework). The main problem with this approach is a typically non-porous nature of the resulting materials, making the loading of the drug and drug delivery impossible. Alternatively, one can consider constructing a MOF out of building components, which are at the same time also active compounds. This has been proposed by McKinlay et al. [46], leading to a concept of a BIOMOF. Application of this approach leads to the drastic reduction of toxicity, elimination of multistage adsorption procedure, and homogeneous distribution of the drug [56,65]. However, among the drawbacks, the synthesis as well as the characterization of these materials can be very time-consuming [65]. He et al. [56] also points out that if the active compounds possess complicated structures, control of the BIOMOF morphology, physiochemical properties and stability during synthesis is challenging.

Despite these issues, a number of BIOMOFs has been already developed. Examples of BIOMOFs include the BioMIL-1 based on the nicotinic acid, and the Fe(III) nicotinate (pyridine-3-carboxylic/niacin/vit B3) [82]. Nicotinic acid is the endogenous compound having pellagra-curative, vasodilating and antilipemic properties. This acid constitutes ca. 71.5% of BioMIL-1 by weight. For comparison, the highest amount of the drug loaded via physisorption route was 1.4 g/g for ibuprofen on MIL-101(Fe) (58% of mass) [23,82]. Another example of BIOMOF synthesized by Kim et al. [83] from glutaric acid (intermediary metabolic product e.g. in tryptophan metabolism) is the Fe(III) glutarate. Also Rieter et al. [84] reported the synthesis of a BIOMOF from disuccinatocisplatin as the ligand (however, it is not easy to determine in this case whether Pt is a part of the ligand, node, or a mixture of both) and Tb as the metallic node. The authors confirmed the therapeutic activity of this system using the angiogenic human colon carcinoma cell line. Next example of a BIOMOF, is a material based on cystine and Zn as described by Ferrera et al. [85]. Also the application of ferritin (T112H) and Zn for a BIOMOF [86] synthesis was reported. Fernández et al. [87] described the synthesis of a new Ca-Alendronate MOF, with potential applicability in the treatment of skeletal disorders. Wang et al. [88] prepared a new Cu-CPP containing 4,4′-dicarboxy-2,2′-bipyridine (H_2DCBP) ligand. This BIOMOF was shown to exhibit particles-size-dependant antibacterial activity. Other examples of MOF containing endogenous ligands include Bi citrate [89], Mg formate [90], Cu aspartate [91], Zn-dipeptide [92], Fe fumarate [93] and Fe muconate [94].

Therapeutically active metals can also be incorporated into a MOF structure. For example, Ag is known for showing antimicrobial activity [95]. Berchel et al. [96] described a MOF structure (containing Ag and 3-phosphonobenzoate), which showed antimicrobial activity against six different bacterial strains, three strains of *Staphylococcus aureus,* one strain *Escherichia coli* and two strains of *Pseudomonas aeruginosa*. Prolonged delivery of antimicrobial ions opens opportunities for the application of BIOMOF materials as topical agents [96], such as for example, the coordination polymer containing 1,3,5-triaza-7-phosphaadamantane-7-oxide (PTA=O) [97]. Slenters et al. [98,99] reported Ag-nicotinate, which was applied in implantology as an antimicrobial agent (coordination polymer was used as coatings on dental implants made from gold alloy and titanium for the prevention of adhesion of bacteria on implant). Another example of a material in this category is Zn-adeninate (BIOMOF-1), which contains a bioactive cation and endogenous ligand [100]. Although this MOF has not been investigated in detail, it is predicted, that this compound can show antimicrobial activity stemming from Zn ions. This MOF however represents an important group of materials where both the cation and the linker are therapeutically active, leading to some synergetic effect. This very interesting group of compounds is currently under extensive development [65].

Some BIOMOF materials can be porous. For example, Zn-CCM (curcumin shows anticancer properties), has surface area around 3000 m^2/g, enabling additional adsorption of therapeutics or other compounds. In this way one can create of multi-purpose delivery system, where both the MOF and the cargo have different and complementary functions [101]. Another example of a porous BIOMOF is Bio-MOF-100, based on Zn (II), adenine, and 4,4-bifenylocarboxylane, with a large surface area of around 4300 m^2/g [102].

To summarize, the BIOMOF structures are very promising and it is certain that this concept will be further developed in the future.

Table 1
Some recent examples of MOF surface modification.

No	Surface agent	Application	Average diameter [nm]	Ref.
1	PEG (poliethylene glycol)	To control carrier interactions with the biological medium, to improve MOFs "stealth" properties and to prolong carrier circulation in the blood stream from a few minutes up to few hours.	~250 (TEM)	[59]
2	Silica	For improving MOF water dispersibility, stablility (to control MOF degradation and drug delivery times) and biocompatibility.	~200 (SEM)	[51,56,80,103]
3	PVP (polivinylopirolidone)	For improving stability.	68.6 ± 10.2 (DLS), ~50 (TEM)	[84]
4	PEG-anisamide	PEG as above and anisamide for targeted anticancer therapy (anisamide has moderate affinity for sigma receptors, which are overexpressed in various tumour cells, especially prostate and lung cancer cells).	124 ± 7 (DLS)	[51,104]
5	Chitosan	For bioadhesive properties, leads to mucoadhesion and permeation enhancement.	204 ± 32 (DLS)	[105,106]
6	Silica and cyclic peptide c(RGDfk)	Silica as above and c(RGDfk) for targeted anticancer therapy (c(RGDfk has specific affinity towards integrin αvβ3 occurring in various cancer cells).	50–100 (SEM, TEM)	[57]
7	1,3,5,7-tetramethyl-4, 4-difluoro-8-bromomethyl-4-bora-3a,4a-diaza-s-indacene) and ethoxysuccinato-cisplatin	For imaging and as prodrug	~200 (SEM)	[80]
8	Lipids	For enhance intracellular uptake, inhibit kinetics of delivery and influence biocompatibility	78 ± 22 – 164 (DLS)	[51,56]. [107,108]
9	Nucleic acids	To effectively enter cells (without the use of cationic or viral transfection agents)	14, 19, 540, 128 ± 3 (TEM, DLS)	[109,110]
10	Folic acid (FOL)	For targeted anticancer therapy	90–120 (TEM) 140–180(DLS)	[111]
11	Amphiphilic dextrin, fluorescein and biotin	For the targeted therapy and imaging	n.a.	[59,112,113]
12	Terb complex and dipicolinic acid	For imaging	~100 (TEM]	[114]

2.3. Surface engineering

Although a synthesized MOF material may not exhibit the desired therapeutic characteristics, additional functionalities and properties can be introduced by judicial surface modifications [51]. This is especially important for the cases of bio-applications since the nature of the surface (surface area and charge, type of ligands, etc.) affects the blood circulation times, biodistribution and the release/availability of the therapeutic agents. Surface modification is also crucial since it can facilitate the crossing of physiological barriers by the drug. Surface modifications can be performed on the surface of pores in the interior of the material but also on the external MOF surfaces by the application of a functionalized ligand during and/or after synthesis. Functionalization can be used to modulate hydrophilicity of the material; it also influences its stability and how it interacts with other species and with the cells. Surface functionalization that makes MOF nanoparticles invisible to the immune system [65], and specifically to the phagocytic system, is particularly interesting in the context of drug delivery as this should increase blood circulation times of the therapeutic agent and its bioavailability. Also so called targeted therapy is possible, in which a drug is transported to the cancer tissues. In this case, appropriate ligands or antibodies (cancer-cells oriented) are bonded to the surface of a carrier. The major purpose of this type of therapy is to pass some biological barriers and concentrate the drug in the specific, target areas, thus increasing its potency and avoiding adverse side effects. In Table 1 we provide some recent examples of MOF surface modification [51,56,57,59,80,84,103–111].

Given the number of MOFs, functionalization agents and functionalization routes, the number of materials that can stem from this strategy is virtually infinite [23]. However, it is important to remember that ultimately, it is the carrier efficiency under physiological conditions, stability, biocompatibility and other factors that determine its promise for biomedical applications and the number of systems that satisfy all these requirements is still rather modest, although rapidly growing.

2.4. Bioimaging and sensor properties

Diagnosis is the first and crucial stage of an efficient therapy against cancer. Some key imaging and sensing techniques for qualitative/quantitative estimation of tumor lesions are highlighted in Table 2.

MOF materials are already being successfully used as potential bioimaging and sensing agents [54,57,66]. In particular, imaging agents can be introduced into the structure (metals, ligands) at the synthesis as well as post-synthesis stage (adsorption, modification). The techniques using MOF materials as contrast agents and/or sensors [54,57,66] are as follows:

- **MRI** is a noninvasive method of the internal body structure mapping, which can provide a wealth of information on the function and state of the body. MRI guarantees high spatial resolution, contrast in soft tissue and penetration; and it does not require strong radiation as other techniques such as X-ray. The method usually detects water protons and this detection depends on the local water density, cellular environment and the rate of nuclear relaxation process. MRI contrasts are based on spin reorientation in paramagnetics such as, for example, Gd(III), Fe(III) and Mn(II). Perfect contrast agents should increase the rate of water proton relaxation as $R1 = 1/T1$ and/or $R2 = 1/T2$ to enhance image contrast, where T1 relaxation is the time taken for the magnetic vector to return to its resting state and T2 relaxation is the time needed for the axial spin to return to its resting state, R1 and R2 are relaxation rates or relaxivities. For example, Gd (III) chelates reduce proton relaxation times and cause the increase of T1-weighted (positive) signal. In contrast, iron oxide nanoparticles increase relaxation time and are applied for the enhancement of T2-weighted (negative) signal [116]. MOF materials are promising contrast agents because they offer a possibility of affecting both T1 and T2, and more information can be obtained from MRI. However, even more important is that the application of MOFs offers simultaneous imaging and delivery of active agents [54,57,66].
- **Optical imaging** is an important and widely applied non-invasive technique, especially in cancer diagnosis, based on using special dyes to colour and locate infected tissues. Usually the dyes absorbing visible light are used, however, the weak visible light permeability of tissues pose certain limitations on the applicability of the method and near IR can be applied instead during *in vivo* imaging. Another technical issue one has to be aware of is the dilution of the dye, which leads to imaging sensitivity decrease [54,57,66].

In general, luminescent MOF materials are being extensively researched at the moment in the context of several optical imaging

Table 2
Summary (advantages and limitations) of principal tumor imaging techniques. Based on Ref. [115].

Comparison of different imaging techniques								
Technique	Source	Typical probes	Resolution	Sensitivity	Time	Depth	Cost	Safety profile
MR imaging	Radio wave	Paramagnetic (Gd(III)), superparamagnetic (Fe_3O_4)	10–100 μm	10^{-9}–10^{-6}	minutes to hours	no limit	Very costly	Non-ionizing radiation
CT imaging	X-ray	Iodine, Barium sulphate, Gold	50–200 μm	10^{-6}	minutes	no limit	Costly	Ionizing radiation
Optical imaging	Light	QDs*, NIRF dyes**	0.3 μm	10^{-12}	sub seconds to minutes	< 10 cm	Low cost	Good

* QD quantum dots, ** near infrared fluorescent (NIRF) dyes.

applications [54,57,66]. Two major strategies have been explored to produce luminescent MOF. The first strategy is the incorporation of a luminescent ligand into a MOF structure. The second strategy is based on the introduction of a ligand possessing a functional dye group during the post-synthesis process. However, the major obstacle of this approach lies in the possible pore blocking by a surface group-dye adduct, and as a result, the loading of the drug inside the structure (if one wanted to create a multifunctional MOF) can be problematic. Unfortunately, a lot of the recently developed luminescent MOFs are either not biocompatible or their excitation wavelengths lie in the blue – to UV range, what is the serious drawback [54,57,66].

Here it is also worth mentioning the use of X-ray scintillating MOFs (constructed from anthracene based organic ligand and metal cluster nodes of high atomic numbers (Z = 72 for Hf and Z = 40 for Zr). The Hf(IV) and Zr(IV) cations in the SBU act as antennas by absorbing X-ray photons and converting them to fast electrons through the photoelectric effect. The generated electrons scintillate/excite multiple anthracene-based optical emitters in the MOF through inelastic scattering, leading to efficient generation of detectable photons in the visible spectrum [117].

- **X-ray computed tomography (CT)** is based on X-rays specimen attenuation. Typically, the elements with large atomic number (barium, iodine etc.) are used for X-rays attenuation to provide good quality, high resolution 3D images. In clinics, iodinated aromatic compounds are applied for intravenous imaging. On the other hand, barium sulfate is applied for gastrointestinal track imaging. However, to achieve satisfactory resolution large doses of compounds must be administrated. This leads to the increasing toxicity, and the appearance of allergic reactions and side effects. Application of MOF materials containing high *Z* elements should improve attenuation, reduce dilution problems and decrease the amount of active agents required for a good contrast. Contrast agent can be introduced into a MOF structure, or into MOF material pores. It the latter case a MOF structure is responsible for a contrast agent stabilization [54,57,66].
- **Sensor properties** of MOF materials can also be applied to facilitate diagnosis and therapy. MOF can detect a variety of chemical species such as cations/anions (Fe(III), Zn(II), Mn(II), Co(II), Cu(II),) or small molecules (O_2) by luminescence of organic and/or inorganic part (luminescent part incorporated or introduced into/onto the MOF structure). Moreover, application of MOFs in sensing and monitoring of pH and temperature have been reported [54,57,66].

2.5. Multitasking and multifunctional MOF materials in biomedicine

2.5.1. Combination therapy

In the combination therapy, a single treatment contains two or more active therapeutic ingredients; and this strategy becomes increasingly important for a number of conditions, particularly, cancer [118]. The variety of possibilities in MOF design, synthesis and modification, makes them an ideal candidate for using in the combination therapy. As an example of the implementation of the combination therapy using MOFs, it is worth to consider a recent study by McKinlay et al. [55] on a multifunctional antimicrobial MOF. Specifically, the authors studied a series of M-CPO-27 (M = Ni, Co, the ligand = 2,5 dihydroxyterephtalate) and the HKUST-1 (M = Cu(II), ligand = 1,3,5 tricarboxylate) materials. Different amounts of two complementary antimicrobial drugs (NO and metronizadole) were loaded onto the materials. Thus, the antimicrobial action of the final material stems from both the loaded active species of two different types, and from the materials themselves, as upon disintegration they release Ni(II) and Cu(II) ions, which also possess antimicrobial properties. Studies of drug delivery in water and in the PBS were performed showing no differences between the two solvents. While the NO delivery was very quick (from 30 min up to 2 hrs for the Ni-CPO-27 and HKUST-1, respectively), metronizadole delivery was slower (from 6 hrs up to 120 hrs for the Ni-CPO-27 and HKUST-1, respectively). Finally, the slowest realease was the delivery of Ni(II) and Cu(II) ions (ca. 4% of ions was delivered after 6 hrs). In addition, the antibacterial

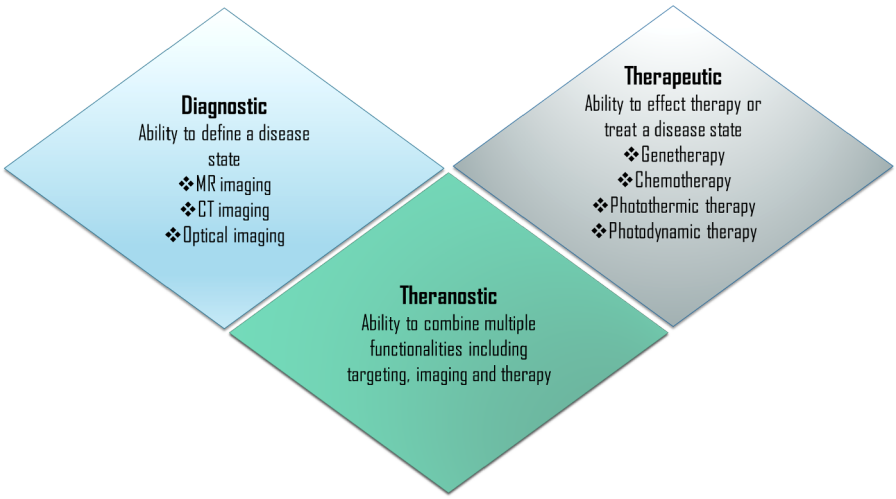

Fig. 5. A schematic description of the theranostic concept.

Table 3
Summary of systemic toxicity parameters recorded for healthy CD1 mice 4 days after tail-vein IV administration of PBS, drug-free FOL-targeted liposomes,# 1.6 mg/kg (MTD) of small-molecule ZOL, or 1.6 mg/kg (MTD) of encapsulated ZOL either from FOL-targeted CaZOL NMOFs or non-targeted CaZOL NMOFs. (N.B. # containing the same amount of lipid coating as in the FOL-targeted CaZOL NMOFs; i.e., each 29–30 g mouse received IV administration of 200 μL of 490 μg/mL of drug-free FOL-targeted liposomes; n = 5 per group; AST = aspartate aminotransferase; ALT = alanine aminotransferase; BUN = blood urea nitrogen; Crea = creatinine; * = above/below the normal range.) Based on results from [131].

Treatment						
	Normal range	PBS	Empty FOL-targeting liposomes	Free ZOL	Non-targeting CaZOL NMOFs	FOL-targeting CaZOL NMOFs
Hematologic toxicity						
White blood cells, $\times 10^3$ μL	2.6–10.1	4.3 ± 0.4	4.9 ± 0.5	4.1 ± 0.7	3.5 ± 0.4	3.2 ± 0.9
Granulocytes, $\times 10^3$ μL	0.4–2.0	0.8 ± 0.1	0.9 ± 0.1	1.1 ± 0.6	0.7 ± 0.2	0.9 ± 0.2
Lymphocytes, $\times 10^3$ μL	1.3–8.4	2.9 ± 0.2	3.5 ± 0.4	2.8 ± 0.5	2.4 ± 0.3	1.8 ± 0.4
Monocytes, $\times 10^3$ μL	0.0–0.3	0.3 ± 0.1	0.2 ± 0.1	0.5 ± 0.1	0.2 ± 0.1	0.3 ± 0.1
Red blood cells, $\times 10^6$ μL	6.5–10.1	8.4 ± 0.2	7.9 ± 0.2	8.4 ± 0.3	8.1 ± 0.3	8.8 ± 0.2
Platelet, fl	780–1540	912 ± 46	809 ± 173	1087 ± 67	1121 ± 41	1156 ± 29
Neptrotoxicity						
BUN, mg/mL	8–33	24 ± 2	27 ± 1	28 ± 1	26 ± 1	28 ± 2
Crea, mg/mL	0.2–0.9	0.2 ± 0.0	0.2 ± 0.0	0.2 ± 0.0	0.2 ± 0.1	0.2 ± 0
Na^+, mmol/L	140–160	155 ± 1	146 ± 3	152 ± 1	147 ± 2	156 ± 1
K^+, mmol/L	5–7.5	2.9 ± 0.1	3.2 ± 0.2	3.2 ± 0.1	3.1 ± 0.2	3.4 ± 0.2
Cl^-, mmol/L	88–110	77 ± 1	81 ± 2	82 ± 2	78 ± 1	76 ± 2
Hepatotoxicity						
AST, U/L	59–247	58 ± 6	89 ± 14	92 ± 23	72 ± 12	89 ± 14
ALT, U/L	28–132	44 ± 4	54 ± 4	64 ± 8	62 ± 2	62 ± 6
Plasma Ca^2 + level						
Ca^{2+}, mg/ml	7.1–10.1	9.8 ± 0.2	10.1 ± 0.3	10.5 ± 0.4	9.0 ± 0.3	10.5 ± 0.5

efficiency of these new systems was confirmed against *Pseudomonas aeruginosa* and *Staphylococcus aureus*.

The example discussed above indicates that a MOF-based combination therapy is a very promising field indeed. Moreover, in this therapy type, the drugs possessing different activity and targets (for example analgesic, antipyretic and anticancer drugs) can be combined and delivered. Other examples of this type of multi-purpose MOF in anticancer therapy [119,120] are discussed below.

2.5.2. Multimodal imaging agents

Similarly to the case of combination therapy (where more than one biologically active compound is applied) one can consider a multimodal MOF, combining several imaging agents or sensors [121–125]. Some selected examples will be discussed below.

2.5.3. Theranostics

Finally, one can envision a combination of both therapeutic and imaging properties in a single MOF, thus making the applicable in theranostics. This indeed becomes a very powerful technique, offering a possibility to monitor in real time the distribution of the drug after dosing [Fig. 5] [66].

For example, Horcajada et al. studied the imaging properties of the MIL-88A containing nontoxic Fe(III) ions possessing relaxation properties [59]. On the MRI image the differences in magnetic-resonance signal intensity of the liver and spleen of rats, comparing to the control, were observed [59].

Lin et al. [80,84,104,126] studied a series of MOF materials as theranostics possessing both imaging and therapeutic properties:

- functionalized prodrug-containing Pt(IV)-MOF.
- DSCP-loaded dye-grafted and silica-coated MIL-101(Fe)_NH_2.
- ESCP-loaded aminofunctionalized $Fe_3(\mu_3\text{-}O)Cl(H_2O)_2(BDC)_3$ particles associated to a fluorophore.
- Zr-MOFs with $[Ru(5,5'\text{-}(CO_2)_2\text{–}4,4'\text{-bpy})(2,2'\text{-bpy})_2]$ as connecting points.

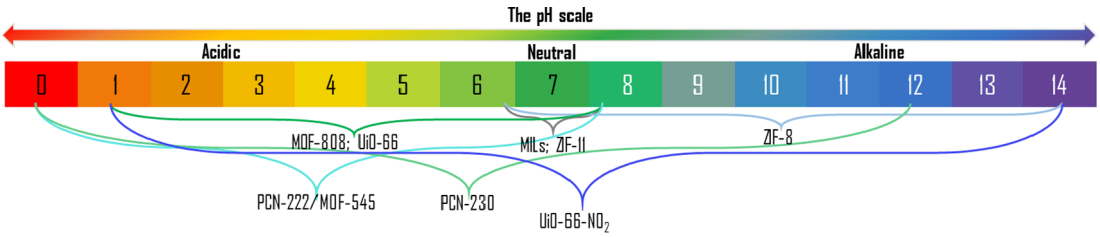

Fig. 6. The chemical (acid-base) stability of some representative MOFs based on the literature data. Based on [16].

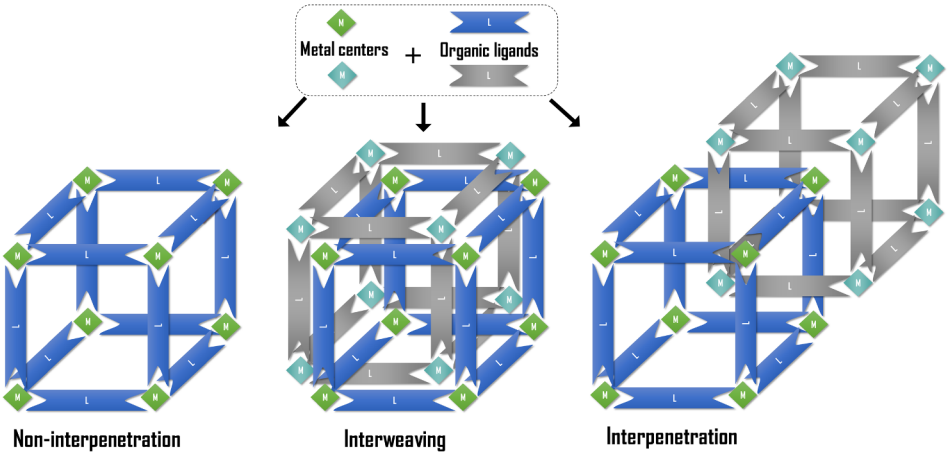

Fig. 7. Schematic representation for the synthesis and formation of the normal and catenated 3D MOF structures: interweaving, in the centre, and interpenetration, on the right.

Rowe et al. [127] published the results for the Gd-MOF containing MTX and covered with different copolymers and fluorophores. The PNIPAM-co-poly(N-acryloxysuccinimide)-co-poly(fluorescein O-methacrylate) (PNIPAM-co-PNAOS-co-PFMA)-wrapped gadolinium (Gd) MOF was synthesized, and its surface was modified with the anticancer drug MTX, with a fluorescent dye, and with the targeted ligand, the peptide (H-glycine-RGD-serine-NH_2 (GRGD-NH_2)). The targeted properties of the drug delivery system were confirmed using the FITZ-HSA cells. Cancer cell growing inhibition properties, similar to MTX, were successfully confirmed. However, comparing to the drug, the new system has additional targeted and imaging theranostic properties.

The examples discussed above confirm the applicability of MOF materials in multifunctional systems. Some additional examples will be discussed later in the article (see Chapter 5.4).

3. Key requirements for medical application of MOFs

3.1. Non-toxicity

MOF materials for biomedical applications should be non-toxic and biocompatible. This requirement can be easily met by various MOF materials due to their steadily growing numbers and building component options. Moreover, some MOFs have appeared, with composition similar to compounds approved for the medical application as drugs. For example, the Fe-fumarate, possessing similar composition to the MIL-88A, is applied in oral iron supplementation [75]. At the same time, it should be pointed out that the general and widely approved toxicity tests of nanomaterials (including MOF materials) still have not been proposed [65]. Until now, four important points of toxicity evaluation have been suggested [24]:

(1) A MOF stability in a biological medium. If a material is non-biodegradible the toxicity can increase due to accumulation in a body;
(2) Initial toxicity estimation using, for example, LD50 (lethal dose parameter, this parameter is defined as the amount of a compound that kills half the members of a tested population after a specific test duration) for constitutive cations and ligands;

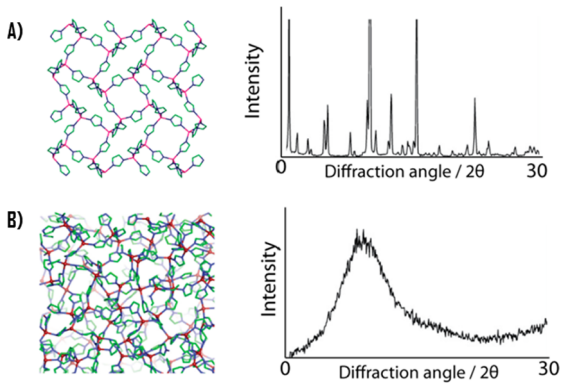

Fig. 8. Structural and PXRD differences between (a) MOF and (b) AMOF. Reprinted with permission from [19]. Copyright 2014 American Chemical Society.

(3) Cytotoxicity of MOFs, initial tests can help understand toxicity on cell level;
(4) Toxicity, studied *in vivo,* which is the most important test, because it provides the most direct and valuable information.

To control the toxicity of a product one should use non-toxic metal cations and ligands. Each cation applied for the MOF preparation is characterized by its own toxicity level from μg/kg (Cd) up to g/kg (Ca). Thus the novel MOFs containing cations playing important roles in human body (for example Mg(II), Ca(II), Fe(III), Zn(II), Cu(II), Mn(II)) and/or being neutral for tissues (Ti(IV), Zr (IV)) have been designed [53]. The toxicity of cations is strongly related to their ability to accumulate in a body. In a different approach, one can use inert metal cations (for example Zr(IV)), which are considered as non-toxic [65]. However, often the toxicity of metals is described for salts or oxides possessing different degradation profiles than MOF materials. Moreover, the toxicity of a cation can depend on the type of organic ligand [75].

The ligand, organic part of a MOF, should be also non-toxic itself, and the toxicity of each ligand should be considered separately [65]. Exo- as well as endogenous substances can act as ligands. In the case of exogenous ligands, possess optimal LD50, it is instructive to present exemplary data on toxicity of some typical organic ligands. Specifically, these are 5 g/kg (terephthalic acid), 8.4 g/kg (trimesic acid), 5 g/kg (2,6 napthalenedicarboxylic acid), 1.13 g/kg (1-methylimidazole), 1.4 g/kg (2-methylimidazole), 5 g/kg (isonicotinic acid), and 1.6 g/kg (5-aminoisophthalic acid), showing that their toxicity is at the acceptable level for bio-

Table 4
Summary of the drugs introduced into a MOF structure.

No	Name of verified chemotherapeutic action drug	Abbreviation
1	Cisplatin	CIS
2	Oxaliplatin	OXA
3	Methotrexate	MTX
4	Doxorubicin	DOX
5	Gemcitabin	GEM
6	5-fluorouracil	5-FU
7	Busulfan	BU
8	Tamoxifen	TMX
9	Mitoxantrone	MTZ
10	Paclitaxel	PTX
11	Daunomycin	DAU
12	Camptothecin	CPT
13	Topotecan (Camptothecin derivative)	TPT
14	7-Ethyl-10-hydroxy-camptothecin (Camptothecin derivative) [156–158]	SN-38
No	**Name of potential chemotherapeutic action drug**	**Abbreviation**
15	Curcumin [159–162]	CCM
16	[Ru(p-cymen)Cl_2(1,3,5-triaza-7-phospaadamantane)] [163]	RAPTA-C
17	S-(N-p-chlorophenyl-N-hydroxycarbamoyl) glutathione [164,165]	CHG
18	Pamidronate [166]	PAM
19	Zolendronate [167,168]	ZOL
20	Alendronate [169]	AL
21	Gallic acid [170–173]	HGAL
22	Olsalazine [174,175]	OLZ
23	Azidothymidine and derivatives [176–178]	AZT, AZT-MP, AZT-TP
24	Polyoxometalates ($H_3PW_{12}O_{40}$) [179–182]	POM
25	Nimesulid [183–185]	NIM
26	Artesunate [186–188]	ART
27	Artemisinin [189–191]	ARS
28	Gold(III) pyrrolidinedithiocarbamato complex [(PDTC)$Au^{III}Cl_2$] [192]	–
29	Gold(I) pyrrolidinedithiocarbamato complex [(PDTC)$Au^{I}Cl_2$] [193]	–
30	Hydrogen sulphide [194,195]	H_2S
31	Nitric oxide [196–199]	NO
No	**Name of photodynamic action drug**	**Abbreviation**
32	Porphyrins and derivatives [200–202]	–
33	Chlorin and derivatives [203,204]	–
34	Ruthenium complexes [205,206] (e.g. $(Ru(2,2'BPY)_3]^{2+}$, $[Ru(1,l0'phenanthroline)_3]^{2+}$, $[Ru(1,l0'phenanthroline)_2$2-(1H-imidazo[5,5-f][1,1-]-phenanthrolin-2-yl)1,l0′phenanthroline $]^{2+}$)	–
35	Pyropheophorbide-lipid (pyrolipid) [207–210]	Pyro
No	**Name of photothermal action drug**	**Abbreviation**
36	Gold nanostar [211,212]	GNS
37	Prussian blue [213,214]	PB
No	**Name of genetherapeutic action drug**	**Abbreviation**
38	Small interfering ribonucleic acid [215–217]	siRNA
39	Deoxyribonucleic acid [218–219]	DNA
No	**Name of immunotherapetic action drug**	**Abbreviation**
40	Vaccine ovalbumin [220,221]	OVA

Table 5
Selected examples of the application of BIOMOFs in drug delivery for the cancer therapy.

Select instances on the application of BIOMOFs in drug delivery
MOFs for drug delivery applications

No.	Metal	Linker	MOF	Surface modification	Tested cell lines and *in vivo* models	Key findings (information)	Ref.
1	Zn(II)	CCM	medi-MOF-1, $[Zn_3(CCM)_2 \cdot 7(DMA) \cdot 3(EtOH)]$	N/D	- BxPC-3 (*in vitro*)	– The MOF possessed very high surface area (Langmuir model: 3002 m^2/g). – The MOF exhibited a comparable cell growth inhibitory performance against cells. – The cytotoxic efficacy of medi-MOF-1 was similar to that of the pharmaceutical ingredient CCM. – To confirm the MOF drug delivery ability the storage and release of ibuprofen was reported.	[101]
2	Tb(III)	DSCP	NCP-1$Tb_2(DSCP)_3(H_2O)_{12}$	PVP, TEOS, C(RGDfK)-enhanced cellular uptake	- HT-29, MCF-7 (*in vitro*)	– C(RGDfK)-targeted NCP-1′-a and NCP-1′-b gave IC50 (50% Inhibitory Concentration) values of 9.7 and 11.9 μM (cisplatin standard had 13 μM). – Targeted nanoparticles were sufficiently internalized presumably *via* receptor-mediated endocytosis. – Nanoparticles in shells of amorphous silica were obtained, and the anticancer efficiacy of Pt-based nanoparticles *in vitro* was demonstrated.	[84]
3	Zr(IV)	DSCP	Zr-DSCP NCP	N/D	N/D	– Zr-DSCP was unstable in PBS.	[107]
4	La(III)	DSCP	La-DSCP NCP	DOPA, CHOL, DOPC, (DSPE–Peg_{2K}), DSPE–Peg_2K–AA	- NCI-H460, A549 (*in vitro*)	– La-DSCP NCP stabilized with Cholesterol/DOPC/DSPE-Peg-lipid or DSPE-Peg-anisamide conjugate were more effective than free cisplatin against (cell NCI-H460 and A549) cell lines.	
5	Zn(II)	Bisphosphonic acids containing CIS and OXA	NCP-1 and NCP-2	DOPA, PEG, DOPC, CHOL, DSPE-PEG_{2k}	- CT26, H460, AsPC-1 (*in vivo* and *in vitro*)	– Nanoparticles that carry cisplatin and oxaliplatin were synthesized. – The drug loadings were equal to 48 ± 3 wt% of cisplatin and 45 ± 5 wt% of oxaliplatin. – Cell viability assays against three cancer cell gave similar IC50 values for studied nanoparticles. – *In vivo* pharmacokinetic studies in mice showed minimal uptake of pegylated nanoparticles by the mononuclear phagocyte system. – Good blood circulation half-lives for the nanoparticles carrying cisplatin and oxaliplatin were reported. – In all tumour xenograft models evaluated pegylated particles showed superior potency and efficacy compared with free drugs.	[233]
6	Zn(II)	MTX	N/D	N/D	- CCRF-CEM (*in vitro*)	– 79.1 wt% of MTX was introduced. – No enhancement in efficacy over free MTX was observed.	[234]
7	Zr(IV)	MTX	N/D	N/D		– 78.2 wt% of MTX was introduced. – No enhancement in efficacy over free MTX was observed	

(*continued on next page*)

Table 5 (*continued*)

Select instances on the application of BIOMOFs in drug delivery
MOFs for drug delivery applications

No.	Metal	Linker	MOF	Surface modification	Tested cell lines and *in vivo* models	Key findings (information)	Ref.
8	Gd(III)	MTX	N/D	DOPE, DSTAP, DOPE-AA	– 71.6 wt% of MTX was introduced. – Lipid-coated and targeted nanoparticles had superior efficacy compared to the as-synthesized particles or free drug in *in vitro* cytotoxicity assays with Jurkat cells. – Also folic acid was introduced into a MOF structure.		
9 **10** **11**	Zn(II) Fe(III) Fe(III)	MTX MTX CHG	MTX-Zn@BIX-Zn MTX-Fe@BIX-Zn CHG-Fe@BIX-Zn	Zn-BIX	- HeLa cells (*in vitro*)	– Core-shell nanostructure was stable under physiological conditions. – The pH-triggered drug release was observed. – Inhibition of the growth of cancer cells, and a higher cytotoxicity against HeLa cells than for core nanoparticles and the free drug *in vitro* was observed.	[235]
12	Hf(IV)	H_2DBP	DBP – UiO NMOF $Hf_6(\mu_3\text{-}O)_4(\mu_3\text{-}OH)_4(DBP)_6$	N/D	- SQ20B (*in vivo* and *in vitro*)	– PDT transport using the porphirine-containing NMOF was reported for the first time. – The loading of DBP was high, and was ewual to 77 wt %. – NMOF worked as an efficient PDT photosensitizer. It was confirmed by $^1O_2$ generation efficiency measurements and *in vitro* cytotoxicity assays. – *In vivo* PDT efficacy studies with subcutaneous xenograft murine models were performed, and tumour reduction were observed (see Fig. 9).	[201]

(*continued on next page*)

Table 5 (*continued*)

Select instances on the application of BIOMOFs in drug delivery
MOFs for drug delivery applications

No.	Metal	Linker	MOF	Surface modification	Tested cell lines and *in vivo* models	Key findings (information)	Ref.
13	Hf(IV)	H_2DBC	DBC-UiO $Hf_6(\mu_3\text{-}O)_4(\mu_3\text{-}OH)_4(DBC)_6$	N/D	- CT26, HT29 (*in vivo* and *in vitro*)	– The first chlorin-based nanoscale MOF was described. – 64% photosensitizer loading was reported. – DBC-UiO was 3 times as efficient as DBP-UiO in generating $^1O_2$ and exhibited much higher PDT cytotoxicity in two colon cancer cell lines. – The superior anticancer efficacy of DBC-UiO compared with DBP-UiO was demonstrated. – Both apoptosis and immunogenic cell death contributed to cell killing induced by DBC-UiO based PDT (see Fig. 10).	[203]
14 **15**	Ca(II) Ca(II)	PAM ZOL	$[Ca(H_2\text{-}PAM)(H_2O)]H_2O$ $[Ca(H_2\text{-}ZOL)(H_2O)]$	DOTAP/DOPE, AA	- H460, AsPC-1 (*in vitro*)	– Lipid-coated and anisamide-targeted nanoparticles displayed superior anti-tumour efficacy compared to the as-synthesized particles (or free bisphosphonates) *in vitro* against human lung and pancreatic cancer cells. – Surface modification was shown as very important. – Pam loading was determined to be 75.5 wt%. – Zol loading of 75.7 wt% was achieved.	[236]
16	Cu(II)	3,5-bis(pyridine-3-ylmethylamino)benzoic acid, (L1)	$[Cu(L_1)(OH)(H_2O)_2]_n$ Cu-CPP	N/D	- MCF-7, HeLa, and NCI-H446. (*in vitro*)	– A ligand was shown cytotoxic. – The results pointed out that antitumour mechanism of coordination polymer particles is still uncertain.	[237]
17	Zn(II)	3,5-bis(pyridine-3-ylmethylamino)benzoic acid (L1)	$[Zn(L_1)(OH)(H_2O)_2]_n$, Zn-CPP			– Amorphous Cu-nanoparticles may act as new metal-based anticancer drugs.	
18	Fe(III)	HGAL	GALFe	N/D	N/D	– GALFe nanoparticles were stable in water across a wide range of pH levels (pH = 4–9). – At low pH (1–3) most of the hydroxyl groups are protonated and this caused a rapid destabilization and disassembly. – Pro-apoptotic properties of gallic acid lead to conclusion that this material is promising candidate in antitumoural therapy.	[238]
19	Ca(II)	ZOL	CaZOL	DOPA, CHOL, DOTAP, DSPE-PEG_{2K}, DSPE-PEG_{2K}-FOL	- H460 and PC3 (*in vivo* and *in vitro*)	– Bioresorbable FOL-targeted CaZOL NMOFs for therapeutic delivery of ZOL to FR-overexpressed tumours were reported. – MOF materials encapsulated more ZOL than existing drug delivery systems. – Good chemical and colloidal stability under physiological conditions was observed. – FOL-targeted CaZOL NMOFs showed higher efficiency than small molecule ZOL at inhibiting cell proliferation and inducing apoptosis in FR-overexpressing cancer cells *in vitro*. – *In vivo* biodistribution study indicated that over 80% of i.v. administrated FOL-targeted CaZOL particles	[131]

(*continued on next page*)

Table 5 (*continued*)

Select instances on the application of BIOMOFs in drug delivery
MOFs for drug delivery applications

No.	Metal	Linker	MOF	Surface modification	Tested cell lines and *in vivo* models	Key findings (information)	Ref.
						were accumulated in the H460 xenograft tumour 48 hrs after administration. – *In vivo* antitumour activity studies in H460 and PC3 xenograft tumour-bearing mice indicated the FOL-targeted CaZOL NMOFs but not non-targeted CaZOL NMOFs improved the direct antitumour efficiencies of ZOL by approximately 80%. – Anticancer properties of FOL-targeted CaZOL MOF materials was shown. – Histopathology study indicated the FOL-targeted CaZOL NMOFs were more efficient than ZOL to normalizing tissue microenvironments, inhibiting cell proliferation, and inducing cell apoptosis in both FR-overexpressing H460 and PC3 xenograft tumours. – FOL-targeted CaZOL NMOFs may be promising to develop as a FR-targeting anti-neoplastic agent.	
20	Mg(II)	OLZ	Mg_2(OLZ)	N/D	N/D	– Olsalazine was shown to inhibit the development of colorectal cancer in patient. – BET surface areas for studied materials were large, across the range of 636–2545 m^2/g. – Over 90 wt% of the Mg_2(OLZ)$(PEA)_2$ material consisted of a therapeutic organic molecule, with 41 and 51 wt% of PEA and olsalazine. – Mg_2(OLZ) desolvated material was composed of 86 wt% olsalazine (see Fig. 11).	[239]
21	Fe(II)	OLZ	Fe_2(OLZ)	N/D	N/D		
22	Co(II)	OLZ	Co_2(OLZ)	N/D	N/D		
23	Ni(II)	OLZ	Ni_2(OLZ)	N/D	N/D		
24	Zn(II)	OLZ	Zn_2(OLZ)	N/D	N/D		
25	Zn(II)	NH_2-BDC	IRMOF-3		- PC12 (*in vitro*)	– High concentrations of IRMOF-3 dose-dependently impaired the differentiation ability of PC12 cells. – The cytotoxicity of high-dose IRMOF-3 resulted from its transport in the endosomes to the proximal perinuclear region, causing dysfunction of transcriptional regulation and synthesis of such proteins as GAP-43 and led to the loss of cell phenotypes and potentially cell death.	[240]
26	Zr(IV)	TCPP	PCN-222/MOF-545	N/D	HeLa (*in vitro*)	– NMOF having particles with diameters across the range of 50–70 nm, 170–210 nm, 330–800 nm were studied. – The results showed that hexagonal PCN-222/MOF-545 nanoparticles, in contrast to TCPP, induced the cancer cell apoptosis upon visible light irradiation (photodynamic therapy). – Apoptotic cell death was preferred over the cell necrosis. – The NMOF phototoxicity was deactivated after several hours.	[241]

Table 6
Selected examples of the application of MOFs in drug delivery by postsynthetic noncovalent loading.

	Select instances on the application of MOFs in drug delivery MOFs for drug delivery applications							
No.	Metal	Linker	MOF	Drug loaded	Surface modification	Tested cell lines and *in vivo* models	Key findings (information)	Refs
1	Fe (II), Fe (III)	cyanide ion	$K_3[Fe(CN)_6]\cdot 3H_2O$	CIS	N/D	- T24 cells (*in vitro*)	– Excellent biocompatibility and physiological stability of hollow Prussian Blue (HPB) nanoparticles was demonstrated. – Obtained HPB exhibited a high surface area (324 m^2/g). – Cisplatin was loaded into the HPB. – Drug adsorption rate was high, also high loading efficiency was observed. However the release percentage was small. – The MTT assay and confocal microscopic observation proved the cell killing ability of the cisplatin-loaded HPB.	[242]
2	Zn (II)	2-MIM	ZIF-8	DOX	N/D	- NCI-H292, HT29 i HL-60 (*in vitro*)	– ZIF-8 with a load of 0.049 g DOX/g of dehydrated MOF was prepared. – Doxorubicin was released in a controlled way with 66% of the drug released after 30 days. – It was shown that the complex DOX-ZIF-8 exhibited lower cytotoxicity than pure DOX for the tested cells.	[243]
3	Fe (III)	BTC	MIL-100	GEM-MP	N/D	- PANC-1 (*in vitro*)	– Maximum reported drug loading was 30 wt%. – Neither degradation nor loss of crystalline structure was observed after drug loading or during particle storage in water. – The MOF was unstable in media containing phosphates, releasing intact GEM-MP cargo. – Drug loaded MOF particles were nine times more effective against pancreatic PANC-1 cells than the free drugs.	[244]
4	Gd (III)	pDBI	Gd-pDBI	DOX	N/D	U 937 (*in vivo* and *in vitro*)	– D-pDBI was grinding mechanically and MG-Gd-pDBI was obtained. – *In vivo* studies on MG-Gd-pDBI revealed its low blood toxicity. – Highest drug loading (12 wt%) of doxorubicin in MOF materials reported to date was observed. – The pH-responsive cancer-cell-specific drug release was observed. – In vitro and *in vivo* experiments demonstrated the biocompatibility of nanoparticles.	[245]
5	Fe (III)	BTC	MIL-100	DOX	N/D	N/D	– 9 wt% of DOX was loaded into a MOF. – DOX, known to be incorporated into MIL-100 (Fe) nanoparticles up to 9 wt%, binds upon the formation of highly stable coordination bonds to CUS of Fe(III) centers and disruption of drug self-associated species.	[246]

(*continued on next page*)

Table 6 (*continued*)

No.	Metal	Linker	MOF	Drug loaded	Surface modification	Tested cell lines and *in vivo* models	Key findings (information)	Refs
Select instances on the application of MOFs in drug delivery MOFs for drug delivery applications								
							– DOX coordination occurred to one or two negatively charged oxygen centers of the B ring, upon deprotonation of the relevant hydroxyl groups. – At MOF contents larger than 0.2 mg/mL, aggregation was observed both in Tris buffer and in water.	
6	Zn (II)	TATAT	N/D	5-FU	N/D	N/D	– MOF loaded with 5-FU (33.3 wt%) was studied. – Delivery in PBS (pH = 7.4) was equal to 42% after 8hrs The remaining part of a drug was delivered after 8 days. – Complete delivery was achieved after one week.	[247]
7	Cu (II)	PI	$[Cu(PI)(H_2O)]_{24}$,	5-FU	PEG_{5K}	N/D	– MOF delivered 20% of 5-FU after 24 hrs – The surface functionalization via click reaction with azide-terminated PEG turned nanoparticles into water-stable colloids. – Controlled release of 5-FU was reported.	[248]
8	Zn (II)	2-MIM	ZIF-8	5-FU	N/D	N/D	– 660 mg of 5-FU/g of the ZIF-8 was achieved. – The delivery to solutions containing the PBS (pH = 7.4) and acetate buffer (pH = 5.0) at 37 °C – was pH responsible. – The drug was released much faster at pH = 5.0 than at pH = 7.4.	[249]
9	Zn (II)	H_6L = 1,2,3,4,5,6-heksakis(3-carboxyphenyloxymethylene)benzen	$[Zn_3(L)\text{-}(H_2O)_2] \cdot 3DMF{\cdot}7H_2O$	5-FU	N/D	N/D	– 5-Fu was adsorbed (0.36 mg 5-FU/mg of a MOF). – The delivery was fast at the initial stage (10 hrs). – The complete drug delivery was observed after 72 hrs. – The encapsulation of La(III) cations was also studied, indicating that MOF could potentially serve as a tunable luminescent material.	[250]
10	Cu (II)	4,4′-BPY;H_2L = diphenylmethane-4,4′-dicarboxylic acid	$[Cu(L)(4,4'\text{-}BPY)(H_2O)]n1.5nCH_3CN$	5-FU	N/D	N/D	– 5-FU (c.a. 27.5 wt%) was adsorbed. – Drug delivery within the "burst effect" was reported. – 21% of drug was delivered after 11 hrs and next 51% was delivered slowly (in a two stage process). – The incorporation of the drug 5-FU into the desolvated MOF was around 27.5 wt% per gram of the dehydrated MOF 1. – 5-FU was released in controlled way with 61% of the drug released after 95 hrs. – Molecular docking calculations were applied to investigate the preferred conformation of 5-FU molecules upon binding to the MOF.	[251]
11	Zn (II)	4,5-di(1H-tetrazol-5-yl)–2H-1,2,3-triazole = L	$[Zn(HL)]{\cdot}DMA$, IFMC-1	5-FU	N/D	N/D	– 5-FU (30.5 wt%) was adsorbed. – The controlled release was achieved from a MOF structure in simulated body fluids (after c.a. 1 h 80%, after 120 hrs − 89.8%).	[252]
12	Cu (II)	BTC	Cu-BTC (BasoliteTM C300)	5-FU	N/D	- NCI-H292, MCF-7,	– 5-Fu in the amount of 45 wt% was adsorbed. – Drug release was observed for 48 hrs.	[253]

(*continued on next page*)

Table 6 (*continued*)

No.	Metal	Linker	MOF	Drug loaded	Surface modification	Tested cell lines and *in vivo* models	Key findings (information)	Refs
Select instances on the application of MOFs in drug delivery MOFs for drug delivery applications								
						HT29, HL60 (*in vitro*)	– 39.4% of the drug was released from the MOF in the first 30 min (the drug in its free form). Next slow release was observed (60% in 15 hrs). The dissolution reached 82.0% after 48 hrs. – 5-fluorouracil incorporated into Cu-BTC MOF induced cell death by apoptosis mechanism to the dose of 10 mg/mL. – 5-Fu loaded MOF materials showed cytotoxicity in MCF-7 and HL60 cells.	
13	Zr (IV)	BDC	UiO-66	AL	N/D	- MCF-7, HepG2 (*in vitro*)	– The AL loading amount was very high (up to 1.06 g/g of UiO-66). – The pH - dependent drug release was observed. – Released drug amount was up to 88.1% after 108 hrs (pH = 7.4). – At the pH = 5.5 the amount was less than 76% within the same time. – New nanoparticles showed remarkable water dispersity. – The drug showed an enhanced growth inhibition effect compared to free AL against cells.	[169]
14	Fe (III)	Muconic acid	MIL-89	BU	N/D	N/D	– New delivery systems possessed similar cytotoxicity to the free drugs.	[59]
15	Fe (III)	Fumaric acid	MIL-88A	AZT-TP, BU	PEG	N/D	– The iron-based cores are endowed with good relaxivities, making these nanoparticles candidates for magnetic resonance imaging (contrast) agents.	
16	Fe (III)	BTC	MIL-100	AZT-TP, BU, DOX	PEG	- CCRF-CEM, RPMI-8226 (*in vitro*)		
17	Fe (III)	NH2-BDC	MIL-101_NH_2	AZT-TP	N/D	N/D		
18	Fe (III)	BDC	MIL-53	AZT-TP, BU	N/D	N/D		
19	Co (II)	DHTP	CPO-27-Co $[Co_2(C_8H_2O_6)\text{-}(H_2O)_2]\cdot 8H_2O$	NO	N/D	N/D	– Two MOF materials $[M_2(C_8H_2O_6)(H_2O)_2]\ 8H_2O$ (M = Co, Ni), were shown good adsorbents for NO. – Water-triggered delivery of this gas was proved. – Each unsaturated metal atom in the structure coordinates to one NO molecule. – All of the stored was available for the delivery even after very long storage of the material (see Fig. 12).	[254]
20	Ni(II)	DHTP	CPO-27-Ni $[Ni_2(C_8H_2O_6)\text{-}(H_2O)_2]\cdot 8H_2O$	NO				
21	Fe (III)	Fumaric acid	MIL-88	NO	N/D	N/D	– 1–2.5 mmol NO/g of a MOF was adsorbed. – NO was delivered after long time (16 hrs). – Release amounts were low but still sufficient enough to ensure a significant release at the biological level over prolonged periods of time.	[255]

(*continued on next page*)

Table 6 (*continued*)

Select instances on the application of MOFs in drug delivery
MOFs for drug delivery applications

No.	Metal	Linker	MOF	Drug loaded	Surface modification	Tested cell lines and *in vivo* models	Key findings (information)	Refs
22	Fe (III)	DOBDC	Fe_2(DOBDC)	NO	N/D	N/D	– Adsorption capacity 16 wt% was achieved. – Moisture-triggered NO delivery after 10 days was studied. – Adsorption isotherms indicated an adsorption capacity greater than 16 wt%, corresponding to the adsorption of one NO molecule per iron center.	[256]
23	Zn (II)	PDC	IRMOF-14,	TMX	N/D	N/D	– Computer simulation results confirmed the application of IRMOF 14 and IRMOF 16 for noncovalent tamoxifen bonding.	[257]
24	Zn (II)	TPDC	IRMOF-16	TMX				
25	Zn (II)	AD, H2TP	ZJU-64 $Zn_{16}(AD)_8(TP)_8O_2(H_2O)_8{\cdot}4HTP{\cdot}36DMF{\cdot}16H_2O$	MTX	N/D	- PC12 (*in vitro*)	– MTX was successfully loaded into MOF particles by a simple impregnation method and the drug payloads reach approximately 13.45 and 10.63 wt% for ZJU-64 and ZJU-64-CH3, respectively.	[138]
26	Zn (II)	AD, CH3-H2TP	ZJU64-$CH_3Zn_{16}(AD)_8(CH3TP)_8O_2(H_2O)_8{\cdot}4HTP{\cdot}36DMF{\cdot}16H_2O$	MTX			– Low cytotoxic activities (to PC12 cells) were recorded. – MTX was delivered at pH = 7.4 and the temperature dependence of this process was studied. – The delivery was faster at higher temperature.	
27	Fe (III)	2-azidoterephtalic acid	MIL-101(Fe)-N_3	DOX	β-CD-SS-BC mono-[6-(1,8 diaza-4,5-dithiaoctyl)- 6-deoxy]-β-cyclodextrin, K (ad) RGDSPEG1900	- COS7, HeLa (*in vitro*) - H22 (*in vivo*)	– Acid environment enhanced, tumour cell uptake, and tumour intracellular GSH_{red} triggered drug release were observed for the studied system. – This was caused by the covalently linked pH - responsive benzoic imine bond and redox responsive disulphide bond. – After surface modification the cytotoxicity of loaded DOX to normal cells was significantly reduced. – The drug loaded TTMOF can inhibit tumour growth effectively with minimal side effects. This was proved *in vivo* experiment.	[130]
28	Zr (IV)	TCPP	PCN 221	MTX	N/D	- PC12 (*in vitro*)	– MTX (40 wt%) was loaded into a MOF structure. – The drug delivery was pH responsible. – After 72 hrs at (pH = 2) 40% of drug was desorbed. – At pH = 7.4 the desorption was total. – Low cytotoxicity was observed (to PC12 cells). – Release without "burst effect" was observed.	[258]
29	Cu (II)	H4L = 3,5-bis(isophthalic acid)-1H-1,2,4-triazole	MOF-1 {$[NH_2(CH_3)][Cu_6(L)_3(OAc)(H_2O)_4]{\cdot}$xsolvent}	5-FU	N/D	N/D	– 5-FU (24.9 wt%) was adsorbed and delivered. – After 30 hrs 52% of the drug was desorbed, and after 80 hrs high desorption rate was recorded (possible structure degradation). – 98% of the drug was released after 120 h in the PBS.	[259]
30	Ni(II)	DHTP	$[Ni_2(DHTP)(H_2O)_2]{\cdot}8H_2O$, Ni-CPO	H_2S	N/D	N/D	– Hydrogen sulfide was adsorbed in a MOF with the CPO-27 structure. – Gas can be stored for several months.	[260]
31		DHTP	Zn-CPO	H_2S	N/D	N/D		

(*continued on next page*)

Table 6 (*continued*)

No.	Metal	Linker	MOF	Drug loaded	Surface modification	Tested cell lines and *in vivo* models	Key findings (information)	Refs
	Select instances on the application of MOFs in drug delivery MOFs for drug delivery applications							
	Zn (II)						– Delivered gas was biologically active in preliminary vasodilation studies of porcine arteries, and the structure of the hydrogen sulfide molecules inside the framework was elucidated using a combination of powder X-ray diffraction and pair distribution function analysis. – The Ni-CPO material showed no degradation of its crystalline structure and only a small loss of deliverable gas capacity over a six month period. – The Zn-CPO material showed a somewhat greater effect on its crystallinity, but still retained a significant delivery of H_2S.	
32	Zn (II)	2-MIM	ZIF-8	DOX	PAA	- MCF-7 (*in vitro*)	– Ultrahigh loading capacity of DOX (1.9 g DOX/g of a material) was observed. – The pH-sensitive drug release occurred. – The DOX-loaded PAA@ZIF-8 NPs could be taken up by MCF-7 cells through endocytosis and released the DOX much faster in mild acidic buffer solution (pH = 5.5) than at the neutral pH of 7.4 in the cytoplasm by CLSM. – At the pH = 7.4 slow release was observed (35.6% after 60 hrs). – At the pH = 5.5 faster release occurred (75.9% after 60 hrs). – The PAA@ZIF-8 NPs were nearly non-toxic to live cells.	[261]
33	Fe (III)	BTC	MIL-100	BU	PEG	- CCRFCEM, RPMI-8226, J774 (*in vitro*)	– MOF nanoparticles showed an unprecedented loading (up to 25 wt%) of busulfan. – The lack of toxicity was observed (up to concentrations equal to 50 μg/ml) for human leukemia CCRFCEM, human multiple myeloma RPMI-8226 and human macrophages J774.	[262]
34	Ni(II)	4,4′-(buta-1,3-diyne-1,4-diyl)bispyrazole	$[Ni_8(OH)_4(O\text{-}H_2)_2(4,4'\text{-}(buta\text{-}1,3\text{-}diyne\text{-}1,4\text{-}diyl)bispyrazolato)_6]n$	[Ru(p-cymen)Cl_2(PTA)] (RAPTA-C),	N/D	N/D	– The loading of a significant (1.1 g of drug/g of a MOF) quantity of the unconventional metallo-drug RAPTA-C was reported. – Adsorption process was reversible as a consequence of physisorption. – RAPTA-C was easily released into simulated body fluid.	[263]
35	Zn (II)	BDP_H	ZnnBDP_H	[Ru(p-cymen)Cl_2(PTA)] (RAPTA-C), MTZ	N/D	- J774 cell (*in vitro*)	– The encapsulation and release of the antitumour drugs mitoxantrone and RAPTA-C was evaluated in the ZnBDP_X series. – High drugs loadings were achieved by using a simple and fast impregnation method. – The incorporation of mitoxantrone was achieved by a simple grinding. – Drug loading was dependent on the BET surface area.	[264]
36	Zn (II)	nBDP_NO_2	ZnnBDP_NO_2	[Ru(p-cymen)Cl_2(PTA)] (RAPTA-C), MTZ				
37	Zn (II)	nBDP_NH_2	ZnnBDP_NH_2					

(*continued on next page*)

Table 6 (*continued*)

Select instances on the application of MOFs in drug delivery MOFs for drug delivery applications

No.	Metal	Linker	MOF	Drug loaded	Surface modification	Tested cell lines and *in vivo* models	Key findings (information)	Refs
				[Ru(p-cymen)Cl_2(PTA)] (RAPTA-C), MTZ			– Two-step RAPTA-C delivery was related to the framework flexibility. While drug release from ZnBDP_X (X = H, NH_2, NO_2) was independent of the matrix stability.	
38	Zn (II)	nBDP_OH	ZnnBDP_OH	[Ru(p-cymen)Cl_2(PTA)] (RAPTA-C), MTZ			– In ZnBDP_OH@RAPTA-C the RAPTA-C delivery was dependent on the kinetics of framework degradation (see Fig. 13).	
39	Mg (II)	HAIP	$[Mg_3(H_2O)_4(5\text{-}AIP)_2(5\text{-}HAIP)_2]\cdot 4DMA$	5-FU, IBU	N/D	N/D	– 5-FU and IBU were loaded into a MOF (21.06 wt% and 16.49 wt%, respectively). – At simulated physiologic conditions (37 °C, pH = 7.4) 83.8% of 5-Fu was desorbed after 6 hrs, and 87.77% of IBU after 8 hrs. – After 45 min very rapid delivery was observed with the "burst effect". – The delivery process was dominated by the MOF decomposition.	[265]
40	Cu (II)	NH2-BDC, 2,2′-BPY	$Cu_{24}(5\text{-}NH_2\text{-}BDC)_{24}(2,2'\text{-}BPY)_6(H_2O)_{12}]$ 72DMA}	5-FU	N/D	N/D	– 5-FU (23.76 wt%) was loaded and delivered in the PBS solution (pH = 7.4) at 37 °C. – Initially, the delivery was fast (80% after 7.5 hrs) and next it was slow (24 hrs). – Rapid delivery was accompanied by the structure degradation (proved by the PXRD study).	[266]
41	Fe (III)	BTC	MIL-100(Fe)	AZT, AZT-MP, AZT-TP	N/D	N/D	– Low AZT loading was observed (1.2 wt%) due to the absence of phosphate groups. – In contrast, phosphorylated drugs were efficiently adsorbed within the NMOF cavities with encapsulation efficiencies close to 100%. – Loadings as high as 36 wt% and 24 wt% were obtained for AZT-MP and AZT-TP, respectively. – AZT-MP molecules were released faster in physiological buffer compared to AZT-TP. However, the release of AZT-MP is still progressive, with less than 60% of the drug released after 8 h of incubation.	[268]
42	Fe (III)	BTC	MIL-100(Fe)	AZT-TP	N/D	- PBMC (*in vitro*)	– MIL-100 quickly adsorbed (24 wt%) of AZT-TP with entrapment efficiencies close to 100%, without perturbation of the supramolecular crystalline organization. – The agreement with molecular modelling predictions was observed. – The drug was adsorbed in the large cages. – Phosphates strongly coordinated with the unsaturated iron(III) sites. – Progressive drug release under physiological simulated conditions was observed.	[268]

(*continued on next page*)

Table 6 (*continued*)

Select instances on the application of MOFs in drug delivery
MOFs for drug delivery applications

No.	Metal	Linker	MOF	Drug loaded	Surface modification	Tested cell lines and *in vivo* models	Key findings (information)	Refs
							– No MOF complexation occurred with AZT leading to poor drug loadings and uncontrolled release.	
43	Zn (II)	AD, BPDC	bio-MOF-1 $[Zn_8(AD)_4(BPDC)_6\text{-}O{\cdot}2Me_2NH_2$, 8DMF, $11H_2O]$	$Ru(2,2'\text{-}BPY)_3]^{2+}$ $[Ru(PHEN)_3]^{2+}$ $[Ru(PHEN)_2HIPP]^{2+}$	N/D	N/D	– A new-type $^1O_2$ generation system was synthesized by exchanging cationic ruthenium complexes (RCs) into anionic bio-MOF-1. – The resulting bio-MOF-1&RCs can be used as effective photocatalysts for $^1O_2$ generation.	[206]
44	Zr (IV)	BDC	UiO-66	PTX, CIS	PCL–TPGS	- U-87 MG, HSC-3 (*in vitro)*	– UiO-66 and UiO-67 nanoparticles with uniform particle size were synthesized and used as drug delivery carriers. – The surfaces of Zr-based NMOF were further microencapsulated within a biocompatible and biodegradable polymeric matrix. – A sustained drug release rate was observed for the cisplatin loaded forms. – For the PTXl loaded nanoparticles a high dissolution rate was observed due to the amorphisation of the drug. – The encapsulation of the drug loaded MOF particles inside the biocompatible and biodegradable polymeric matrix enhanced the sustained release and the decrease of the "burst effect" was observed. – Very low toxicity for the polymer coated forms was observed even at high concentrations.	[269]
45	Zr (IV)	BPDC	UiO-67	PTX, CIS				
46	Zn (II)	BTCA	ZnBTCA, $Zn_3(AD)(BTC)_2(H_2O){\cdot}(CH_3)2NH_2{\cdot}xDMF{\cdot}yH_2O$	$[(PDTC)Au^{III}Cl_2]$	N/D	- A2780, A2780cis (*in vitro*)	– Anticancer active gold(III) pyrrolidinedithiocarbamato complex after metalation was found to display an up to 33-fold higher anti-cancer potency towards cisplatin-resistant A2780cis line. – Incorporating gold(III) complex in a zinc-based biodegradable MOF could significantly enhance its anti-cancer activity.	[192]
47	Zn (II)	BPDC, AD	BIO-MOF-1, $Zn_8(AD)_4(BPDC)_6\text{-}O{\cdot}2Me_2NH_2$,8DMF, $11H_2O$	$[(PDTC)Au^{III}Cl_2]$	N/D	N/D		
48	Zn (II)	AD, TATB	PCN 530, $Zn_3[Zn_2(\mu_2\text{-}H_2O)]_3(AD)_6(TATB)4(DMF)$,	$[(PDTC)Au^{III}Cl_2]$	N/D	N/D		
49	Zn (II)	BTCA	ZnBTCA, $Zn_3(ad)(BTC)_2(H_2O){\cdot}(CH_3)2NH_2{\cdot}xDMF{\cdot}yH_2O$	$[(PDTC)Au^{I}Cl_2]$	N/D	- A2780, A2780cis (*in vitro*)	– The MOF ZnBTCA (surface area = 3057.5 m^2/g), was studied as a drug carrier. – The cellular survival percentages of around 95% were recorded, whereas longer incubation periods (more than 24 hrs) resulted in a decrease of cellular survival percentage to around 50%. – Au(I) complex compounds loaded MOF materials can be successfully applied as anticancer nanoparticles.	[193]

(*continued on next page*)

Table 6 (*continued*)

No.	Metal	Linker	MOF	Drug loaded	Surface modification	Tested cell lines and *in vivo* models	Key findings (information)	Refs
	Select instances on the application of MOFs in drug delivery MOFs for drug delivery applications							
50	Zn (II)	2-MIM	ZIF-8	5-FU	FMN - Phosphorylated vitamin B2	– 4 T1, MCF-7, HepG2 (*in vitro*) - Balb/c (*in vivo*)	– The ZIF-nanoparticles could partially enter the cells via clathrin- and macropinocytosis-mediated pathways. – The drugs were released under the intracellular acidic environment. – The ZIF-nanoparticles affected the membrane integrity at a high dose and increased membrane mediated ROS, which substantially contributed to their cytotoxicity. – This toxicity was different from inorganic ZnO nanoparticles in respect of biointeraction, and ROS-generation mechanisms. – Studied type of vehicle exhibited a relatively very high concentration in lung. The drug levels dropped with time, with more than 70% removal on the 7th day following a four times i.v. administration. – At the normal doses, ZIF-nanoparticles exhibited acceptable system and blood biocompatibilities, and minimal effects on the liver and renal functions, immune cells, inflammatory factors, etc. – Consistent with their high distribution to the lung, 5-FU@ZIF-NPs significantly improved the therapeutic outcome in a nude mouse model with tumour lung metastasis.	[270]

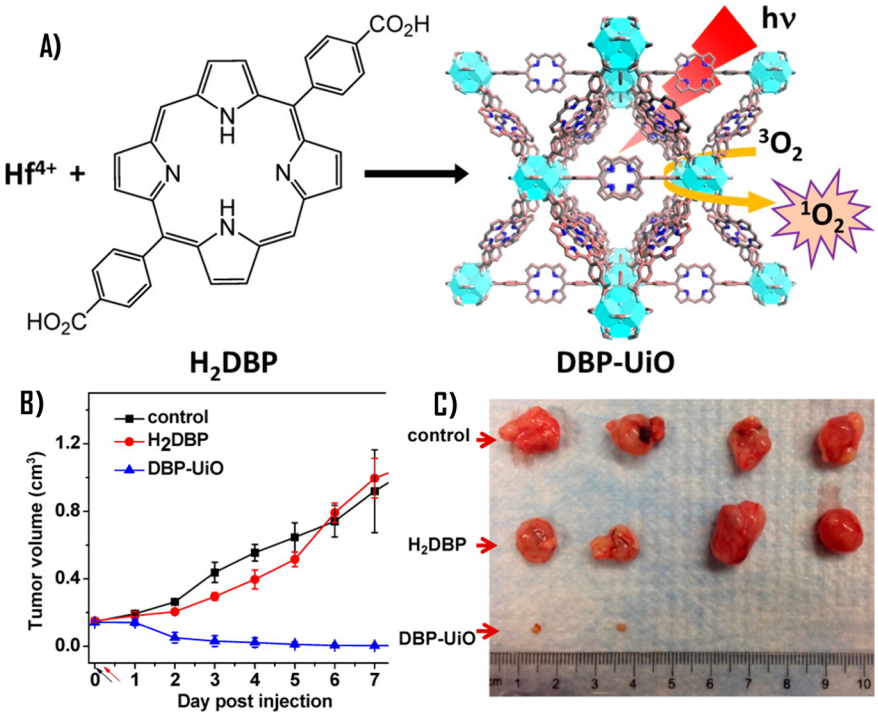

Fig. 9. (A) Schematic synthesis and singlet oxygen generation by Hf-DBP NMOF; (B) Tumor growth inhibition curve after PDT treatment on SQ20B tumor bearing mice. Black and red arrows refer to injection and irradiation time points, respectively (i.e. time 0); (C) Photo of tumors of each group after PDT. Two tumors in the DBP–UiO group were completely eradicated at the end point. Adapted from reference [201] (an open-access article by ACS AuthorChoice. This is an unofficial adaptation of an article that appeared in an ACS publication. ACS has not endorsed the content of this adaptation or the context of its use). (For interpretation of the references to colour in this figure legend, the reader is referred to the web version of this article.)

applications [51]. The advantage of exogenous ligands is the possibility of adding functional substituents. This enables the modification of the ADME (absorption, distribution, metabolism and excretion) process, and influences the drug-carrier interactions, making the delivery process more controllable. The second possibility is the application of endogenous ligands and in the ideal situation, the ligand is metabolized, after MOF degradation. An example of such a linker would be fumaric acid. However, only a small number of MOF structures based on endogenous ligands show appropriate porosity and stability [52]. Some of the best known examples of these materials are two MOFs based on γ-cyclodextrin, namely: [(γ-CD) $(KOH)_2$] and [(γ-CD)$(RbOH)_2$] [128].

Considering MOF toxic properties, the full toxicity evaluation (cytotoxicity and *in vivo* studies) is crucial and determines the applicability of a MOF *in vivo*. This can be a serious obstacle, limiting application of MOF materials in biomedicine. Recent toxicity studies on a series of porous nanoMOF materials (two cell lines were applied, namely: J774 and HeLa) lead to the following conclusions: (i) MOF nanoparticles show low cytotoxicity, and it is comparable to other commercially applied nanosystems, (ii) the results reveal strong correlation between the composition and cytotoxicity (the materials containing Fe(III) were less toxic than those containing Zn(II)) [65]. However, it is well known that the cytotoxicity results do not always correlate with the *in vivo* toxicity. Probably the first reported toxicity study *in vivo* [129] was performed for the Fe(III) carboxylates: MIL-100, MIL-88A, MIL-88B_4CH3. The MOF nanoparticles were administered to Wistar rats, and the toxic properties and ADME process were determined. Biochemical and enzymatic parameters as well as histopathological examination, revealed the absence of acute or subacute toxicity symptoms. The uptake of MOF particles was quick, and the particles were accumulated in liver and spleen where the degradation process occurred. The excess of Fe(III) and a ligand was removed from the body in urine and feces [65]. Subsequent MOF toxicity data were published by Wang et al. [130]. To check the anticancer properties of DOX loaded PEG-RGD-B-CD-SS-MIL-101(Fe) (TTMOF) mice infected with hepatoma H22 were used. It was established that the DOX in TTMOF exhibits lower toxicity than the free DOX. This is caused by the partial elimination of side effects. To summarize, the results of *in vivo* studies suggest that DOX loaded into TTMOF exhibits slightly better chemotherapy efficiency and remarkable limitation of side effects.

Another set of results was reported by Au et al. [131], who performed the *in vivo* MOF toxicity studies on CD-1 mice (the maximum ZOL dose as equal to 1.6 mg/kg). Table 3 presents the toxicity data 4 days after the administration. The results for mice subjected to the treatment are similar to the results observed for the control (PBS was administrated). By contrast, the biodistribution studies revealed, that CaZOL NMOF was accumulating in liver and kidneys however, no remarkable hepatho- and nephrotoxicity was recorded. These results are very promising but still systematic toxicity studies, performed for a wide group of MOF materials are necessary [65]. The lack of adequate results is the probable reason for the delay in MOF clinical applications [75].

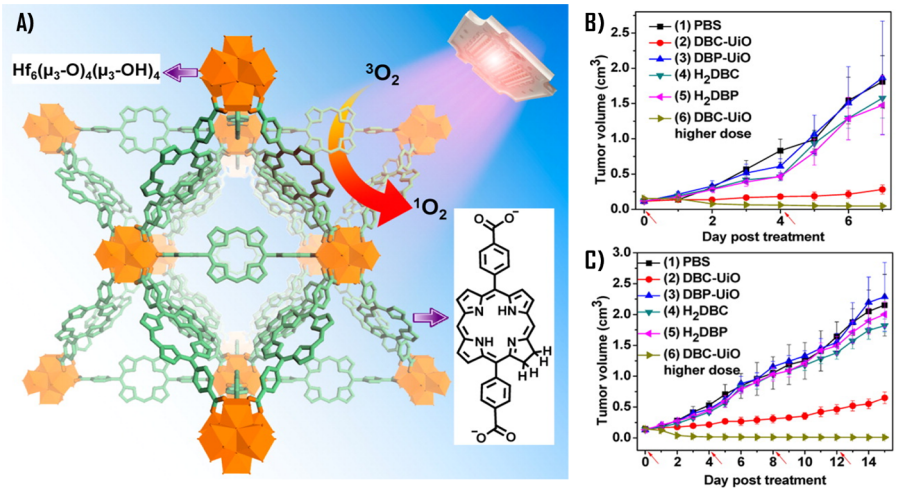

Fig. 10. (A) Schematic Description of Singlet Oxygen Generation by DBC-UiO; Tumor growth inhibition curves after *in vivo* PDT treatment in the (B) CT26 and (C) HT29 models. Red arrows refer to treatment time points (for group 6 in the HT29 model, only one treatment was received). Reprinted with permission from [203]. Copyright 2015 American Chemical Society. (For interpretation of the references to colour in this figure legend, the reader is referred to the web version of this article.)

3.2. Stability in aqueous and biological media environments

The perception and understanding of MOF stability has changed over the last several years. In the earlier stages of MOF development, these materials were seen as rather sensitive, or gentle, not very moisture resistant, and generally not very stable compared to more traditional zeolite materials. This remains true for most of MOFs. However, it is now also apparent that within the vast universe of MOFs, there are some materials that are actually very stable with respect to moisture, heat, pressure and harsh chemical environments [16]. Sheer number of building blocks, available for MOFs, suggests that one can design a MOF material suitable for specific targets and stable at required chemical conditions; however, generally, there is still a lack of systematic procedures for the estimation of a MOF stability in acidic, neutral and basic solutions [16]. It is also important to recognize that different applications may impose very different requirements on the material in terms of stability. Industrial applications typically require materials, such as zeolites, that are very stable thermally, chemically and mechanically. In contrast, the moderate MOF stability can be the advantage in biomedical applications since. Specifically, a biodegradable MOF alleviates the problem of carrier accumulation in the body [73]. In this context, it is also important to understand and control the lifetime of the carrier in the body, as the MOF structure should remain intact and functional until the drug is delivered to the target, and only after this mission is accomplished MOF should be metabolized [53,65] [Fig. 6]. The propensity of a MOF to degrade, in its turn, depends on the type of metal and ligand, diameter of the nanoparticle, physiological conditions, etc. [75]. If a drug is included as a part of MOF framework (as a ligand, for example), the kinetics of delivery is then governed by the kinetics of the degradation process [65]. So far, relatively rapid delivery of drugs has been a serious limitation for this application of MOFs [52].

The stability of many MOF structures upon exposure to water is an important issue [25]. Thus, systematic determination of stability of MOFs in water and in selected body fluids is still crucial for their application in biomedicine. For example, the MIL-100(Fe) and UiO-66 are quite stable in water however, in more complex solutions (such as, for example, in the PBS) invigorated degradation process is observed [53,65,106]. The stability can be controlled to some extent by functionalization and by the judicious selection of MOF constituents. Unfortunately, until to date, little information is available on the stability of MOF materials at the physiological conditions, and a larger number of *in vivo* studies is necessary [53].

3.3. Accurate control of MOF particle size

An important challenge is the control of MOF particle size to avoid agglomeration. This is also crucial for some methods of drug administration [75], for example in the case of injection, the size of particles should not exceed 200 nm. This is why the synthesis of nanoscale drug delivery systems (i.e. NMOFs) has become such an important strategy [53,75]. Moreover, the size of particles determines the biodistribution *in vivo*. The smallest particles (having the size across the range of 20–30 nm) undergo mostly the renal elimination. On the other hand, larger particles (30–300 nm) can be rapidly taken up by the mononuclear phagocytic system cells and are found mainly in the liver, the spleen and the bone marrow [61]. In the case of biological applications bulk MOF materials having sizes of micro and even millimetres often are inappropriate. To obtain nanometer-sized particles, microwave, ultrasound and growth inhibitor (Fe(III) acetate or pyridine [61]) – assisted synthesis is performed [66]. The detailed discussion on this subject can be found in the study published by Cai et al. [51]. It is postulated [75] that NMOFs having smaller size should cause smaller side effects in the body, moreover, small size of MOF particles also leads to more homogeneous solutions formed in the body, hence improving stability. Size control is also important for the consistent and reproducible behaviour of drug delivery platforms, such as patches, capsules,

Table 7
Selected examples on the application of MOFs in drug delivery using ship-in-a-bottle approach.

Select instances on the application of MOFs in drug delivery.
MOFs for drug delivery applications

No.	Metal	Linker	MOF	Drug loaded	Surface modification	Tested cell lines and *in vivo* models	Key findings (information)	Refs
1	Fe(III)	2-NH2-BDC	S-NMOF and F-NMOF	DOX	N/D	- A549 (*in vitro*)	– S-NMOF and F-NMOF were synthesized in different solvents (DMSO – S-MOF and DMF – F-NMOF). – Solvents influenced the magnetic properties of nanoparticles. – DOX was encapsulated, and the drug delivery was slow (15 days). – The NMOF materials were well uptaken by cells *in vitro* and this process was magnetically targeted. – Cell viability assays showed that the blank NMOF materials were non-toxic, even at a high dosage (700 μg/ml). – Drug-encapsulated NMOF particles showed dose dependent toxicity, with the IC50 value of the encapsulated drug (~1.5 μM) much lower than that of the free drug. – The cell uptake and drug-induced toxicity of the F-NMOFs can be further enhanced by magnetic targeting.	[271]
2	Zn(II)	2-MIM	ZIF-8	DOX	N/D	- MCF-7, MDA-MB231, MDA-MB-468 (*in vitro*)	– ZIF18 crystals loaded with the DOX were studied. – The pH responsive release was observed. – The efficacy of new system on breast cancer cell lines was higher than that of free DOX. – The drug was not released at physiological condition (PBS, pH = 7.4). – Controlled release at low pH (5.0–6.5) was observed. – The DOX@ZIF18 system showed a synergistic effect, and its cytotoxicity was higher than for the free DOX (see Fig. 14)	[272]
3	Zn(II)	2-MIM	ZIF-8	CCM	N/D	- HeLa (*in vitro*)- U14 (*in vivo*)	– High drug encapsulation efficiency (88.2%), good chemical stability and fast drug release in tumour acidic microenvironments were recorded. – Cytotoxicity of CCM@NZIF-8 was higher than that of free CCM towards HeLa cells. – The *in vivo* anticancer experiments indicated that CCM@NZIF-8 nanoparticles exhibited much higher antitumour efficacy than free drug. – The CCM@NZIF-8 NPs possessed high DLE (88.2%) and DLC (12.7 wt%), excellent biocompatibility and was stable at physiological conditions. – The *in vitro* and *in vivo* anticancer experiments confirmed that CCM@NZIF-8 NPs display much higher antitumour efficacy than free CCM (see Fig. 15).	[273]
4	Zn(II)	BIX	Zn(BIX)	DOX, SN-38, CPT, DAU	N/D	- HL60 (*in vitro*)	– Ship in the bottle synthesis was performed and the nanoparticles having the diameters across the range of 100–1500 nm were obtained. – Free DOX and DOX from DOX/Zn(BIX) spheres gave similar IC50 values. – DOX/Zn(BIX) spheres had similar cytotoxic effects against HL60.	[48]
5	Fe(II)	BBI	Fe(BBI)	DOX	TEOS, FOL	- HeLa (*in vitro*)	– Novel kind of coordination polymer sphere with superior stability and pH sensitivity was prepared by simple deposition method. – A targeted drug delivery system based on in-situ encapsulation of anticancer drugs into the MOF was constructed. – The release of encapsulated drug from studied system was pH-dependent with a sustained release pattern. – Receptor-mediated endocytosis led to a lower cytotoxicity to normal tissues and greater anticancer efficiency.	[274]

(*continued on next page*)

Table 7 (*continued*)

Select instances on the application of MOFs in drug delivery.
MOFs for drug delivery applications

No.	Metal	Linker	MOF	Drug loaded	Surface modification	Tested cell lines and *in vivo* models	Key findings (information)	Refs
6	Zn(II)	2-MIM	ZIF-8	CPT	CTAB	- MCF-7 (*in vitro*)	– Small molecules were encapsulated into the ZIF-8 frameworks, with high control of loading. – This unique mechanism of incorporation was in situ trapping, and can be generalized to small molecules of varying physicochemical properties. – The cytotoxicity of the ZIF-8 spheres was moderate and comparable to other organic and inorganic drug carriers. – The particles were endocytosed by cells and the pH-triggered disintegration of the ZIF-8 framework in these acidic compartments resulted in drug release. – The versatility of these ZIF-8 nanospheres by introducing the anticancer agent CPT and magnetic nanoparticles was demonstrated. – Several small molecules (including fluorescein and the anticancer drug camptothecin) were encapsulated inside the ZIF-8 framework. – Evaluation of fluorescein-encapsulated ZIF-8 nanospheres in the MCF-7 breast cancer cell line demonstrated cell internalization and minimal cytotoxicity. – The 70 nm particle size facilitated cellular uptake, and the pH-responsive dissociation of the ZIF-8 framework resulted in endosomal release of the small-molecule cargo, thereby rendering the ZIF-8 scaffold an ideal drug delivery vehicle. – Camptothecin encapsulated ZIF-8 particles showed enhanced cell death, indicative of internalization and intracellular release of the drug. – To demonstrate the versatility of this ZIF-8 system, iron oxide nanoparticles were also encapsulated into the ZIF-8 nanospheres, thereby endowing magnetic features to these nanospheres (see Fig. 16).	[81]
7	Fe(III)	BTC	MIL-100	TPT	N/D	- A549, MiaPaCa-2, PANC1 (*in vitro*)	– TPT was encapsulated in a biodegradable NMOF particles. – Inside the pores, monomers aggregated in a “ship in a bottle” fashion, thus filling practically all of the NMOF available free volume and stabilizing their crystalline supramolecular structures. – Highly efficient results were found with the human pancreatic cell line PANC1. – One- and two-photon light irradiation emerged as a highly promising strategy to promote stimuli-dependent drug release from the NMOF particles.	[275]
8	Zn(II)	2-MIM	ZIF-8	CAT, AlPcS4	cancer cell membrane	- HeLa, SCC-7, 4 T1, COS7, RAW (*in vitro*) - HeLa (*in vivo*)	– After intravenous injection, CAT-AlPcS4-ZIF@Mem might exhibit the immune escape and homologous targeting capabilities, which was beneficial for tumour preferential accumulation and uptake. – Subsequently, the high level of intracellular H_2O_2 was catalyzed by CAT to produce O_2 at the hypoxic tumour site, facilitating the formation of cytotoxic O_2 killing cells under the NIR irradiation. – ZIF-8 nanospheres, an O_2 self-sufficient cell-like biomimetic nanoplatform was developed for highly specific tumour imaging and precise PDT *in vivo*. – Owing to the cloaking of CAT- AlPcS4-ZIF with cell membrane, it had a relative long retention time in blood circulation with enhanced immune escape and would preferentially accumulate in tumour tissues after tail vein injection. – The self-sufficiency of O_2 during the PDT process could facilitate the generation of ROS under NIR irradiation regardless of the hypoxia environment of tumour tissues. – The NMOF porous structure provided a pathway for facile diffusion of ROS. This cell-like PDT agent demonstrated highly selective and effective PDT with much reduced side effects to normal tissues.	[276]

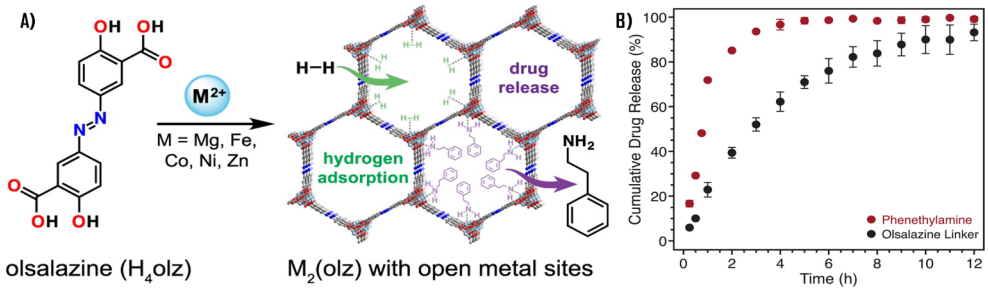

Fig. 11. (A) Schematic synthesis of MOF with the olsalazine as a ligand; (B) Release of phenethylamine and olsalazine from $Mg_2(OLZ)(PEA)_2$ under simulated biological conditions (PBS, pH = 7.4, 37 °C). Error bars represent standard deviation for release from triplicate pellet samples. Reprinted with permission from [239]. Copyright 2016 American Chemical Society.

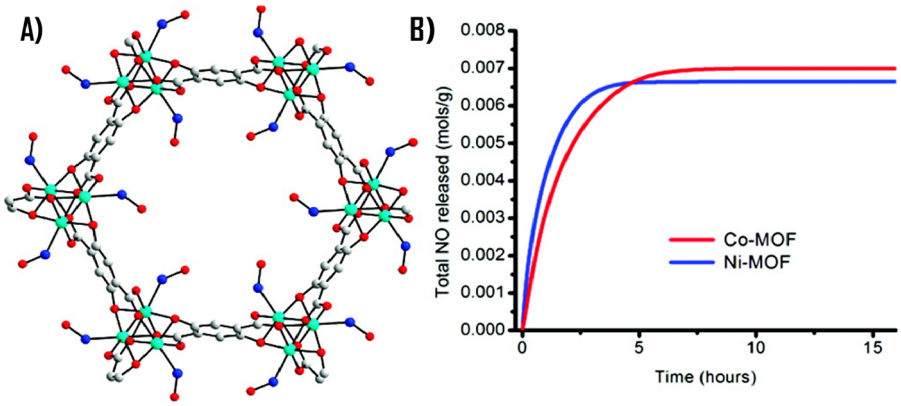

Fig. 12. (A) Binding of NO to the metal site in SBU; (B) The total amounts of NO released by the two materials normalized per gram of activated solid. Reprinted with permission from [254]. Copyright 2008 American Chemical Society.

tablets and pills [53].

4. New concepts to overcome challenges in medical applications of MOFs

Biomedical applications require well-defined physicochemical and biological materials to avoid undefined and undesirable effects. It is important from this point of view to ensure stability, absence of toxicity, high loading of API, and optimal release kinetics as key requirements for any drug delivery system. The same requirements apply to MOFs in these applications, hence here we review the strategies to achieve them.

4.1. Heterogeneous MOF structures

In a typical MOF material the structure is formed by connecting one type of a metal cation and one type of a ligand. However, it is possible to mix different metal cations and different ligands, leading to heterogeneous MOF crystal structures [132]. Early reports showed that two organic building unit can be used, in particular $[Cu_2(BPDC)_2\text{-}(DABCO)]$ (BPDC = biphenyl-4,4′-dicarboxylate, DABCO = 1,4-diazabicyclo[2.2.2]octane) was synthesized for high-pressure CH_4 storage [133]. Moreover, MOFs have been prepared by employing two types of metal ion, forming two different SBU. In 2003 Zhao et al. [134] prepared MOF from a series of lanthanide metals (Ln = Pr, Gd, and Er) with Mn and pyridine-2,6-dicarboxylic acid (H2DIPIC), resulting in $[\{[Ln(DIPIC)_3Mn_{1.5}\text{-}(H_2O)_3]\cdot nH_2O\}_\infty]$ structure. A comprehensive review of this "Heterogeneity within Order" concept was published in 2015 by Furukawa et al. [132].

Nowadays the heterogeneity of MOF materials can be introduced by using several strategies [132]:

- mixing of organic linkers within the MOF framework,
- mixing of the metal-containing secondary building units (SBUs),
- mixing of both the SBUs and organic linkers within the same MOF framework,
- mixing of functional groups on the framework (MTV-MOF),
- MOF materials with random and ordered defects,
- attaching MOF materials to functional surfaces,

Table 8
Selected examples of the application of MOFs in drug delivery by postsynthetic covalent loading.

	Select instances on the application of MOFs in drug delivery. MOFs for drug delivery applications							
No.	Metal	Linker	MOF	Drug loaded	Surface modification	Tested cell lines and *in vivo* models	Key findings (information)	Refs
1	Fe(III)	NH_2-BDC	MIL-101 Fe_3-(μ_3-O)Cl(H_2O)$_2$(BDC)$_3$,	ESCP	Silica, c(RGDfK)	- HT-29 (*in vitro*)	– Studied nanoparticles showed similar IC50 value to free CIS. – The released drug would presumably become active inside cells via reduction to cisplatin by endogenous biomolecules such as glutathione. – To increase the cytotoxicity the silica shell was functionalized with silyl derived c(RGDfK). – Cytotoxicity tests of RGD-targeted nanocarrier gave a cytotoxicity (IC50) 21 μM - similar to that of cisplatin (IC50 = 20 μM) (see Fig. 17).	[80]
2	Zr(IV)	2-azidoterephtalic acid	UiO-66-N_3 ($Zr_6O_4OH_4(C_8H_3O_4 - N_3)_6$)	DNA functionalized with dibenzylcyclooctyne	N/D	- HeLa (*in vitro*)	– A novel class of nucleic acid - MOF nanoparticle conjugates was obtained. – They were stable, showed different cellular transfection capabilities compared to unfunctionalized MOF nanoparticles. – This class of nanostructures can be important in various areas of chemistry, biology, and materials science (see Fig. 18).	[110]
3	Zn(II)	NH_2-BDC	IRMOF-3	NO	N/D	N/D	– The NO-release studies showed that NONOate modification is specific to MOF particles containing the NH_2-BDC ligand, and that large amounts of NO can be liberated. – The results showed that covalent PSM provides an excellent avenue for the production of NO-releasing MOFs.	[277]
4	Zn(II)	NH_2-BDC	UMCM-1_NH_2	NO	N/D	N/D		
5	Zr(IV)	NH_2-BDC	UiO-66-NH_2	5-FU	positive charged quaternary ammonium salt (Q) stalks, (CP5)	- HEK 293 (*in vitro*)	– A benign activation mechanism was developed for targeted drug release systems combining mono-disperse NMOFs with CP5-based stimuli-responsive supra-molecular switches as nanovalves for CNS disease therapy. – Zn(II)-triggered drug release with extremely low premature release suggested an especially advantageous approach for brain disease therapy. – External heating (as a part of treatment therapy) was introduced to regulate the drug release from NMOF nanocarriers.	[278]

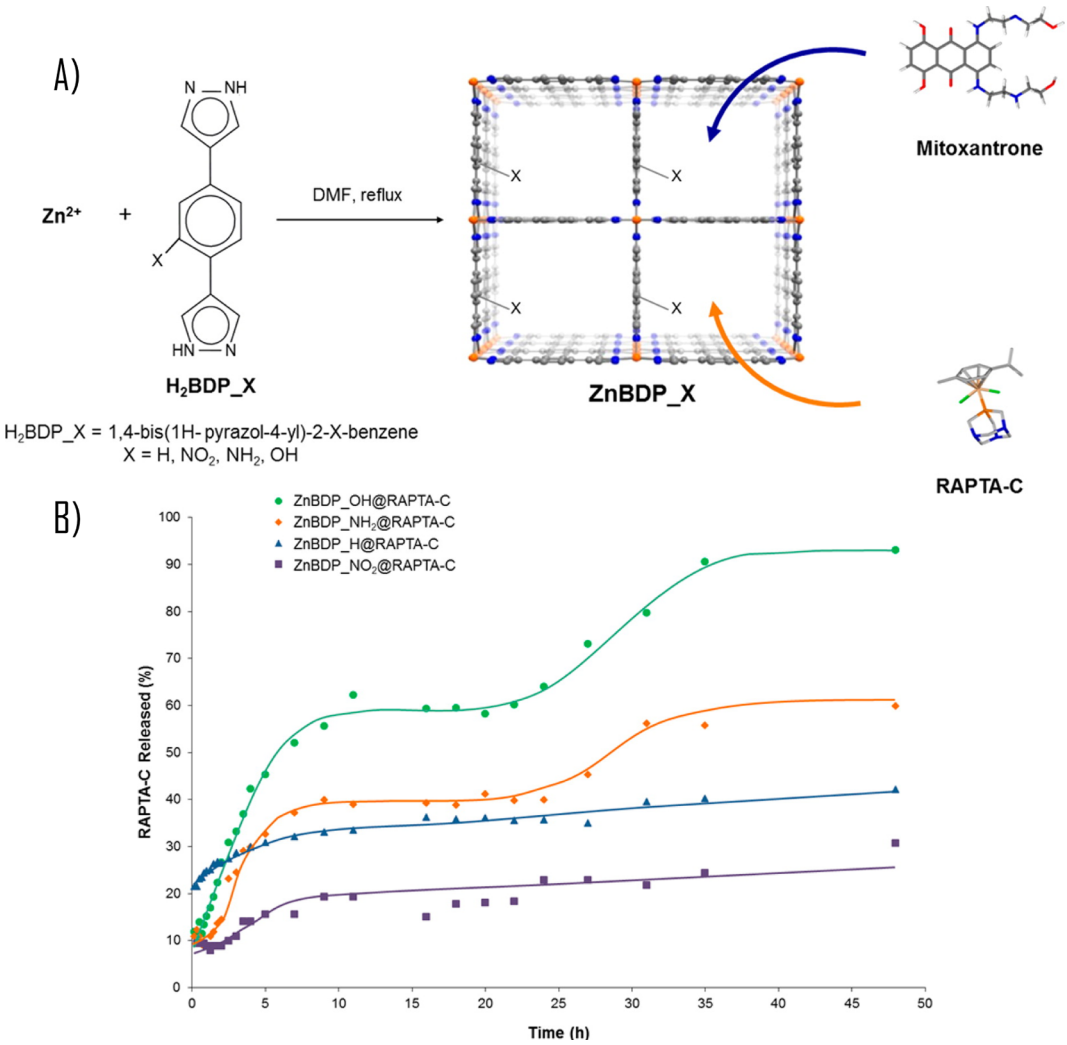

Fig. 13. (A) Schematic representation of the reaction between Zn(II) and the functionalized ligands H2BDP_X to obtain the isoreticular ZnBDP_X series for the encapsulation of nonconventional anticancer drugs RAPTA-C and mitoxantrone. Zn, N, and C atoms are in orange, blue, and gray, respectively. (B) RAPTA-C release from ZnBDP_X@RAPTA-C (X = H, NH_2, NO_2, OH) (10 mg) into SBF (150 mL) at 37 °C (top). Reprinted with permission from [264]. Copyright 2016 American Chemical Society. (For interpretation of the references to colour in this figure legend, the reader is referred to the web version of this article.)

- combining inorganic nanocrystals and MOF nanoparticles,
- MOF materials with heterogeneous pores (macro and mesoporous etc.).

To summarize, strategies to introduce heterogeneity in MOFs lead to new materials and topologies. In this way the toxicity can be decreased, therapeutic molecules or contrast agents can be introduced into MOF structures, and multifunctional systems can be at the same time created, thus expanding possibilities for MOF application in biomedicine.

4.2. Stimuli-responsive structures

Stimulus-responsive solids belong to the relatively new group of MOF materials. Stimulus can be considered as any factor (or a combination of factors) that leads to structural changes in a MOF material. In general, these changes can be reversible or irreversible. However, in the context of stimuli-responsive MOFs, it is the reversible changes that are of a particular interest, where the MOF returns to the original structure once the stimulus is removed or an antagonistic factor is applied. For biomedical applications, important types of stimulus can be of physical (temperature, light, pressure, ultrasounds, magnetic or electric field stimulation, adsorption etc. [135]) or chemical (pH level change, interaction between ions, redox stimulation etc. [136]) nature. If the response of a MOF to stimuli can be precisely controlled or predicted to a high level of accuracy, this can be exploited in a number of applications, leading to a concept of so-called “smart” MOFs.

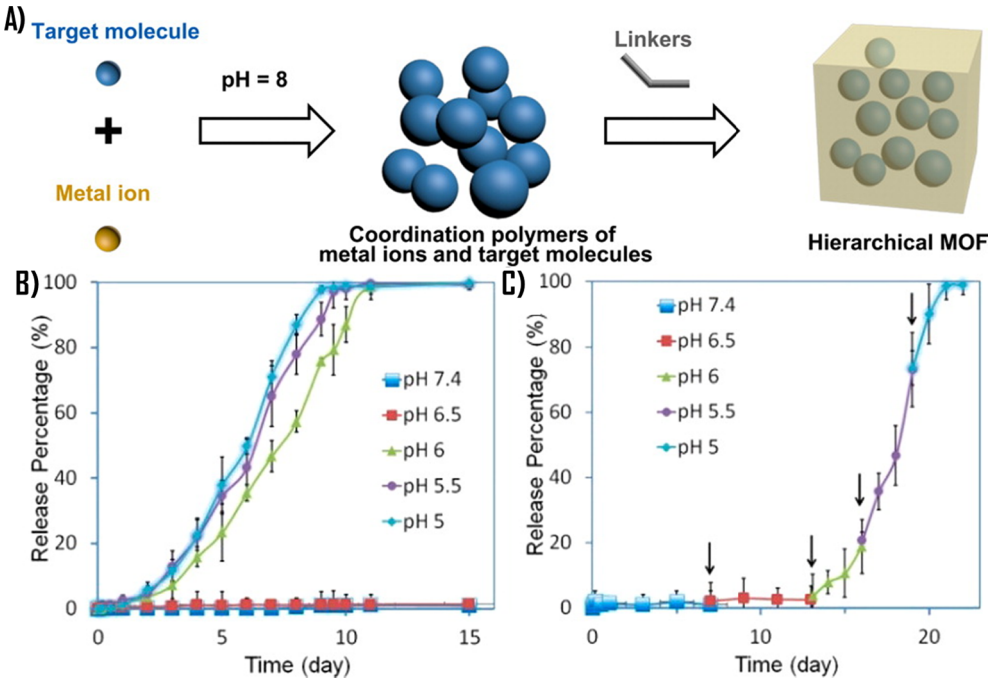

Fig. 14. (A) Schematic pH-induced ship in the bottle synthesis of MOFs with encapsulated target molecules; The pH-responsive release of DOX from DOX@ZIF-8 particles determined by UV–vis spectrophotometry. (B) The typical release system. (C) The stepped release system. Results are presented as means ± standard deviation (SD) (n = 3). Reprinted with permission from [272]. Copyright 2016 American Chemical Society.

For example, stimuli responsive behaviour can be applied for the construction of MOF-based sensors [137]. In particular, among the most investigated areas is pH-sensitive behaviour [138]. Some MOF materials can reveal different pH-dependent behaviour, and it depends on the type of components forming a structure. The design of a smart-MOF can be performed at the stage of synthesis and/or at the stage of functionalization [136]. It is expected that multi-responsive MOF materials (i.e. materials that have various responses to different type of stimuli) will be of greater use, and the new stimuli-responsive MOFs will eventually be discovered [135,136].

The possibility of stimuli-responsive MOF materials synthesis is very important in the biochemical applications because different tissues can show different properties, for example pH levels (in cancer cells pH level is lower than in the healthy ones) temperature, concentration of selected chemical compounds, etc. Also external sources (for example irradiation) can be applied to activate a desired action.

4.3. Additional structural changes

In the case of MOF materials, additional structural changes can be achieved using two approaches; namely catenation and amorphization. Catenation (providing ordered structures) can happen at the synthesis stage. Amorphization, leading to disordered structures, can also take place at the synthesis stage, or later. Catenation is an internal interpenetration of two or more independent structures [139,140] [Fig. 7]. It can lead to the increase in the mechanical stability of a MOF and prevent hydrolysis process, thus improving chemical stability. The stabilization effect can be caused by limiting access of water molecules to the bonds between a node and a ligand by the reduction of the water clusters size existing in a MOF structure, or it may arise from structure – structure interactions [16].

On the other hand, the amorphous MOF materials (AMOF) possess the same components (ligands and nodes) and the type of connections as occurring in the crystal structures however, no periodic arrangement is observed. In other words, one can call them porous or nonporous amorphous coordination polymers [56]. Amorphization can be achieved by a grinding, heating etc. Nonperiodic arrangement of atoms leads to the appearance of humps (wide peaks) on diffractograms [Fig. 8]. Partial structure destruction or a collapse can improve the transport process of ions and a MOF mechanical stability (comparing to crystal counterparts, this is very important for industrial applications) and prolonging drug delivery time. In this way AMOF materials offer a wide range of potential practical applications however, this subgroup of MOF materials has not been explored to any significant extent (till date around 30 structures of AMOF exist) [19].

The application of AMOF for drug delivery was discussed by Orellana-Tavra et al. [73]. The UiO-66 [$Zr_6O_4(OH)_4(BDC)_6$] (S_{BET} = 1200 m^2/g) was applied as a drug delivery system for a model compound, calcein. Amorphization was achieved using grinding of the MOF material with preadsorbed calcein. The delivery time was prolonged from 2 up to 30 days and the delivery process was more stable. Moreover, the rise in calceine thermal stability in the MOF structure was observed (the degradation

Table 9
Selected examples of the application of MOFs in MR imaging.

Select instances on the application of MOFs in MR imaging.
MOFs for biomedical imaging

No.	Metal	Linker	MOF	Active substance	Surface modification	Tested cell lines and *in vivo* models	Key findings (information)	Refs
1	Gd(III)	BDC	$Gd(BDC)1.5(H_2O)_2$	Gd(III)	N/D	N/D	– Obtained NMOF nanopartcles exhibited large R1 and R2 relaxivities. – Doping of luminescent lanthanide ions was demonstrated (Fig. 19).	[122]
2	Gd(III)	1,2,4-BTC	$[Gd(1,2,4\text{-}BTC)\text{-}(H_2O)_3]$ H_2O	Gd(III)	N/D	N/D		
3	Gd(III)	BHC	$[Gd_2(BHC)(H_2O)_6]$	Gd(III)	PVP	N/D	– Two different Gd containing NMOF materials were synthesized using a surfactant-assisted method. – The materials possessed different particle sizes and morphologies. They were obtained using identical building blocks as a result of different metal - ligand coordination modes that are dependent on the pH value of the reaction medium. – The potential use of new materials as contrast agents for magnetic resonance and optical imaging was shown.	[281]
4	Gd(III)	BHC	$[Gd_2(BHC)(H_2O)_8]$ $(H_2O)_2$	Gd(III)	N/D	N/D		
5	Gd(III)	BDC	$Gd(BDC)1.5(H_2O)_2$	Gd(III)	N/D	N/D	– Reverse microemulsions techniques were shown to be useful to synthesize Gd MOF nanoparticles for application in MRI. – By incorporating hydrotropes into the reverse microemulsion nanoparticles the size and shape can be controlled. – MRI studies demonstrated that all of the Gd MOF nanoparticles exhibited higher relaxivities than that of the conventionally employed Magnevist®.	[282]
6	Gd(III)	1,2,4-BTC	$[Gd(1,2,4\text{-}BTC)\text{-}(H_2O)_3]$ H_2O	Gd(III)	N/D	N/D		
7	Gd(III)	1,2,4-BTC	$[Gd(1,2,4\text{-}BTC)\text{-}(H_2O)_3]$ H_2O	Gd(III)	poly[N-(2-hydroxypropyl) methacrylamide], poly(N-isopropylacrylamide), polystyrene, poly(2-(dimethylamino)ethyl acrylate), poly(((poly)ethylene glycol) methyl ether acrylate), and poly(acrylic acid)	N/D	– A method for the surface modification of Gd MOF nanoparticles was developed by reducing the RAFT homopolymers with the addition of hexylamine, providing thiolate polymer end groups for attachment to the GdMOF nanoparticles. – To evaluate the potential of the RAFT homopolymer modified nanoparticles to be employed as clinically viable positive contrast nanoparticle agents, *in vitro* MRI was performed. – Gd MOF nanoparticles, had the ability to tailor and tune the r1 values, thus providing greatly enhanced T1 relaxation values in comparison to the unmodified structure and widely used small molecule contrast agent.	[283]
8	Mn(II)	BDC	$Mn(BDC)(H_2O)_2$	Mn(II)	N/D	N/D	– Mn NMOF materials with controllable morphologies were obtained and demonstrated as potential materials for MR contrast enhancement. – Surface functionalization of the Mn NMOF particles with a cell targeting molecules enhanced their delivery to cancer cells allowing target-specific MR imaging.	[103]
9	Mn(II)	BTC	$Mn_3(BTC)_2(H_2O)_6$	Mn(II)	Silica, rhodamine B, c(RGDfK)	- HT-29 (*in vitro*)		

(*continued on next page*)

Table 9 (*continued*)

Select instances on the application of MOFs in MR imaging.
MOFs for biomedical imaging

No.	Metal	Linker	MOF	Active substance	Surface modification	Tested cell lines and *in vivo* models	Key findings (information)	Refs
10	Fe(III)	Fumaric acid	MIL-88	Fe(III)	PEG	- Wistar female rats (*in vivo*)	– The favourable *in vivo* detection of the iron carboxylate MOF nanoparticles makes them interesting candidates for contrast agents. The first example for iron-based MOF application for this purpose was reported. – Reported MOF nanoparticles possessed not only paramagnetic iron atoms, but also an interconnected porous network filled with metal coordinated and/or free water molecules. – The relaxivity values were related not only to the iron content, but also to the size of the nanoparticles. – The iron-based core is responsible for the favourable relaxivities and imaging properties of the MOF nanoparticles.	[59]
11	Fe(III)	BTC	MIL-100	Fe(III)	PEG	- Wistar female rats (*in vivo*)		
12	Gd(III)	H2CMP	$[Gd(H_2CMP)(H_2O)]$	Gd(III)	N/D	N/D	– The r2 values of $[Gd(H_2CMP)(H_2O)]$ MOF particles were much larger than those measured for xanthan coated Gd_2O_3 nanoparticles.	[284]
13	Gd(III)	FC	FC-Gd	Gd(III)	Silica, RBITC, RGD Peptide	- U87MG, MCF-7 (*in vitro*) - U87MG (*in vivo*)	– The fabrication of nanoparticles for targeted T1 - and T2 -weighted MR imaging of tumours *in vivo* was reported for the first time. – Unique Fc-Gd@SiO_2 (RBITC)-RGD NCPs for dual-mode targeted T1 - and T2 -weighted MR imaging of cancer cells *in vitro* and *in vivo* were obtained. – The formed multifunctional nanoparticles were water dispersible, stable, and exhibited a low cytotoxicity at concentrations up to 200 μ g/mL.	[285]

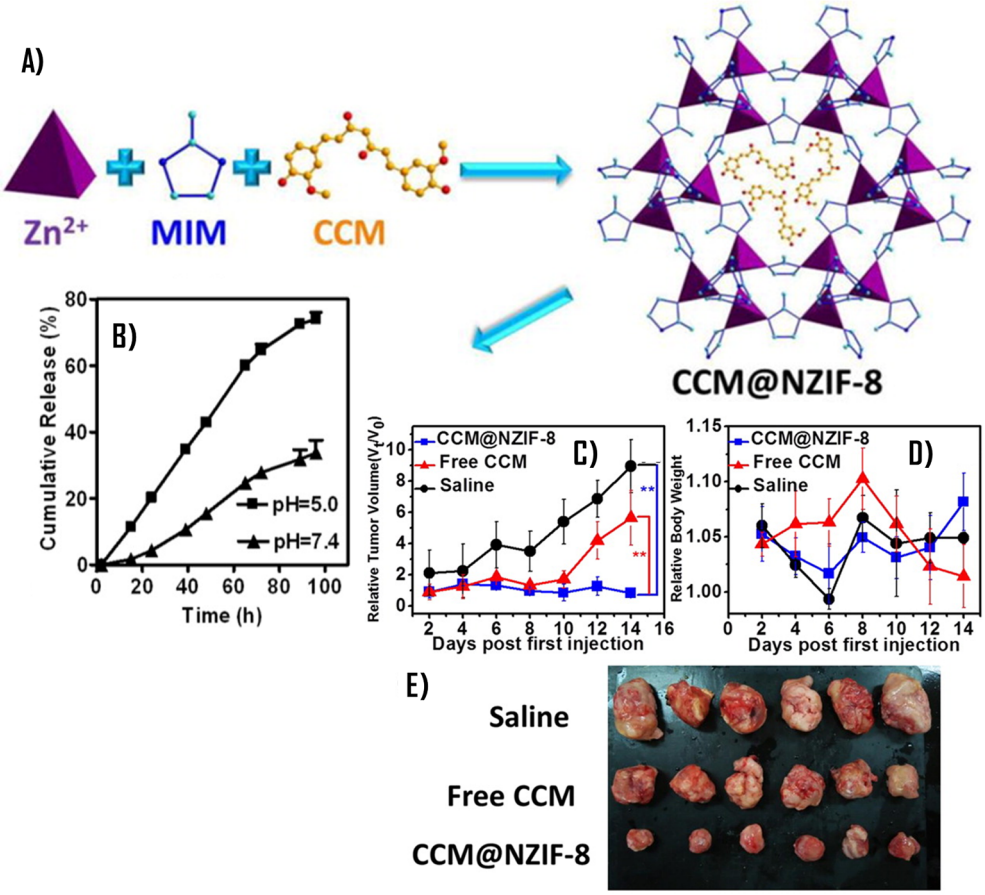

Fig. 15. (A) Schematic illustration of the preparation of CCM@NZIF-8 (B); CCM; (B) release profiles from CCM@NZIF-8 in PBS solution (pH 5.0 and 7.4) containing 1 wt% of Tween-80; *In vivo* antitumor efficacy of CCM@NZIF-8 (of the U14 cancer bearing mice as a function of time (2.5 mg CCM)/(kg body weight), represents by (C) the relative tumor volume and (D) relative body weight; (E) Photo of the excised tumors on the 14th day. Reprinted with permission from [273]. Copyright 2015 American Chemical Society.

temperature for the pure compound is 165 °C and increases up to ca. 400 °C in the MOF structure). The structural variations such as catenation and amorphization make possible to use known MOF materials in new contexts and applications.

4.4. Composites

One effective avenue to prepare a material with a desired combination of properties, is synthesis of a composite material [141], exhibiting properties of the constituent materials. Composites are created by the fusion of at least two chemically different materials (matrix/*continous* phase and dispersed/*discountinuous phase)* in such a way, that in spite of the phase boundary existing between components, their form durable and robust system, with even distribution of the dispersed phase within the matrix. In contrast to alloys, each component retains its chemical, physical and mechanical properties [142]. Also nanocomposites, where at least one component is a nanomaterial, have been discovered. The synthesis of nanocomposites can be performed with the application of the same methods as for the synthesis of conventional composites (for example *in-situ*, solvent method etc. [141]). Currently a number of MOF composites (containing nanoparticles of metals/metal oxides, quantum dots, silicas Si-containing compounds, organic polymers, polyoxometalates (POM), biomolecules, and carbon materials) exists [144,144]. In MOF-containing composites, MOF plays a role of *discountinuous* and/or *continous* phase [145]. Composites based on MOF-5, HKUST-1 and MIL or ZIF types of MOF materials have been reported [143]. For example, to obtain a MOF-carbon composite the in situ *one pot synthesis* method was employed, where MOF precursors and a carbon material were in the same solution [144]. An example of *ex situ* method is mixing of the synthesized MOF with carbon material [144,146]. Also step by step methods are used, for example, layering [144]. For metal/MOF composites techniques, such as solid grinding, encapsulation, impregnation, infiltration, solid grinding, coprecipitation [145] are commonly used.

In a new class of composites, carbon materials with well-known and useful properties in medical applications are combined with MOFs to achieve new add-on functionalities. Usually activated carbons, carbon monoliths and nanotubes are used for this purpose [143]. Consider for example, a composite prepared by the incorporation of a MOF in the pores of activated carbon [143,147]. This

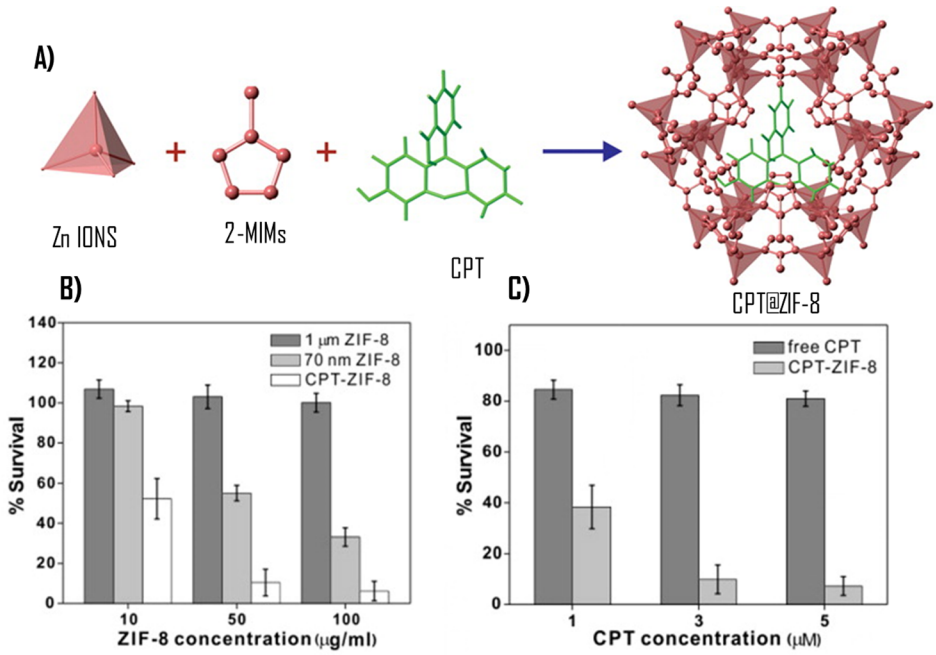

Fig. 16. (A) Encapsulation of small molecules (CPT) into the frameworks during synthesis; (B) Cell viability when incubated with micron-sized ZIF-8 (dark gray), 70 nm ZIF-8 (light gray), and CPT-encapsulated ZIF-8 (white); (C) Cell viability when incubated with free CPT (dark gray), and CPT-encapsulated ZIF-8 (light gray) for 24 h. Reprinted with permission from [81]. Copyright 2014 American Chemical Society.

composite was synthesized at the hydrothermal conditions. Different activated carbon concentrations were added during the synthesis of Ln-succinate (Ln = Tb and Eu). The composite was successfully applied for *aldicarb* (well-known pesticide) adsorption at high pH level in the Wistar rat stomach.

Another nanostructural carbon material, often used for composites with MOF, are carbon nanotubes. CNT dispersed in a MOF (CNT@MOF) is a particularly interesting class of materials since they possess good thermal/mechanical properties and are chemically resistant. Typically in the synthesis procedure, CNTs are dispersed in the organic solvent (e.g. DMF) solution of MOF precursors followed by the actual MOF synthesis. This type of composite was synthesized for the first time by Yang et al. [148] (MWCNT@MOF-5). The presence of multiwalled carbon nanotubes has improved the material's moisture resistance. At the same time the surface area increased from 2160 up to 3550 m^2/g. Hydrogen adsorption also increased from 1.2 up to 1.52% m/m (at T = 77 K, and p = 1 bar) and from 0.3 up to 0.61% m/m (at T = 298 K and p = 95 bar).

As it is shown above, the synthesis of composites is very promising method for modulating properties of materials. One can conclude that the application of MOF-based composites in biomedicine is expected to grow significantly in coming years.

5. MOF materials in anticancer therapy

Cancer is, in general, uncontrollable proliferation of cells, leading to intense recession of normal cells/tissues, and in consequence, to death [149]. Cancer diseases are among one of the major problems of modern medicine and the "World Cancer Report 2014″ [150] indicates that this is also a truly global problem. The weight of the problem, socio-economic costs and the society expectations clearly confirm that the oncology requires a priority place in health research around the world. To address this problem, new breakthroughs are required in both early detection and prevention of cancer (which should be the priority strategy in the longer term perspective) and in treatment of the existing cases.

It is also important to acknowledge that our understanding of cancer etiology and biology has made substantial progress within last several decades and was also paralleled by the development of advanced therapies and diagnostic methods [149,151]. So far, a number of anticancer therapeutics, e.g. small molecular inhibitors [152], antibodies [153], chemotherapeutics [154] and gene therapeutics (drugs based on nucleic acids) [155], have been identified, patented and commercialised. In fact, it is now recognized that further development of anticancer therapies cannot rely on the discovery of new targets and active therapeutic agents alone, and must address drug delivery and bioavailability issues as well [56]. This is where MOFs can lead to important breakthroughs, as has been advocated throughout this review.

The most often described in literature, and also the most promising, is the MOF materials application as prodrugs and/or drug delivery systems. This application is a natural niche for MOF materials due to their specific properties, such as organic–inorganic nature of the structure, high surface areas, different modification techniques, which offer a possibility of highly tailored properties and "targeted therapy", and at the same time, biocompatibility. This explains the significant list of different therapeutic agents (with well documented, or potential anticancer properties) that have been introduced into MOFs as DDS, as summarized in Table 4, in a

Table 10
Select instances on the application of MOFs in CT imaging.

	Select instances on the application of MOFs in CT imaging. MOFs for biomedical imaging							
No.	Metal	Linker	MOF	Active substance	Surface modification	Tested cell lines and *in vivo* models	Key findings (information)	Refs
1	Cu(II)	I_4-BDC-H_2	[Cu(I_4-BDC)(DMF)$_2$]	I_4-BDC-H_2	N/D	N/D	– Novel iodinated coordination polymers as well as corresponding nanoparticle phases with controllable morphologies were synthesized. – Their potential for CT contrast enhancement was demonstrated. – These new nanomaterials were capable of delivering high payloads of iodine.	[286]
2	Cu(II)	I_4-BDC-H_2	[Cu(I_4-BDC)(DEF)$_2$(H_2O)]	I_4-BDC-H_2	N/D	N/D		
3	Cu(II)	I_4-BDC-H_2	[Cu(I_4-BDC)(H_2O)$_2$]·2H_2O	I_4-BDC-H_2	N/D	N/D		
4	Zn(II)	I_4-BDC-H_2	[Zn(I_4-BDC)(DMF)$_{2.5}$]	I_4-BDC-H_2	N/D	N/D		
5	Zn(II)	I_4-BDC-H_2	[Zn(I_4-BDC)(EtOH)$_2$]·2EtOH	I_4-BDC-H_2	N/D	N/D		
6	Zr(IV)	BDC	UiO-66 (Zr)	Zr(IV)	N/D	N/D	– NMOF materials with Zr or Hf metal connecting points were synthesized and evaluated for their potential as CT contrast agents. – Both amorphous Hf-NMOF and crystalline Hf-NMOF of the UiO structure were prepared for the first time. – The materials were coated with silica and then functionalized with PEG to make the particles suitable for *in vivo* CT imaging. – New materials could be used as contrast agents for imaging the spleen or liver.	[287]
7	Hf(IV)	BDC	UiO-66 (Hf)	Hf(IV)	TEOS (silica), PEG	- Mice model (*in vivo*)		
8	Hf(IV)	BDC	Hf-NMOF (Hf)	Hf(IV)	TEOS (silica), PEG	- Mice model (*in vivo*)		

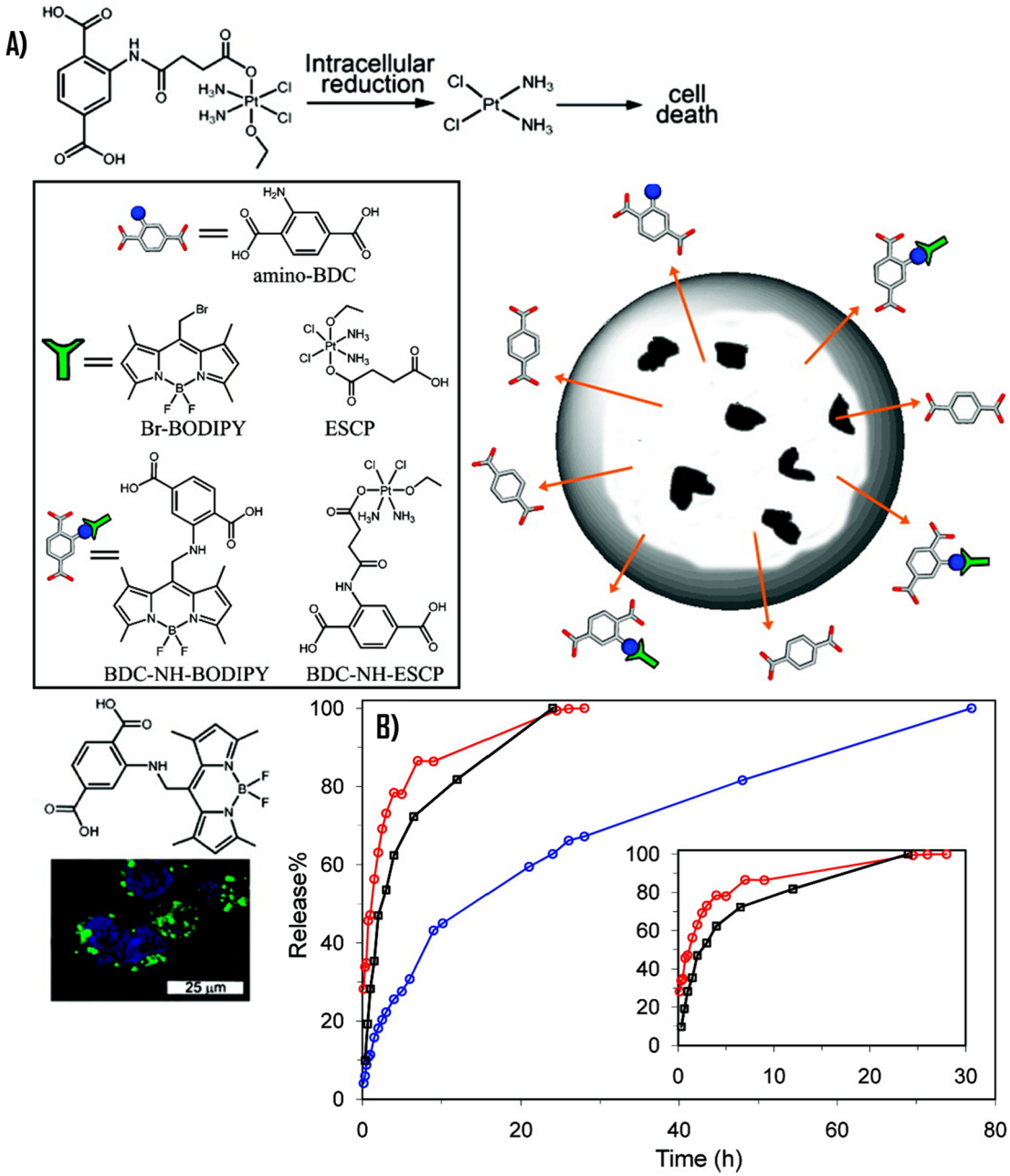

Fig. 17. (A) Schematic representation of release ESCP and BODIPY; (B) Release profile of the BDC-NH-BODIPY dye from the particles of MOF in PBS buffer at 37 °C (black) as determined by fluorescence spectroscopy. Release profiles of the BDC-NH-ESCP from the particles of MOF (red) and MOF@silica (blue) in PBS buffer at 37 °C as determined by ICP-MS. The expanded release profiles for 1b and 1c are shown in the inset. Reprinted with permission from [80]. Copyright 2009 American Chemical Society. (For interpretation of the references to colour in this figure legend, the reader is referred to the web version of this article.)

search of the advanced therapies.

Various properties of MOFs reviewed earlier lead not only to the application in therapy, but also to application in diagnostics. In this field MOF materials are successfully applied in MRI, CT and optical imaging, as was discussed above. It is important and interesting to note that the specific properties of MOF-based materials are often better than those of commercial imaging agents (such as, for example, OmniScan® [54]). The next important logical step is synthesis of multifunctional or smart materials. Here the most interesting materials would be the ones suitable for simultaneous delivery of several drugs (in so called combined therapy) or several diagnostic agents (multimodality) or even for the combined therapy and diagnostics (so called theranostics).

Specifically, in the field of cancer diagnosis and anticancer therapy the MOF materials offer a wide range of possibilities. Cancer

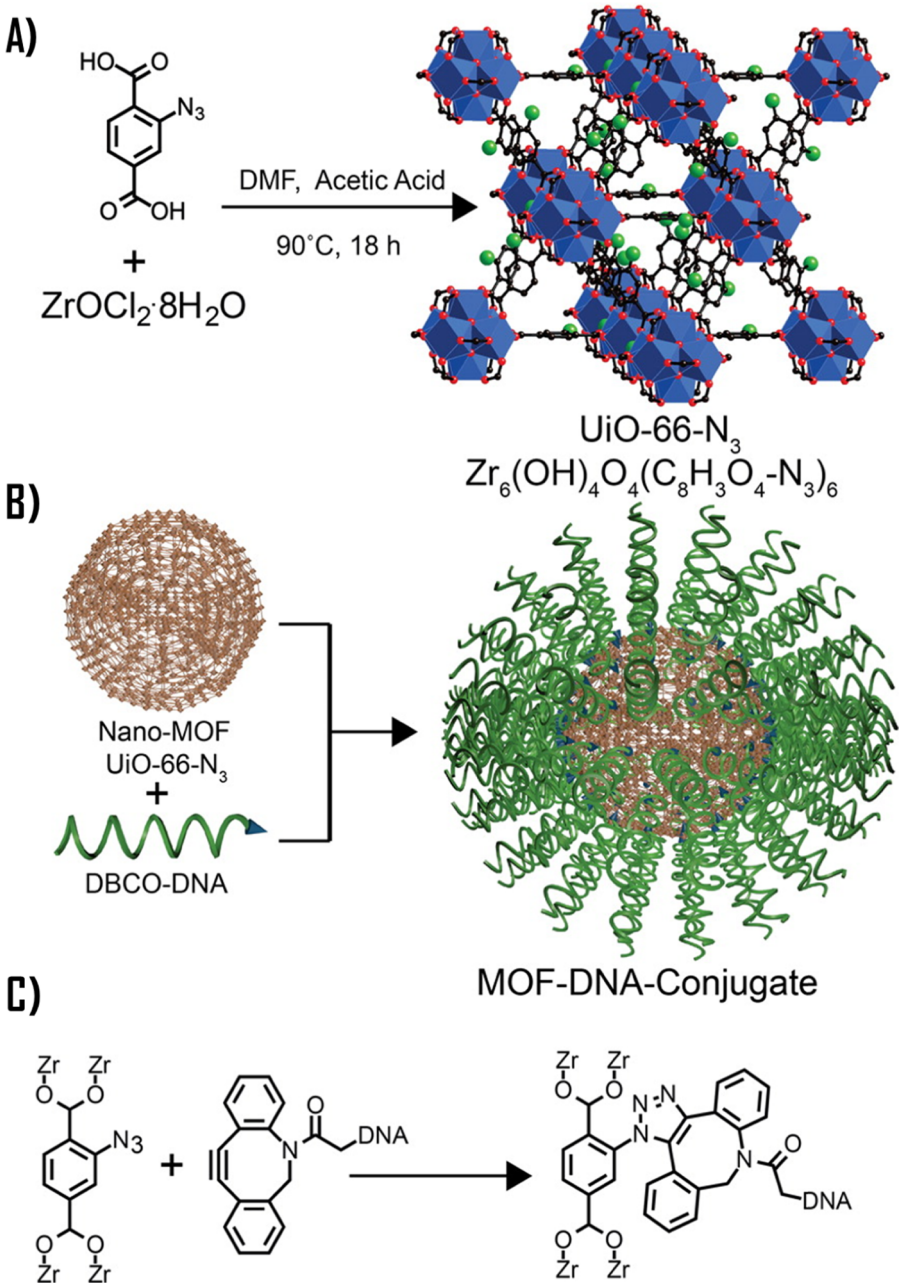

Fig. 18. (A) Synthesis of UiO-66-N3 ($Zr_6O_4OH_4(C_8H_3O_4\text{-}N_3)_6$); (B) DNA functionalization of UiO-66-N_3 nanoparticles, utilizing DNA functionalized with dibenzylcyclooctyne (DBCO); (C) Strain promoted click reaction between a metal–organic framework (MOF) strut and DNA. Zirconium atoms = blue; oxygen atoms = red; carbon atoms = black; azide groups = green. Hydrogen atoms are omitted for clarity. Reprinted with permission from [110]. Copyright 2014 American Chemical Society. (For interpretation of the references to colour in this figure legend, the reader is referred to the web version of this article.)

cells in many cases are characterized by lower pH [222], sometimes higher temperature [223,224], lower concentration of oxygen [225] and higher concentration of H_2O_2 [226], than it is observed in healthy cells. These differences can be exploited in sensing and location of affected tissues, followed by target drug delivery. MOFs can potentially carry out this task since sensing abilities of MOF nanoparticles have been already reported in the context of this application. For example, MOFs have been applied for determination of pH [227], temperature [228], and concentration of different substances (among them oxygen [229]). Moreover, thermometric properties of MOFs make real-time determination of temperature in cells possible, and this is especially important in the case of hyperthermia therapy for cancer treatment. Other functionalized MOF materials have been reported to detect PSA [230] (a biomarker for prostate and breast cancer present in serum), and LPA [231] (biomarker for ovarian cancer) biomarkers. Additionally, the results

Table 11
Selected examples of the application of MOFs in optical imaging.

	Select instances on the application of MOFs in optical imaging. MOFs for biomedical imaging							
No.	Metal	Linker	MOF	Active substance	Surface modification	Tested cell lines and *in vivo* models	Key findings (information)	Refs
1	Tb(III)	BTB	Tb-BTB-1	Tb (III)	N/D	N/D	– A simple one-step approach for the selective synthesis of RE-BTB ICP hollow spheres, especially Tb-BTB was described. – The parameters affecting the fabrication of the hollow spheres were reported, and the mechanism of the process was proposed. – Multicolour emission was initiated in the Eu^{3+}doped Tb-BTB hollow spheres. – Due to porosity and photoluminescence properties, the new materials can find application in different areas like catalysis, chemical sensing, for construction of photonic devices, in bioimaging, drug delivery etc.	[288]
2	Fe(III)	Calcein	Calcein-Fe,	Calcein	Zn-BIX	N/D	– Adsorption of CHG and MTX was studied. – Calcein was introduced into a MOF structure. This drug can be monitored by the confocal microscopy.	[235]
3	Zn(II)	BSB	Zn-BMSB-Zn	BSB	N/D	N/D	– A new class of materials (a metal-metalloligand particles) was presented. – The materials were obtained by a synthesis between metalloligands and precursor solution of metal ions. – The materials were unstable at physiological conditions.	[289]
4	Cu(II)	BSB	Cu-BMSB-Cu	BSB	N/D	N/D		
5	Ni(II)	BSB	Ni-BMSB-Ni	BSB	N/D	N/D		
6	Zn(II)	[Ru-{5,5′-$(CO_2H)_2$–2,2′-BPY}(2,2′-BPY)$_2$]$(PF_6)_2$ = ([L-H_2]$(PF_6)_2$)	[Zn_2L-$(C_2O_4)_2$]·2 DMF·3H_2O	Ru-{5,5′-(CO_2H)2–2,2′-BPY}(2,2′-BPY)$_2$] $(PF_6)_2$ = [L-H_2]$(PF_6)_2$	N/D	N/D	– Phosphorescent MOF with extremely high dye loadings were synthesized. – The Zr-based nanoparticles were stabilized with thin shells of amorphous silica.	[104]
7	Zr(IV)	[Ru-{5,5′-$(CO_2H)_2$–2,2′-BPY}(2,2′-BPY)$_2$]$(PF_6)_2$ ([L-H_2]$(PF_6)_2$)	N/D	Ru-{5,5′-$(CO_2H)_2$–2,2′-BPY}(2,2′-BPY)$_2$] $(PF_6)_2$ ([L-H_2]$(PF_6)_2$)	Silica, PEG, AA	- H460 (*in vitro*)	– Next the structures were coated with PEG and PEG-anisamide. – The anisamide-targeted particles are efficient optical imaging contrast agents and exhibit cancer specificity.	
8	Fe(III)	NH2-BDC	MIL-101(Fe)	1,3,5,7-tetramethyl-4,4-difluoro-8-bromomethyl-4-bora-3*a*,4*a*-diaza-*s*-indacene (Br-BODIPY)	1,3,5,7-tetramethyl-4,4-difluoro-8-bromomethyl-4-bora-3*a*,4*a*-diaza-*s*-indacene (Br-BODIPY), silica	- HT-29 (*in vitro*)	– A new MOF ($Fe_3(\mu_3$-O)Cl$(H_2O)_2(BDC)_3$ (where BDC was functionalized with amino groups) having the structure of MIL-101 was synthesized. – Anticancer drugs and an optical imaging contrast agent were loaded into structure. – The Br-BODIPY loading was across the range of 6–12%. – BODIPY delivery time in 8 mM PBS (T = 37 °C) was equal to 2.5 hrs. – MOF was Si covered and after this the delivery half-time was reduced down to 16 hrs Imaging in cells was reported. – The highest fluorescence signal was observed at 0.38 mg/ml.	[80]

(*continued on next page*)

Table 11 (*continued*)

Select instances on the application of MOFs in optical imaging.
MOFs for biomedical imaging

No.	Metal	Linker	MOF	Active substance	Surface modification	Tested cell lines and *in vivo* models	Key findings (information)	Refs
9	Fe(III)	BTC	MIL-100(Fe)	fluorescein dye	DOPC	- T24 (*in vitro*)	– Novel MOF nanoparticles encapsulated by a lipid membrane were obtained.	[108]
10	Cr(III)	BDC	MIL-101(Cr)	fluorescein dye	DOPC	- T24 (*in vitro*)	– The MOF@lipid system could effectively store dye molecules. – The improvement of colloidal stability of nanoparticles was discussed. – New nanoparticles were absorbed by cancer cells.	
11	Gd(III)	AMP	5′-AMP/Gd^{3+}	carboxyl-QDs605, carboxyl-QDs525, amino-QDs605	N/D	N/D	– Enfolding of quantum dots by coordination networks was studied. – The formation of core–shell nanoparticles with carboxyl-QDs605 cores was generally observed for a wide range of nucleotides and lanthanide ions. – Luminiscence core–shell nanoparticles were obtained.	[290]
12	Gd(III)	AMP	5′-AMP/Gd(III)	Cyanine dye (NK 1881), 5,10,15,20-Tetrakis(4-carboxyphenyl)porphyrin platinum (II) complex, perylene-3,4,9,10-tetracarboxylic acid	N/D	N/D	– Dyes confined in CNPs were conformationally restricted and stable against molecular oxygen – Nanostructures obtained from this polymer were able to encapsulate fluorescent dyes, metal nanoparticles, and proteins. – The confined environment remarkably enhanced the luminescence intensity of the functional dyes, induced circular dichroism, and showed barrier properties against dissolved molecular oxygen.	[291]
13	Gd(III)	AMP	5′-AMP/Gd(III)	Perylene-3,4,9,10-tetracarboxylic acid (dye 4) and other 7 dyes, AuNP	N/D	- HeLa (*in vitro*)- Mice model 4-week-old mice (ddY, male) (*in vivo*)	– Different nucleotide/lanthanide combinations were applied for creation of new nanoparticles. – The following ions were studied: Sc(III), Y(III), La(III), Ce(III), Pr(III), Nd(III), Sm(III), Eu(III), Gd(III), Tb(III), Dy(III), Ho(III), Er(III), Yb(III) and Lu(III). – The system nucleotide/Gd(III) revealed higher contrast compared to the case of Magnevist®. – The fluorescence was observed only from the liver. – Eight different dyes and AuNP were included into MOF structure.	[292]
14	Tb(III)	dAMP	dAMP/Tb(III)	[(dAMP + 1)/Tb(III)]	N/D	n/D	– 3-hydroxypicolinic acid was used to switch on the luminescence of nucleotide/lanthanide nanoparticles. – Sensitized luminescence properties were observed.	[293]

(*continued on next page*)

Table 11 (*continued*)

Select instances on the application of MOFs in optical imaging.
MOFs for biomedical imaging

No.	Metal	Linker	MOF	Active substance	Surface modification	Tested cell lines and *in vivo* models	Key findings (information)	Refs
15 **16**	Tb(III) Tb(III)	dG_2MP dGMP 2′-	dG_2MP/Tb(III) dGMP-Tb(III)	dG_2MP/Tb(III) dGMP-Tb(III)	N/D N/D	N/D N/D	– Nanoparticles showed strong emission bands in the visible region (dG_2MP/Tb(III): 489 nm and 544 nm), dGMP-Tb(III) (489 nm, 544 nm, 586 nm, 621 nm). – Nanofibers were successfully obtained from dimeric dG_2MP upon coordination with lanthanide ions. – Monomeric and dimeric forms of guanine nucleotides gave totally different coordination environments for Tb^{3+} ions and specific supramolecular architectures. – Dimeric dG_2MP adopted a unique pincer-like conformation, and the difference in nucleotide molecular structures was expressed as characteristic hierarchical self-assemblies and luminescent properties. – The controlled hydration of lanthanide ions in supramolecular nanostructures was crucial to develop magnetic resonance contrast agents and we envisage potential applications of these nanofiber systems in such imaging technologies.	[294]
17	Zn(II)	PK	PZn QD	PZn QD	N/D	- A498 (*in vitro*)	– PZn quantum dots were obtained. – They showed good water dispersibility, high photoluminescence, and photostability. – The new material can be applied especially for long-term cell imaging.	[295]
18	Yb(III)	PVDC	nano-Yb-PVDC-3	nano-Yb-PVDC-3	N/D	- HeLa, NIH 3 T3 (*in vitro*)	– The nano-Yb-PVDC-3, emitting in the NIR was obtained. – The material can be applied as a NIR imaging agent in cells.	[296]
19	Hf(IV)	9,10-bis(p-benzoic acid)anthracene	$Hf_6(\mu_3\text{-}O)_4(\mu_3\text{-}OH)_4$(9,10-bis(*p*-benzoic acid) anthracene)$_{12}$	Hf (IV), 9,10-bis(*p*-benzoic acid) anthracene	N/D	N/D	– Hf-MOF and Zr-MOF materials effectively converted X-rays into visible light luminescence. – The materials possessed high BET surface area values (2187 and 2776 m^2/g for the Hf-MOF and Zr-MOF, respectively) offering multifunctional applications. – The high atomic number of Hf(IV) and Zr(IV) ions in the SBUs served as effective X-ray antenna by absorbing X-ray photons and converting them to fast electrons through the photoelectric effect. – The generated electrons scintillated/excited multiple anthracene-based optical emitters in the MOF through inelastic scattering, leading to efficient generation of detectable photons in the visible spectrum (see Fig. 20).	[117]
20	Zr(IV)	9,10-bis(p-benzoic acid)anthracene	$Zr_6(\mu_3\text{-}O)_4(\mu_3\text{-}OH)_4$(9,10-bis(*p*-benzoic acid) anthracene)$_{12}$	Zr (IV), 9,10-bis(*p*-benzoic acid) anthracene	N/D	N/D		

Table 12
Selected examples of the application of MOFs as sensors.

	Select instances on the application of MOFs in sensors. MOFs for drug delivery applications							
No.	Metal	Linker	MOF	Active substance	Surface modification	Tested cell lines and *in vivo* models	Key findings (information)	Refs
1	Al(III), Eu(III)	H2BPY-5,5′-DC	MOF-253	Eu(III) complex with H2BPY-5,5′-DC, Eu(III) complex with TTA	TTA	N/D	– Modified MOF-253 was applied for the construction of ratiometric pH sensor. – No external calibration was necessary for this sensor across the pH range of 5.0–7.2.	[227]
2	Zr(IV)	amino-TPDC	UiO-68-NH_2	FITC	FITC	- H460	– The first example of NMOF materials application for real time intracellular pH sensing in live cells was shown. – FITC conjugated UiO NMOFs was stable, showed fluorescence efficiency, pH responsibility, and efficient cellular uptake. – The first insight into the endocytosis and intracellular trafficking process of NMOFs was reported based on the obtained nanosystem (see Fig. 21).	[297]
3	Cu(II)	BTC	$Cu_3(BTC)_2$	anti-PSA TCNQ –	anti-PSA TCNQ –	N/D	– $Cu_3(BTC)_2$ thin films were obtained on the surfaces of the custom-made gold screen printed electrodes. – This system was used for immunosensing of an important cancer marker. – The new immunosensor was developed (using targeting of specific antibodies – i.e. anti-prostate cancer antigen), and showed good performance for the quantitative analysis of PSA.	[230]
4	Pb(II)	β-cyclodextrin	Pb(II)-β-CD	Ag(I), $K_2S_2O_8$, Pb (II)-β-CD	Anti-PSA, $K_2S_2O_8$	N/D	– The electrochemiluminescence (ECL) immunosensing platform was developed by using Ag@Pb(II)-β-CD as the ECL sensing indicator. – It showed stable ECL behavior, thus some MOF materials can be used to fabricate ECL sensors. – The ECL mechanism of Ag@Pb(II)-β-CD/$K_2S_2O_8$ system was additionally investigated. – developed sensor could be preliminarily applied for the determination of PSA in serum samples.	[298]
5	Tb(III), Eu(III)	H2BPY-6,6′-DC	MZMOF-3, $Eu_{0.6059}Tb_{0.3941}$-ZMOF	Tb(III), Eu(III)	N/D	N/D	– Two lanthanide zeolite-like MOF materials (Ln-ZMOFs) Tb-ZMOF and Eu-ZMOF, were constructed. – By changing the Tb(III)/Eu(III) ratio during synthesis three materials having variable Eu:Tb stoichiometry were obtained. – The suspensions of freshly obtained mixed crystals showed selective detection of lysophosphatidic acid (LPA), a biomarker for ovarian cancer and other gynecologic cancers. – Studied materials showed the potential to act as a self-referencing and self-calibrating fluorescent indicators for LPA. – The energy transfer mechanism was explained.	[231]
6	Hf(IV)	H_2QPDC-NH_2, H_2DBP-Pt	M – UiO	H_2DBP-Pt,	RITC	- CT26 cells (*in vitro*)	– Phosphorescence/fluorescence dual-emissive NMOF (R-UiO) was applied as intracellular oxygen sensor. – The sensor contained O_2-sensitive Pt(II)-porphyrin ligand, and O_2-insensitive Rhodamine-B isothiocyanate ligand as a reference probe. – The material exhibited good crystallinity, stability, and luminescence response to O_2. – The applicability of R-UiO as an intracellular O_2 biosensor was confirmed by *in vitro* study results.	[299]

(*continued on next page*)

Table 12 (*continued*)

No.	Metal	Linker	MOF	Active substance	Surface modification	Tested cell lines and *in vivo* models	Key findings (information)	Refs
	Select instances on the application of MOFs in sensors. MOFs for drug delivery applications							
							– Mtv-MOF (mixed ligand) were studied.	
7	In(III)	BTC	$In_3O(OH)(H_2O)_2[BTC]_2$ MIL- 100(In)	Tb(III), BTC	N/D	N/D	– Tb(III)-based luminescent MOF films were constructed using the method of postfunctionalization of indium MOF films, CPM-5 and MIL-100(In). – The luminescent MOF films revealed fast and reversible detection of oxygen.	[300]
8	Zn(II)	AD, BPDC	Bio-MOF-1, $[Zn_8(ad)_4(BPDC)_6O{\cdot}2Me_2NH_2,8DMF,11H_2O]$	Yb(III),	N/D	N/D	– O_2 detection experiments using Yb(III)@bio-MOF-1 were performed and reported.	[229]
9	Zr(IV)	BDC	UiO-66	carboxyfluorescein (FAM)-PNA21, cyanine 5 (Cy5)-PNA96and 6-carboxy-X-rhodamine (ROX)-PNA125b	carboxyfluorescein (FAM)-PNA21, cyanine 5 (Cy5)-PNA96and 6-carboxy-X-rhodamine (ROX)-PNA125b	- MCF-7 and MDA-MB-231 (*in vitro*)	– In the presence of target miRNA, the dye-labeled PNAs are released from NMOF and hybridize with the target miRNAs, leading to the fluorescence recovery of PNA probes – The applicability of this system for miRNA (cancer biomarker) biosensing was demonstrated – sensitivity of NMOFbased miRNA detection in the present work (10 pM) is much lower than the standard methods such as RT-PCR that are able to detect only a few copies (aM ~ fM) of miRNA – This miRNA sensor not only enables quantitative and highly specific detection of multiplexed miRNAs in living cancer cells, but also allows precisely monitoring the spatiotemporal changes of miRNA expression in situ.	[301]
10	Cu(II)	BTC	MOF-199	N/D	electrospun polystyrene	N/D	– New composite – a nanofibres layer composed of electrospun polystyrene/MOF-199, were applied as new adsorbents (in thin film microextraction (TFME) process) for sensing aldehydes in urine. – At the optimal conditions the detection limit was across the range of 4.2–17.3 nmol/L (for the analysis of six aldehydes – aldehydes have been considered as potential biomarkers of lung cancer [302]). – The TFME-HPLC method with PS/MOF-199 was also applied to the analysis of aldehyde metabolites contained in complex sample matrices (urine) of lung cancer patients and healthy people. – The method possesses advantages of being simple, rapid, cost-effective, sensitive and non-invasive.	[232]
11	Fe(II), Fe(III)	cyanide ion, BDC	$K_3[Fe(CN)_6]{\cdot}3H_2O$,MIL-101(Fe)	3,3′,5,5′-tetramethylbenzidine (TMB), o-phenylenediamine (OPD), and 2,2′-azinobis-(3-ethylbenzthiazoline-6-sulphonate) (AzBTS)	TEOS, APTES (3-aminopropyltriethoxysilane), PEG, FOL	MCF-7 (*in vitro*)	– New composite PB/MIL-101(Fe) was possible to oxidise catalytically 3,3′,5,5′-tetramethylbenzidine (TMB), o-phenylenediamine (OPD), and 2,2′-azinobis-(3-ethylbenzthiazoline-6-sulphonate) (AzBTS) with H2O2 in solution, leading to the observable change in colour of the solution. – PB/MIL-101(Fe) and PB/MIL-101(Fe) functionalized with FOL (small molecules, which could target the folate receptor present on the surface of tumor cells) was tested *in vitro* with MCF-7 cancer cells. In the presence of TMB and H2O2, the absorbance changes can be monitored by the UV–vis spectrophotometry. PB/MIL-101(Fe)-FA expressed much stronger binding to MCF-7 cells than that of PB/MIL-101(Fe) which is observable by absorbance increasing with the number of MCF-7 cells. However both compounds confirmed colorimetric detection of cancer cells.	[303]

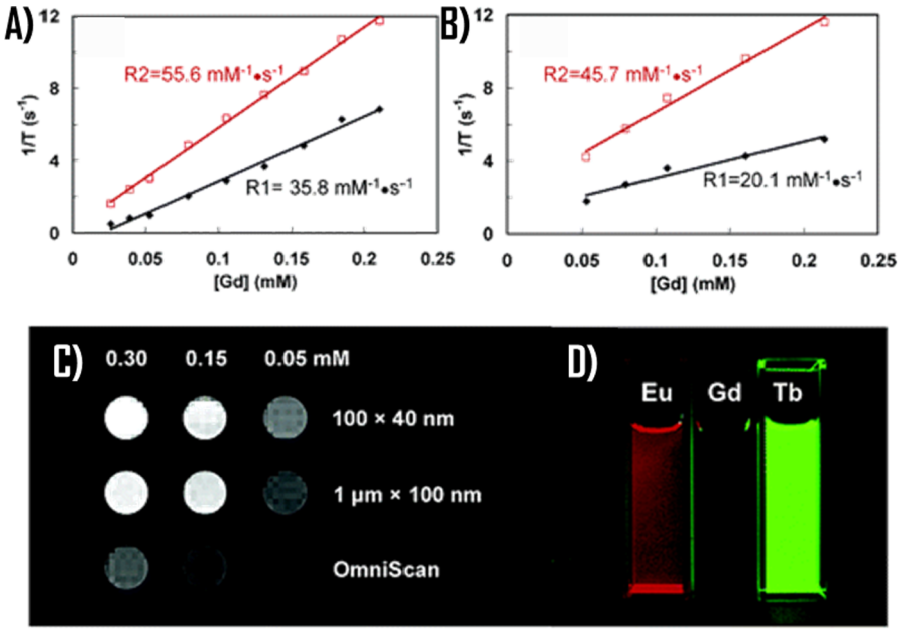

Fig. 19. (A) *R*1 and *R*2 relaxivity curves of $Gd(BDC)_{1.5}(H_2O)_2$ = 1 of ~100 nm in length by ~40 nm in diameter; (B) *R*1 and *R*2 relaxivity curves of MOF of ~1 μm in length by ~100 nm in diameter. In comparison, OmniScan gave an *R*1 of 4.1 $mM^{-1}{\cdot}s^{-1}$ under these conditions; (C) *T*1-weighted MR images of suspensions of (1) in water containing 0.1% xanthan gum. (D) Luminescence images of ethanolic suspensions of 1, 1a (1 doped with 5 mol% of Eu(III)), and 1b (1 doped with 5 mol% of Tb(III)). Reprinted with permission from [122]. Copyright 2006 American Chemical Society.

have been published showing application of MOF materials as sensors detecting human metabolic products (for initial diagnosis [232]). A drug-sensitive MOF can be also applied to check if the drug penetrates the internal part of a cell, or if it is still inside a cell (this can be used to determine the time of a drug internalization).

To summarize, MOF materials can be applied at every stage of anticancer therapy. Below we present the review of the reports confirming this thesis. In order to provide this information in a comprehensive, compact, useful, and easy to navigate form we summarized it as tables presented below.

5.1. Drug delivery

5.1.1. BIOMOF materials

The major conclusions from the studies presented in Table 5 can be formulated as follows:

- BIOMOFs in most cases do not posses high porosity [84,107,235,237,238], however some of the BIOMOFs are porous [101,239–241], especially in the case of ZnCCM it is possible to obtain the BIOMOF with high BET surface area value (3000 m^2/g). The occurrence of porosity is a MOF structure is not a necessary condition for drug delivery application. In this case,drug delivery is achieved by structure degradation.
- Better drug efficacy, comparing to a free drug, is observed for BIOMOFs [131,233,235,236].
- High drug loadings can be achieved because the drug is a part of the MOF structure [131,201,203,233,234,236,239].
- Even drug distribution in the whole structure is observed.
- A time-consuming synthesis and characterization procedures are often necessary.
- A drug can change structure and/or can be destroyed at the synthesis stage. The chemical structure of a drug should be controlled.
- BIOMOFs can be used to enhance chemotherapeutics efficiency via change in pharmacokinetics of the drug toward cancer cells.
- BIOMOF structures can be used as starting point for the synthesis of more advanced materials.
- The BIOMOF strategy can lead to fully biocompatible structures and to incorporate bioactive agents with well documented chemotherapeutic, photodynamic and anticancer properties.

5.1.2. Postsynthetic noncovalent loading systems

The main conclusions from the studies presented in Table 6 can be summarized as follows:

- Highly porous materials are necessary for drug delivery using post-synthetic non-covalent loading [59,130,138,169,192,193,206,242–270].
- Encapsulation efficacy depends on the properties of the active compound. Drug distribution can be heterogeneous influencing the desorption kinetics and making it hardly controllable.

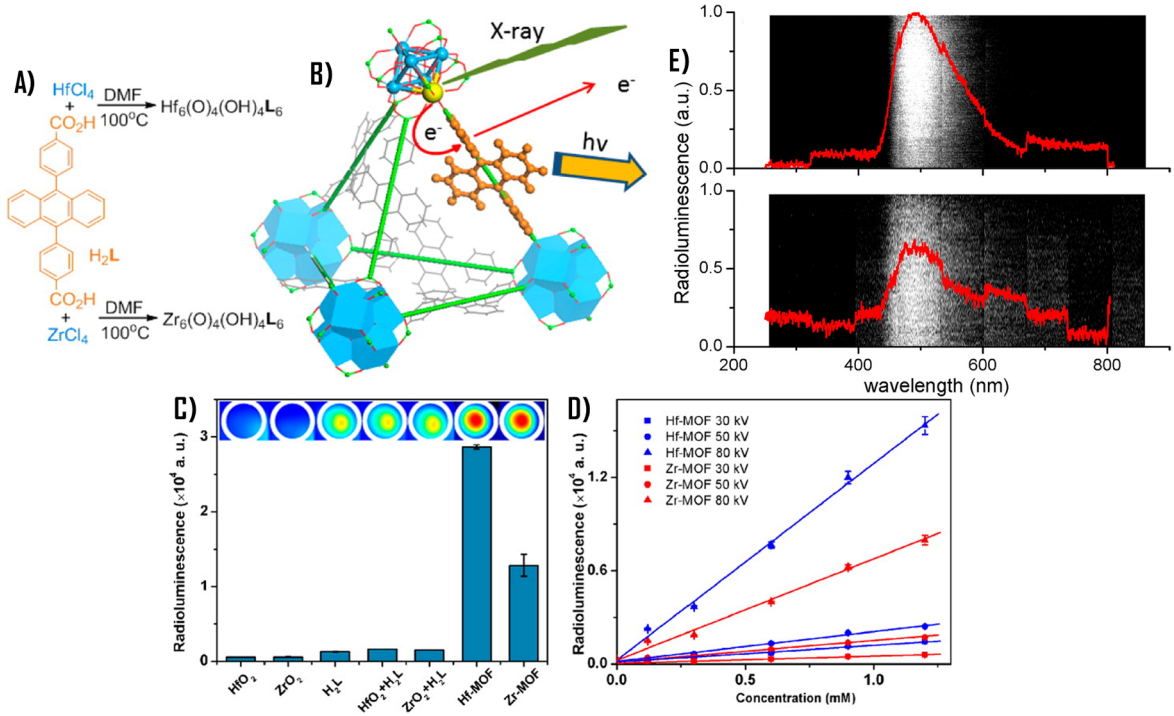

Fig. 20. (A) Synthesis of Hf-MOF and Zr-MOF; (B) Scheme Showing X-ray Induced Generation of Fast Photoelectrons from Heavy Metals Followed by Scintillation of the Anthracene-Based Linkers in the Visible Spectrum; (C) Radioluminescence signals of Hf-MOF, Zr-MOF, and control samples (from left to right): HfO_2 and ZrO_2 colloidal nanoparticles, H_2L alone, H_2L + HfO_2 colloid, H_2L + ZrO_2 colloid, Hf-MOF, and Zr-MOF. The concentrations of H_2L or Hf or Zr in the samples are 1.2 mM. The X-ray dosages are 1 Gy/10 s with effective X-ray energy ~18.9 keV (40 kV tube voltage, 0.08 mA tube current) and detection gain of 200; (D) Radioluminescence signals of Hf-MOF and Zr-MOF with different concentrations and different radiation tube voltages; (E) Optical spectra of (a) Hf-MOF and (b) Zr-MOF induced by X-ray irradiation at a dose of 6 Gy/min. Adapted from reference [117] (an open-access article by ACS AuthorChoice. This is an unofficial adaptation of an article that appeared in an ACS publication. ACS has not endorsed the content of this adaptation or the context of its use).

- Drug loading is usually lower than for the BIOMOF approach [138,243–246,248,250–252,256,259,262,265,267,268], however there are exceptions with very high drug loading efficiency [169,261,263].
- A procedure of drug loading is relatively simple.

5.1.3. *Ship-in-a-bottle systems*

The main conclusions from the studies presented in Table 7 can be summarized as follows:

- In the ship-in-the-bottle approach, drug molecule can be incorporated into the structure even if the pore limiting diameter is smaller than the kinetic diameter of the molecule, which is a typical problem for post-synthetic non-covalent bonding.
- Drug delivery is typically linked with structure disintegration [48,81,271–276].
- Usually, drug loadings are lower than for the noncovalent loading, however ZIF-8 shows good loading efficiency [273].

5.1.4. *Postsynthetic covalent loading systems*

The main conclusions from the studies presented in Table 8 can be summarized as follows:

- Covalent binding of the drug molecules to the host structure [80,110,277,278] – leads to more stable systems as compared with noncovalent loading of the drug. As a result, a prodrug is created, with the drug dissociation and release properties controlled by how it is connected to the host matrix. For the drug release applications, it is important to establish precise conditions for this dissociation.
- Heterogeneous distribution of a drug can occur within the host material, with the drug located usually on the external surface of a solid.
- A drug covalently bonded to a bridge ligand will be delivered after decomposition of the NMOF, which is another factor to take into consideration when designing release strategies.

5.1.5. *Miscellaneous studies*

Here we review few miscellany studies, that could be also seen as related to biomedical applications of MOFs. Torad et al. [279]

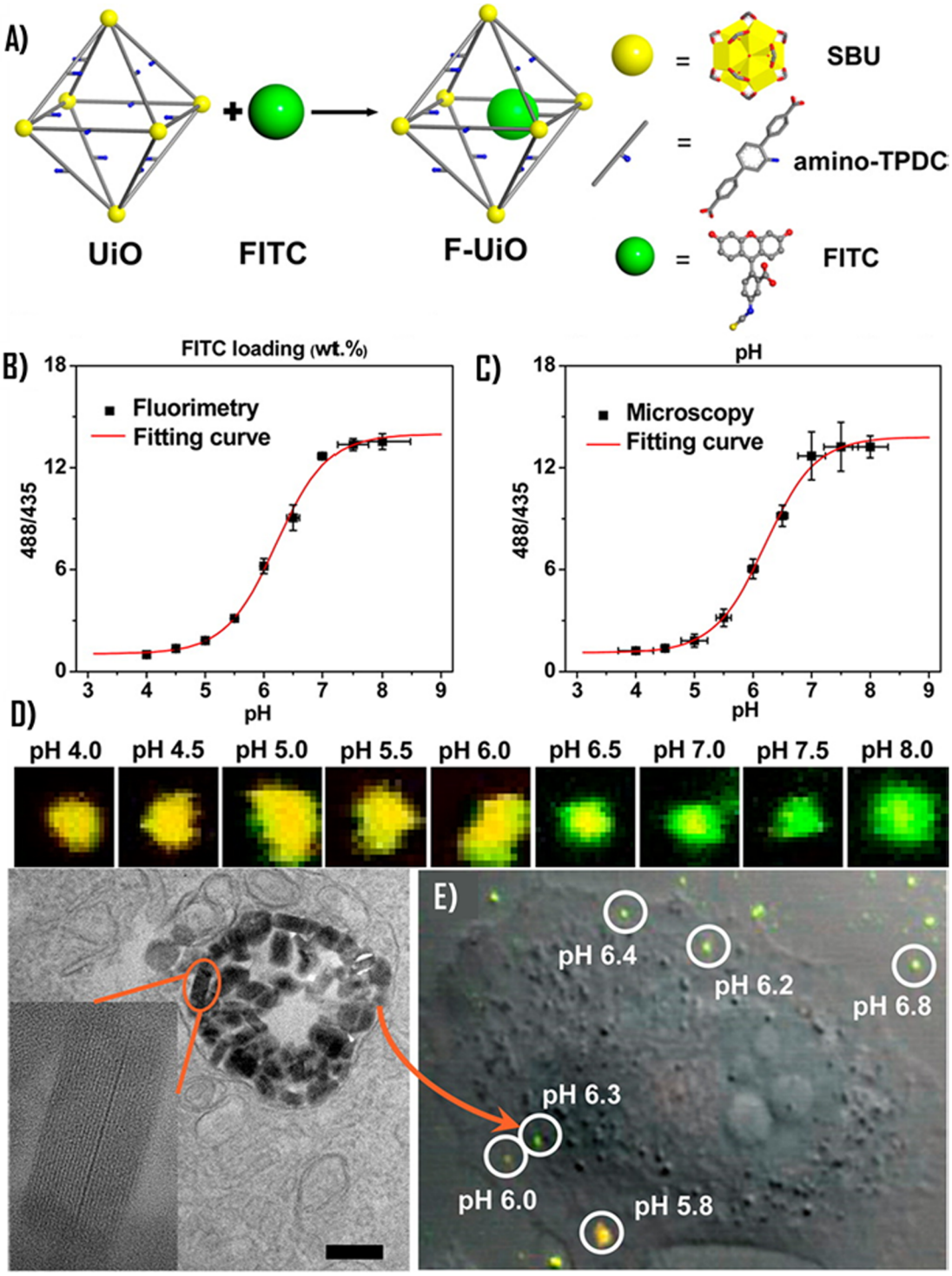

Fig. 21. (A) Schematic presentation of F-UiO synthesis; pH calibration curves of F-UiO acquired by (B) fluorimetry and by (C) CLSM. 488/435 in the Y-axis represents I488/520/I435/520. (D) CLSM images showing the overlay of green (488 nm excitation) and red (435 nm excitation) colors of F-UiO particles in HBSS buffers with different pH values; (E) inter-cellular pH determination using F-UiO. Adapted from reference [297] (an open-access article by ACS AuthorChoice. This is an unofficial adaptation of an article that appeared in an ACS publication. ACS has not endorsed the content of this adaptation or the context of its use). (For interpretation of the references to colour in this figure legend, the reader is referred to the web version of this article.)

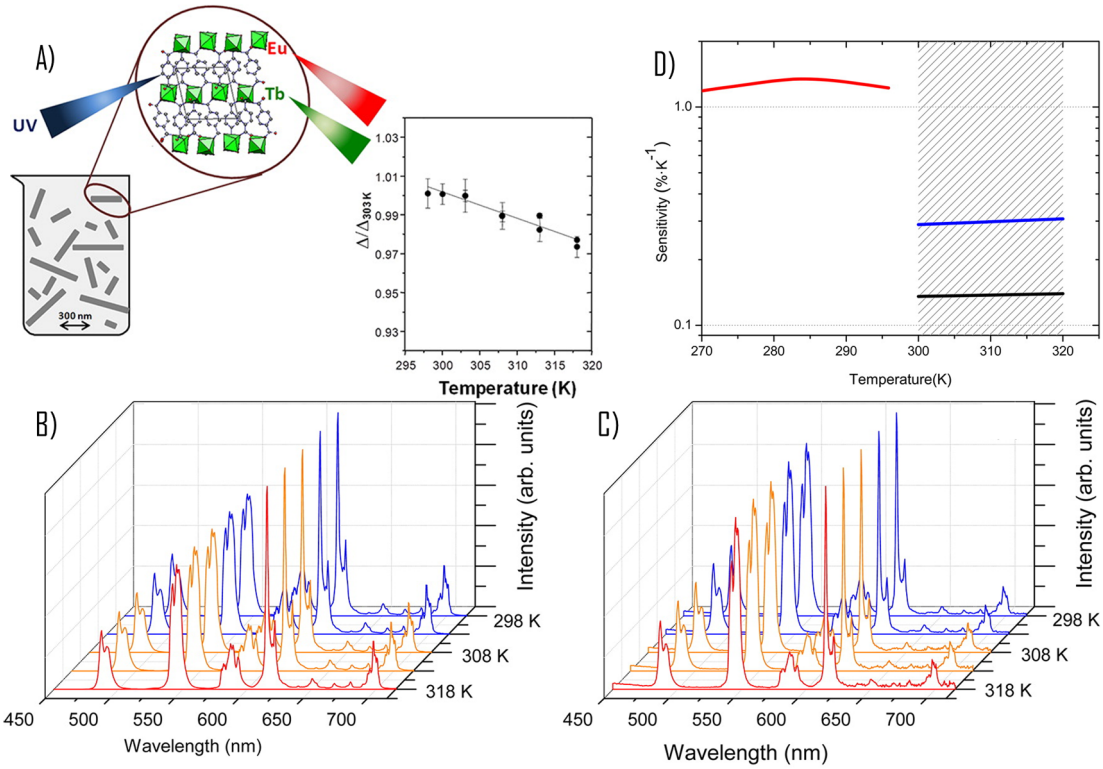

Fig. 22. (A) Schematic description of temperature dependent emission of $Tb_{0.99}Eu_{0.01}(BDC)_{1.5}$-$(H_2O)_2$; Emission spectra of $Tb_{0.99}Eu_{0.01}(BDC)_{1.5}$-$(H_2O)_2$ in (B) the solid state and (C) aqueous suspension (0.36 g·L^{-1}) in the physiologic-temperature range excited at 320 nm; (D) Relative sensitivity of the thermometers $Tb_{0.99}Eu_{0.01}(BDC)_{1.5}$-$(H_2O)_2$, in solid state (black) and aqueous suspension (blue), and $(Eu_{0.0069}Tb_{0.9931})_2(DMBDC)_3(H_2O)_4$·DMF·$H_2O$ (red). The physiological temperature range is shadowed. Reprinted with permission from [305]. Copyright 2013 American Chemical Society. (For interpretation of the references to colour in this figure legend, the reader is referred to the web version of this article.)

synthesized the ZIF-8 NMOF materials (diameter 50 nm) and next, after carbonisation, MOF-NC was obtained. Cisplatin was next encapsulated in the structure of MOF-NC (6.26 mg cisplatin/mg of the MOF-NC). Although MOF-NC nanopaticles themselves were nontoxic for HepG2 cells, the results of cytotoxicity tests for cisplatin-loaded material were not presented.

Reynolds et al. [280] used a MOF for catalytic NO synthesis. The $Cu_3(BTC)_2$ was used in the polyurethane/MOF composite material ($Cu_3(BTC)_2$ and polymer SG-80A) as a catalyst of S-nitrosothiols decomposition. The rates of NO release from each of the substrates with the MOF catalyst varied based on the substitution of the R groups. This work highlights the feasibility of incorporating embedded catalysts into MOF to produce biomedical device, with the capacity to effectively generate NO from bioavailable sources.

The key points from the studies discussed above can be summarized as follows:

- A MOF can be transformed into a new material during (for example) carbonisation process.
- A MOF can be a catalyst during reactions taking place inside cells. Some bioactive products (for example NO) can be created during this kind of reactions.

5.2. Biomedical imaging using MOFs

5.2.1. MR imaging

The key points from the studies presented in Table 9 are as follows:

- Magnetic elements can be introduced into a MOF structure for MR imaging [59,103,122,281–285].
- For some cases achieved relaxivities are higher than for commercially applied contrast agents (for example Magnevist®, OmniScan) [282], which is an encouraging result.

5.2.2. CT imaging

The key points from the studies presented in Table 10 can be summarized as follows:

- The elements with large atomic numbers can be introduced into a MOF structure as nodes [287] or in ligands [286].
- MOF contrast shows slightly higher X-ray attenuation than commercial contrast agent (Iodixanol).

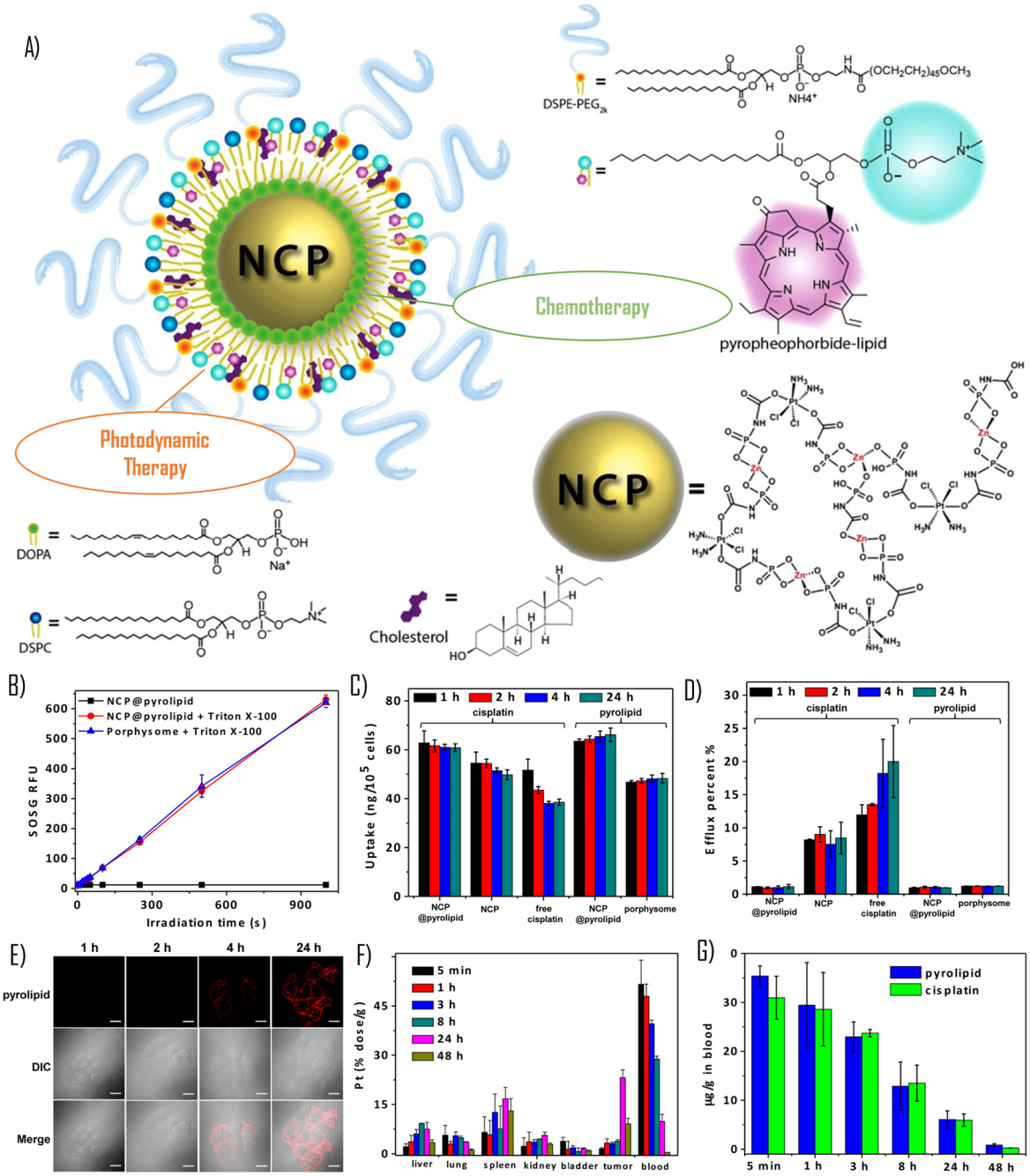

Fig. 23. (A) Schematic description of the composition of self-assembled NCP@pyrolipid core–shell nanoparticle with PEG and pyrolipid in the outer lipid layer; (B) Time-dependent $^1O_2$ generation by NCP@pyrolipid and porphysome in PBS reported by the SOSG fluorescence intensity (670 nm, 120 mW/cm^2) for intact particles *versus* particles with disrupted lipid bilayer. Data expressed as means ± SD (N = 3); (C) Cellular uptake of NCP@pyrolipid, NCP, free cisplatin, and porphysome in SQ20B cells determined by ICP-MS (cisplatin uptake) and fluorimetry (pyrolipid uptake). Data expressed as means ± SD (N = 3); (D) Efflux of cisplatin and pyrolipid of NCP@pyrolipid, NCP, free cisplatin, and porphysome in SQ20B cells. Data expressed as means ± SD (N = 3). (E) CLSM images showing the internalization and intracellular distribution of pyrolipid coated on the NCP in SQ20B cells. Channels are pyrolipid (405 nm laser, red) and DIC. Bar = 20 µm; (F) Tissue distributions of Pt at time points of 5 min, 1, 3, 8, 24, and 48 h after intravenous injection of NCP@pyrolipid; G) Time-dependent pyrolipid and cisplatin concentrations in blood after intravenous injection of NCP@pyrolipid. Reprinted with permission from [209]. Copyright 2015 American Chemical Society. (For interpretation of the references to colour in this figure legend, the reader is referred to the web version of this article.)

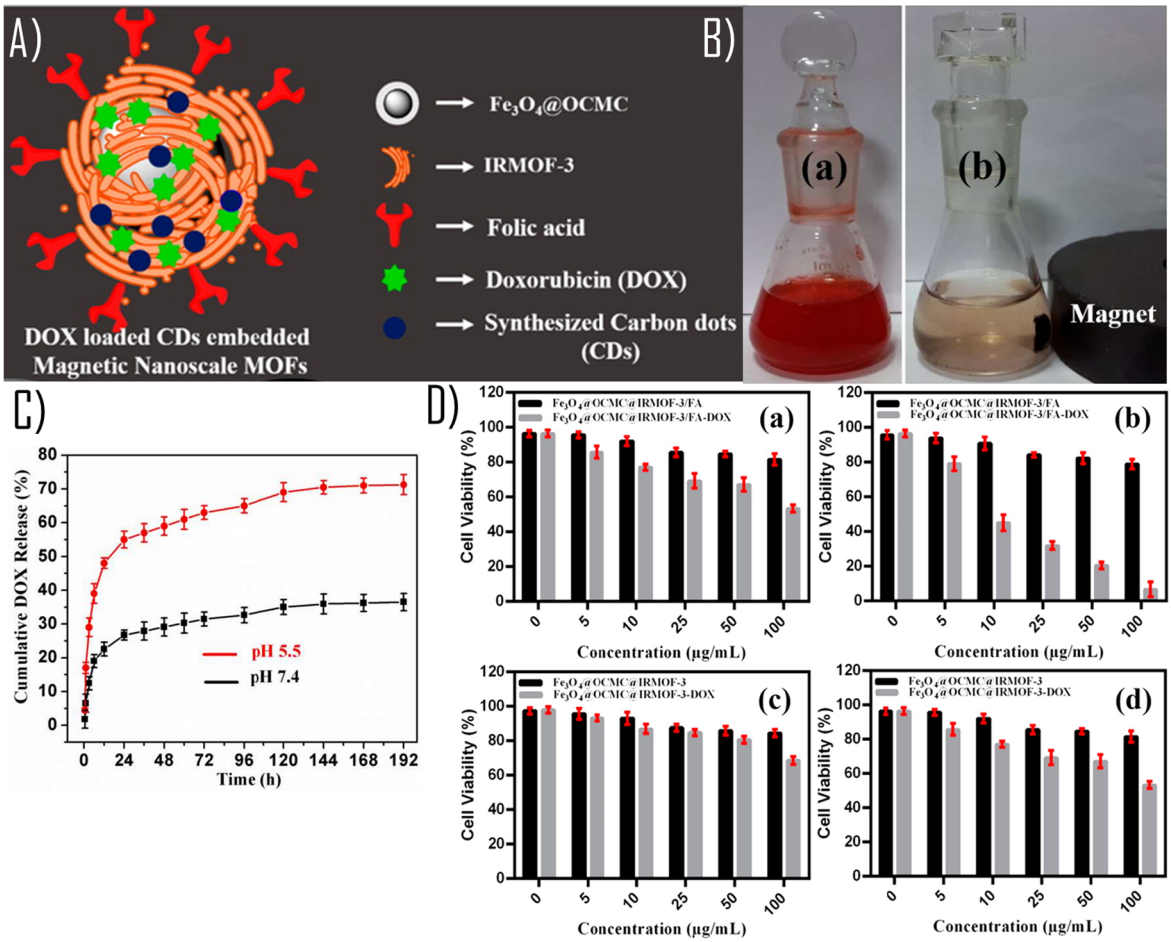

Fig. 24. (A) Schematic description of obtained structure; (B) Camera photo image of (a) Free doxorubicin solution (b) magnetic separation of doxorubicin loaded Fe3O4@OCMC@IRMOF-3/FA nanoparticles from solution; (C) In vitro cumulative DOX-release profiles for DOX-loaded Fe3O4@OCMC@IRMOF-3/FA measured at pH5.5 and 7.4 at 37 °C; (D) Cell viability of folic acid conjugated nanoprobes in (a) L929 and (b) HeLa cell lines and without folic acid conjugated nanoprobes in (c) L929 and (d) HeLa cell lines. Reprinted with permission from [327]. Copyright 2016 American Chemical Society.

- Large amount of a contrast agent can be introduced into a MOF.

5.2.3. Optical imaging

The key points from the studies presented in Table 11 can be summarized as follows:

- Different substances possessing fluorescent properties can be introduced into a MOF (for example: metal nanoparticles [292], metal ions [117,288,293,294], complexes [104,289,291], organic dyes [80,108,235,291,292], quantum dots [290,295]).
- Good optical properties have been confirmed for these structures.

5.3. Biodetectors based on MOFs

5.3.1. Cancer detection

Tha main conclusions from the results presented in Table 12 can be summarized as follows:

- Different substances with sensing properties can be introduced into a MOF structure (for example: metal ions [229,231], complexes [227], dyes [297,299,301]).
- MOF-based sensors can report pH levels [227,297], oxygen concentration [229,299,300], the concentration of cancer biomarkers (PSA, LSA, miRNA) [230,231,298,301], aldehydes in urine [232].
- MOF could catalytically oxidise organic dyes [303].
- MOF-based sensors can possess high sensitivity and selectivity.
- A variety of procedures exists to introduce active compounds into a MOF (incorporation into a structure, postsynthetic loading, covalent and noncovalent bonding, etc).

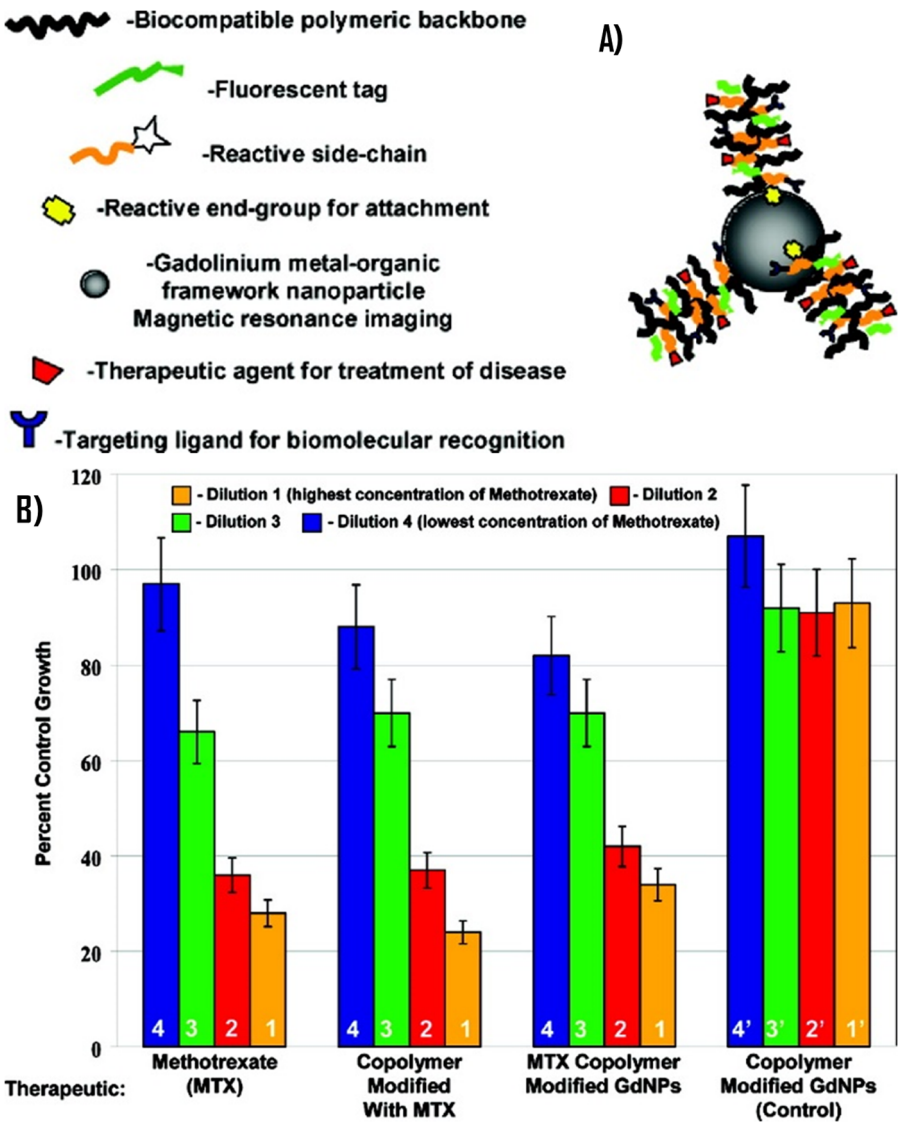

Fig. 25. (A) Polymer-modified Gd metal–organic framework; (B) Cell growth inhibition studies for reagents involved in multifunctional nanoparticle formation, including: Methotrexate (MTX), PNIPAM-*co*-PNAOS-*co*-PFMA tailored with MTX, gadolinium (Gd) metal–organic framework (MOF) nanoparticles modified with PNIPAM-*co*-PNAOS-*co*-PFMA tailored with MTX. Finally, the control, Gd MOF nanoparticles modified with PNIPAM-*co*-PNAOS-*co*-PFMA, without the MTX therapeutic, is shown for comparison. Dilutions (10-fold) of each sample were carried out, with Dilution 1 having the highest concentration of the therapeutic, MTX, and Dilution 4 having the lowest concentration of MTX. The concentration of MTX for each dilution of each therapeutic sample is as follows: Dilution 1 = 1.15 mM, Dilution 2 = 0.115 mM, Dilution 3 = 0.0115 mM, and Dilution 4 = 0.00115 M. Again, there is no MTX in Dilutions 1′, 2′, 3′, and 4′. Reprinted with permission from [127]. Copyright 2009 American Chemical Society.

5.3.2. Nanothermometer

The main conclusions from the studies presented in Table 13 can be summarized as follows:

- In case of many diseases, such as cancer, cellular pathogenesis is characterized by extraordinary heat production. This can be exploited in new diagnostic and imaging technologies, where the intracellular temperature is accurately monitored.
- Nanothermometers can be applied for measuring the temperature inside cells. In hyperthermia therapy, nanomaterials can be also used to heat cancer cells leading to their elimination, while leaving the healthy cells unharmed.
- Small variations in temperature can be determined very precisely using the new generation of MOF-based technologies.
- MOF-based nanothermometers usually contain Tb(III), Eu(III) and Nd(III) [228,304–314].

5.3.3. Biodetecting anticancer drugs

MOFs can be also used to detect active substances used in cancer therapy. This sensing functionality can be used to confirm that

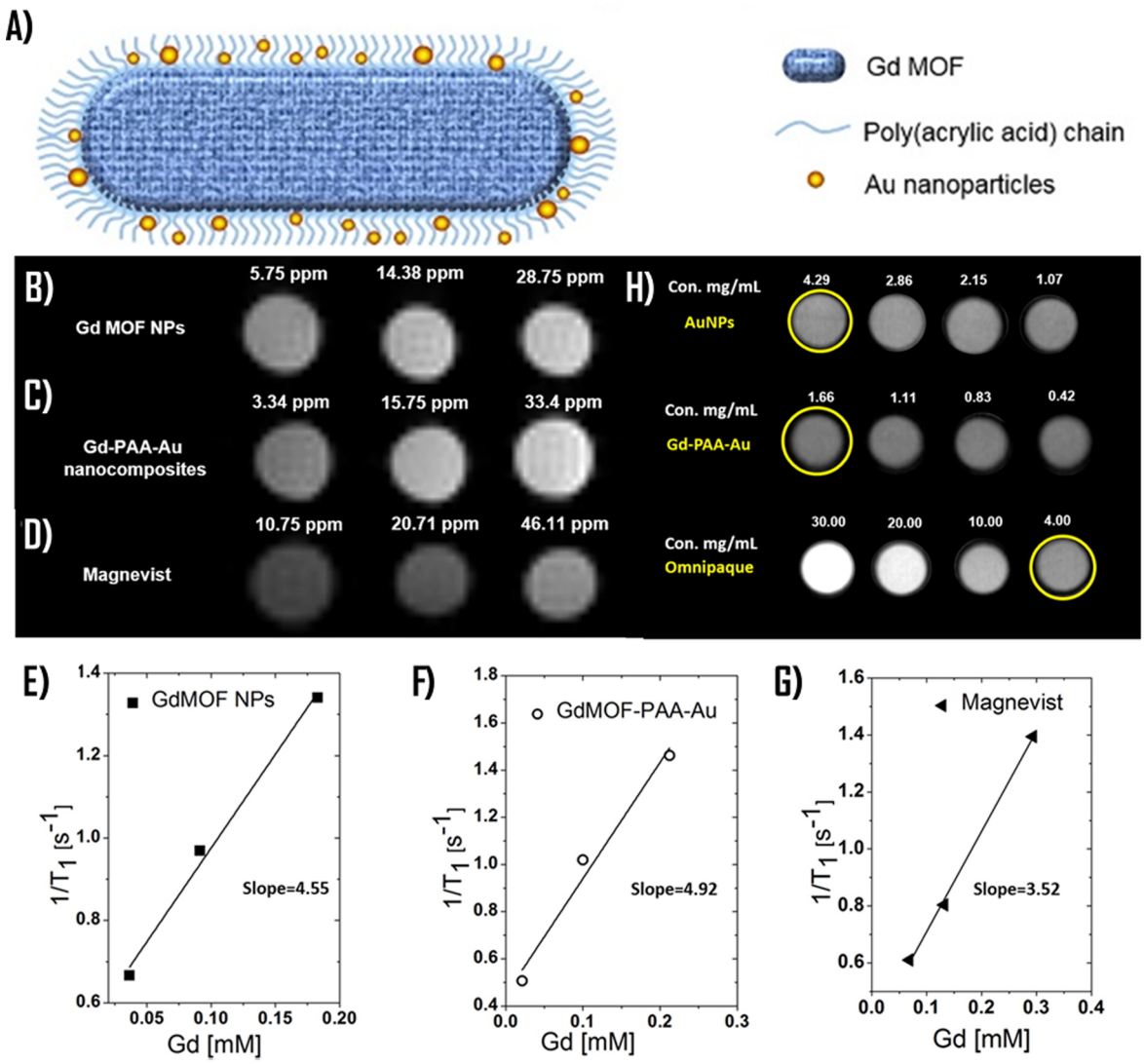

Fig. 26. (A) Schematic of the structures produced; T_1-weighted MRI images of (B) unmodified GdMOF nanoparticles; (C) GdMOF–PAA–Au nanocomposite, and (D) chelate-based Gd contrast agent (Magnevist®) at various Gd concentrations in DIUF water; Relaxation rate ($1/T_1$) of (E) unmodified GdMOF nanoparticles and (F) GdMOF–PAA–Au nanocomposite, and (G) chelate-based Gd contrast agent (Magnevist®) as a function of the Gd concentration; (H) CT images of plain AuNPs, GdMOF–PAA–Au nanocomposite, and the iodine-based contrast agent Omnipaque with different Au or iodine concentrations. All concentrations are listed on top of each sample's CT image. Reprinted with permission from [125]. Copyright 2015 American Chemical Society.

drug entered into the target (i.e. cell) or to ascertain that drug is metabolized (this can be used to determine the time of a drug internalization or to avoid interaction with the next API from the next treatment). Florea et al. [315] obtained a MOF-based GEM sensor. Very good reproducibility of results, high detection limit (of 3 fM) and the application for biological systems were recorded. Wu et al. [316] synthesized a NMOF containing Cu(II)/Eu(III) and tricarboxytriphenyl amine (H_3TCA) for NO detection. Cu-TCA fluorescence drastically increases after NO appearance. The applicability of this system was demonstrated for MCF-7 cancer cells.

These are just few examples of using MOFs in the additional capacity of sensors and monitoring devices, however this field has been also attracting significant attention in recent years and further studies are expected to emerge.

5.4. Multifunctional MOFs

The main conclusions from the studies presented in Table 14 can be summarized as follows:

- MOFs alone or in more complicated systems could work as multidrug delivery system [109,119,200,208,209,220,317,321,324,330,332,335,336], multicontrast/sensor system [121,125,333,334] or theranostics [127,211,318–320,322,323,325–329,331]

Table 13
Selected examples of the application of MOFs in nanothermometers.

Select instances on the application of MOFs in nanothermometers.
MOFs for temperature sensing

No.	Metal	Linker	MOF	Surface modification	Tested cell lines and *in vivo* models	Key findings (information)	Refs
1	Tb(III), Eu(III)	DMBDC	$Eu_{0.0069}Tb_{0.9931}$-DMBDC	N/D	N/D	– Mixed lanthanide MOF idea was used for the construction of the first MOF thermometer based on two emissions at a wide temperature range which was robust, reliable, and instantaneous. – Time-dependent DFT calculation were used to find the efficient organic linker. – The new luminescent MOF thermometer is a significant step forward in cryogenic temperature sensors.	[304]
2	Tb(III), Eu(III)	BDC	$Tb_{0.99}Eu_{0.01}(BDC)1.5(H_2O)_2$	N/D	N/D	– Nanorods of $Tb_{0.99}Eu_{0.01}(BDC)_{1.5}(H_2O)_2$ were studied as ratiometric nanothermometers operating in aqueous suspension in the physiological range of temperatures. – The Tb(III)/Eu(III) co-doped MOF nanoparticles were prepared by a micro-emulsion method. – The photoluminescence properties of materials were studied across the temperature range of 298–318 K. – New materials displayed an excellent performance as ratiometric luminescent nanothermometers showing that NMOF particles can be applied for physiological temperatures measurements (see Fig. 22).	[305]
3	Tb(III), Eu(III)	PDA	$[(Tb_{0.914}Eu_{0.086})_2(PDA)_3(H_2O)]\cdot 2H_2O$	N/D	N/D	– The nanoparticles of $[(Tb_{0.914}Eu_{0.086})_2(PDA)_3(H_2O)]$ were prepared and applied as nanothermometers. – The operating temperature range was across the range of 10–325 K. – Studied system is the most sensitive cryogenic nanothermometer reported so far.	[306]
4	Tb(III)	(H_3TATAB)	$Tb(TATAB)\cdot(DMF)_4(H_2O)(MeOH)_{0.5}$ (TbTATAB)	N/D	N/D	– A Tb-based MOF possessing 1-D channel was synthesized and characterized. – A luminescent dye was encapsulated into the channel. – Luminescence studies showed that this new composite can be applied as a ratiometric, self-calibrated thermometer, working across the temperature range of 100–300 K.	[307]
5	Nd(III), Yb(III)	BTB	$Nd_{0.866}Yb_{0.134}(BTB)(H_2O)(DMF)_3$ ($Nd_{0.866}Yb_{0.134}$BTB)	N/D	- PC12	– The NIR luminescent MOF $Nd_{0.866}Yb_{0.134}$BTB was developed as a self-calibrated thermometer in the physiological range. – High sensitivity and resolution and good biocompatibility prefer this material for biomedical applications.	[308]
6	Nd(III), Yb(III)	H_2BDC-F_4	$(Nd_{0.577}Yb_{0.423})_2(BDCF_4)_3(DMF)(H_2O)\cdot DMF$ ($Nd_{0.577}Yb_{0.423}$BDC-F_4)	N/D	N/D	– A NIR pumped luminescent MOF thermometer $Nd_{0.577}Yb_{0.423}$BDC-F_4, was constructed. – The excellent sensitivity across the physiological temperature range of 293–313 K was proved.	[309]

(*continued on next page*)

Table 13 (*continued*)

Select instances on the application of MOFs in nanothermometers.
MOFs for temperature sensing

No.	Metal	Linker	MOF	Surface modification	Tested cell lines and *in vivo* models	Key findings (information)	Refs
7	In(III)	H2BPY-5,5′-DC	In(OH)(H2BPY-5,5′-DC)			– Radiometric luminescent thermometers were described based on Ln(III) post-functionalized MOF. – New materials possessed enhanced sensitivity and self-referencing output.	[310]
8	Eu(III), Tb(III)	D-H2CAM, H3IMDC	$[Eu_{0.7}Tb_{0.3}(cam)(Himdc)_2(H_2O)_2]_3$	N/D	N/D	- $[Eu_{0.7}Tb_{0.3}(D\text{-}CAM)(HIMDC)_2(H_2O)_2]_3$, was demonstrated as good temperature sensor across the temperature range of 100–450 K. – It was highly stable in a wide pH range, and pH sensing (across the range of 2–11).	[311]
9	Tb(III), Eu(III)	(H_2PIA	$Tb_{0.9}Eu_{0.1}(C_{13}H_7O_4N)(C_{13}H_8O_4N)(H_2O)_{2.5}$, $Tb_{0.9}Eu_{0.1}PIA$	N/D	N/D	– A new mixed La-MOF thermometer $Tb_{0.9}Eu_{0.1}PIA$ with the significantly high. – Sensitivity was synthesized.	[312]
10	Tb(III), Eu(III)	H_2DSTP, OA	$Tb_{0.98}Eu_{0.02}(OA)_{0.5}(DSTP)\cdot 3H_2O$	N/D	N/D	– Two types of highly stable and sensitive thermometers were obtained. – The working temperature was across the range of 77–275 K.	[313]
11	Tb(III), Eu(III)	H_3CPDA	$Tb_{0.957}Eu_{0.043}CPDA$, $Tb_{0.957}Eu_{0.043}(H_2cpda)(Hcpda)(H_2O)\cdot 6(H_2O)$	N/D	N/D	– A lanthanide coordination polymer $Tb_{0.957}Eu_{0.043}cpda$ was obtained. – It was demonstrated working as ratiometric and colorimetric luminescent thermometer across the temperature range of 40–300 K.	[314]
12	Eu(III)	H_4QPTCA	ZJU-88, ZJU-88 ($[Eu_2(QPTCA)(NO_3)_2(DMF)_4]\cdot(CH_3CH_2OH)_3$)	N/D	N/D	– A novel ratiometric thermometer was developed by luminescent perylene dye incorporation into the pores of the Eu MOF ZJU-88. – The new thermometer was highly temperature-sensitive across the physiological temperature range of 293–353 K.	[228]

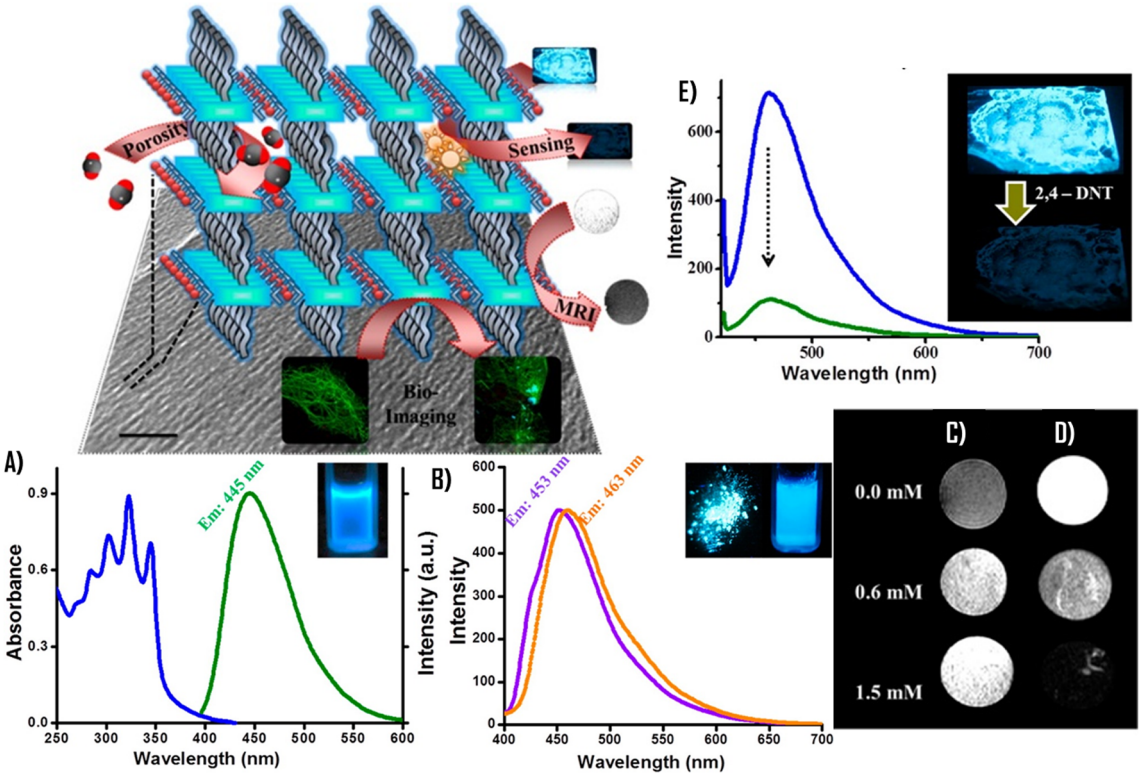

Fig. 27. (A) Absorbance (blue) and fluorescence spectra (green) of NCP-1 dispersed in ethanol; (B) Fluorescence spectra of NCP-1 in PBS buffer (violet) and solid state (orange). Inset: Images of NCP-1 in ethanol (left), solid state and PBS dispersion (right) under UV light, respectively; (C) T1- and (D) T2-weighted MR images of microfuge containing NCP-1 in 0.5% agarose; (E) fluorescence quenching behaviour of NCP-1 coated on quartz (0.7 × 1.2 cm) glass after exposure to 2,4-dinitrotoluene (2,4-DNT) vapours with time. Inset: enlarged images of quartz glass plate coated with NCP-1 under UV light before and after 2,4-DNT exposure. 2,4 DNT. Reprinted with permission from [121]. Copyright 2014 American Chemical Society. (For interpretation of the references to colour in this figure legend, the reader is referred to the web version of this article.)

- Systems with very high control of drug release upon internalization in the cells are now possible.
- More effective systems are obtained if there is a synergic effect between different drugs.
- The detailed mechanisms of drug action can be discovered, if drug release function is also combined with imaging function (that is in theranostics).
- Multifunctional systems containing MOFs usually also contain other building components, such as Fe_2O_3 and Au nanoparticles, folic acid, PVP, PEG, etc. and in this way they have complex structure with better selectivity, more controllable delivery time, better biocompatibility.

6. Computational simulations of MOFs for biomedical applications

Considering the very rapid increase in the number of synthesized MOFs, it is not possible to test every single MOF material for drug storage and drug delivery applications using purely experimental efforts. Highly accurate computational methods that can predict the drug storage and delivery performances of MOFs for particular molecules are very valuable to screen large numbers of MOFs in a time efficient manner and to direct the experimental efforts, time, and resources to these promising candidates. Molecular simulations are specifically useful to study storage and release of drug molecules from the MOFs' pores. These simulations are able to provide molecular-level, fundamental insights into the drug-MOF interactions in addition to offering the knowledge on the adsorption and diffusion mechanisms of drug molecules in MOFs. These insights can be useful to guide the design and development of new MOFs with better performances, such as higher drug loadings and more controllable delivery of guest molecules.

The number of molecular simulation studies of MOFs on the drug storage and delivery is still limited compared to the molecular simulations of the same materials on the gas adsorption and separation. This is due to the difficulty of molecular modeling of larger drug molecules compared to smaller gas molecules within the pores of MOFs. Confinement of large drug molecules in the frameworks requires large computational resources and times. Details of computational methods, density functional theory (DFT) calculations and molecular simulations, used to compute drug storage and delivery in MOFs can be found in the literature [337]. Ibuprofen (IBU) is one of the most studied drug molecules for storage in MOFs. In one of the earliest studies, Babarao and Jiang [338] used molecular simulations to study the microscopic behavior of IBU in two mesoporous MOFs, MIL-101 and UMCM-1, and showed that predicted maximum loading of IBU is in good agreement with the experimental measurements. These MOFs were found to offer approximately

Table 14
Selected case stdies of the application of multifunctional MOFs in drug delivery and imaging.

Select instances on the application of multifunctional MOFs in drug delivery and imaging.
MOFs as multifunctional systems

No.	Metal	Linker	MOF	Drug loaded (active substance)	Surface modification	Tested cell lines and *in vivo* models	Key findings (information)	Refs
1	Zn(II)	GEM-MP, (dach)Pt (BP)	NCP-1	GEM, OXA	DOPA, DSPE/DSPE-PEG	- CT26, AsPc-1, BxPc-3 (*in vitro and in vivo*)	– A NCP-based formulation for the co-delivery of oxaliplatin and GEM as a combination therapy for the treatment of pancreatic cancers was developed. – The synergistic effect of oxaliplatin and GEM against pancreatic cancer cell lines during *in vitro* studies was proved. – A new system showed a long blood circulation half-lifewith and high drug accumulation in tumours, and inhibited tumour growth *in vivo*.	[317]
2	Zn(II)	2-MIM	ZIF-8	c-dots, 5-FU	N/D	- Hela, DU145, L929 (*in vitro)*	– Green fluorescent carbon nanodots@ZIF-8 were obtained. – Tunable fluorescence intensity allowed to use a new system for simultaneous pH-responsive drug delivery and fluorescence imaging of cancer cells.	[318]
3	Zn(II)	DSCP	Zn-CIS	CIS, PYRO	DOPA, DSPC, PYRO/CHOL//DSPC DSPE-PEG2	- SQ20B, JSQ3, HNSCC135, SCC61 (*in vitro*)- Q20B (*in vivo*)	– A novel NCP-based nanotherapeutic material combing two treatments: chemotherapy and PDT, into one single platform was prepared. – Using NCP@pyrolipid high loadings of cisplatin and pyrolipid, the controlled drug release, and the reduction of drugs efflux were achieved. – At the same time enhanced anticancer effect *in vitro* was observed, causing significant tumour regression at very low drug doses (see Fig. 23).	[209]
4	Zn(II)	2-MIM	ZIF-8	POM $H_3PW_{12}O_{40}$, 5-FU	N/D	N/D	– The controlled release of MB and 5-FU from BIT-1 was studied. – For MB 80% of release occurred over 32 days and for 5-FU 93% after 50 hrs. – Reported study shows a *ship in the bootle* synthesis type application.	[319]
5	Mn(II)	ZOL	N/D	ZOL	DOPA, DOPC, CHOL, DSPE-PEG_{2k}, AA	- AsPC-1, MCF-7 (*in vitro*)	– High loadings of ZOL (ca. 63 wt%) and Mn(II) ions (ca. 13 wt%) were observed for Mn-bisphosphonate NCP. – The Mn-bisphosphonate NCP was further modified by coating with lipid and PEG and by the functionalisation with anisamide. – Enhanced cytotoxicity against human breast and pancreatic cancer cells was reported. – New system is also an effective contrast agent thus can be used in theranostics.	[320]
6	Zr(IV)	amino-TPDC	UiO-68-NH_2	CIS, siRNA	N/D	- SKOV-3, A2780, PC-3, MCF-7 H460, A2780/CIS (*in vitro*)	– Cisplatin and siRNA were loaded into UiO by encapsulation, and coordinating to metal sites. – The MOF protected siRNA from degradation and finally led to enhancement in chemotherapeutic efficacy of cispltain.	[109]

(*continued on next page*)

Table 14 (*continued*)

Select instances on the application of multifunctional MOFs in drug delivery and imaging.
MOFs as multifunctional systems

No.	Metal	Linker	MOF	Drug loaded (active substance)	Surface modification	Tested cell lines and *in vivo* models	Key findings (information)	Refs
7	Zn(II)	DSCP	N/D	CIS, siRNA	DOPA, DOTAP, CHOL, DSPE-PEG_{2k}	- ES-2, OVCAR-3, SKOV-3, A2780, A2780/CIS (*in vitro*)- SKOV-3 (*in vivo*)	– MOF nanoparticles were applied for simultaneous deliver of cisplatin and pooled siRNAs to cisplatin-resistant ovarian cancer cells. – NCP-1/siRNAs could mediate effective gene silencing in cisplatin-resistant ovarian cancer cells to overcome MDR and re-sensitize the cells to cisplatin treatment. – The co-delivery of cisplatin and pooled siRNAs drastically enhanced the *in vivo* chemotherapeutic effects in cisplatin-resistant SKOV-3 ovarian cancer mouse model.	[321]
8	Ni(II)	DHTP	CPO-27-Ni, $[M_2(C_8H_2O_6)(H_2O)_2]\cdot(H_2O)_8$	NO, [Ru(p-cymene)Cl_2(PTA)] (RAPTA-C)	N/D	N/D	– The concomitant adsorption of NO and RAPTA-C into the pores of CPO-27-Ni material was studied. – Due to saturating different adsorption sites in the structure, the adsorption capacity for both species was unaffected by the presence of each other. – The release of the trapped Ru-metallodrug into SBF was shown independent on the previous loading of NO into the structure. – The kinetics of NO desorption in the presence of a humid flowing gas was significantly faster for the CPO-27-Ni@RAPTA-C than for the original material.	[119]
9	Gd(III)	GEM-MP	N/D	AuNS, GEM-MP	PEG	– 4 T1 cells (*in vitro and in vivo*)	– A composite containing Au nanoparticle and a MOF shell and gemcitabine-5′-monophosphate (GEM-MP) was obtained. – The gold core provided plasmonic photothermal effect, while the MOF shell provided drug delivery and MR imaging.	[211]
10	Hf(III)	TCPP	Hf-TCPP	TCPP, HF	PEG	– 4 T1, HeLa, NIH3T3 (*in vitro*) – 4 T1 (*in vivo*)	– A simple solvothermal method of synthesis based on Hf and a porphyrin derivative, TCPP was reported. – After PEGylation, NMOF-PEG nanoparticles were stable in physiological solutions. – Small *in vitro* cytotoxicity, long blood circulation time, and efficient tumour homing were recorded for nanoparticles. – Anticancer therapeutic efficacy *in vivo* was enhanced by the combined RT and PDT based on such Hf-TCPP NMOF-PEG.	[200]
11	Zn(II)	NH_2-BDC	IRMOF-3	Fe_2O_3, PTX	FOL	- HeLa , NIH3T3 (*in vitro*)	– Folic acid targeted magnetic nanoscale MOF labeled with florescent molecule RITC was synthesized and loaded with Paclitaxel. – The Fe_3O_4@IRMOF-3/FA nanoparticles showed very good internalization into HeLa cells. – Paclitaxel loaded Fe_3O_4@IRMOF-3/FA nanoparticles achieved excellent effectiveness for targeting and killing the cancer cells.	[322]

(*continued on next page*)

Table 14 (*continued*)

Select instances on the application of multifunctional MOFs in drug delivery and imaging.
MOFs as multifunctional systems

No.	Metal	Linker	MOF	Drug loaded (active substance)	Surface modification	Tested cell lines and *in vivo* models	Key findings (information)	Refs
							– Simultaneously Fe_3O_4 nanoparticles were used as MRI contrasting agents. They can be also used for magnetic guided drug delivery.	
12	Zn(II)	2-MIM	ZIF-8	iron oxide nanoparticles (Fe_3O_4NPs), AuNC, DOX	N/D	- HepG-2 (*in vitro*)- Balb/c H-22 (*in vivo*)	– Multifunctional Fe_3O_4@polyacrylic acid/gold nanoclusters/zeolitic imidazolate framework-8 NPs (Fe_3O_4@PAA/AuNCs/ZIF-8 NPs) were used as theranostic agents. – Tri-modal (MR, CT and fluorescence) imaging was used. – Dual pH-responsive controlled drug release and nontoxicity were reported.	[323]
13 **14**	Zr(IV) Zr(IV)	BDC NH2-BDC	UiO-66 UiO-66-NH2	CIS, NO CIS, NO	N/D	- A549, The Alamar Blue cell (*in vitro*)	– UiO-66 i UiO-66-NH_2 based MOF nanoparticles were synthesized. – The loading with cisplatin was performed using two approaches: encapsulation and conjugation. – UiO66-NH_2 conjugation allowed higher loading than encapsulation however, led to greater *in vitro* cytotoxicity. – The amount of released drug (CIS,NO) from UiO-66 was larger than for UiO-66-NH_2. – The cisplatin loaded MOFs were successfully loaded with NO, and NO release was not affected by the conjugation of the prodrug to UiO-66-NH_2.	[324]
15	Tb(III)	DSCP	N/D	CIS	PVP, silica, LS301	N/D	– A new cisplatin based MOF containing Tb was synthesised. – The material was PVP and silica contained, and LS301 was attached. – In this way a new theransotic agent was obtained.	[325]
16	Zn(II)	BTC	Zn(BTC)	TMPyP	GPTS,Cy3-labelled, H_2N-PEG-(FOL)	- HeLa (*in vitro*)	– Porphyrin and dye-labelled peptide were encapsulated in a MOF. – The singlet oxygen quantum yield of porphyrin was increased by 6.2 times. – The new MOF was biocompatible. – High phototoxicity for therapy against cancer cells was proved.	[326]
17	Zn(II)	NH2-BDC	IRMOF-3	Fe_3O_4, Doxorubicin, carbon dots	FOL, carbon dots	- HeLa, L929 (*in vitro*)	– The composite Fe_3O_4@OCMC@IRMOF-3/FOL was synthesized (see Fig. 24).. – DOX (96 wt%) was adsorbed and carbon quantum dots were attached. – The pH responsible delivery was observed. The process was faster at pH = 5.5 than at pH = 7.4. – NMOF materials were very stable in biological solution (1 month at pH = 7.4).	[327]

(*continued on next page*)

Table 14 (*continued*)

Select instances on the application of multifunctional MOFs in drug delivery and imaging.
MOFs as multifunctional systems

No.	Metal	Linker	MOF	Drug loaded (active substance)	Surface modification	Tested cell lines and *in vivo* models	Key findings (information)	Refs
							– Carbon dots encapsulated magnetic NMOF materials for the optical bio-imaging were reported for the first time.	
18	Zr(IV)	BDC	UiO-66	Fe_3O_4, Doxorubicin	N/D	- HeLa, 3 T3 (*in vitro*)- HeLa (*in vivo*)	– A novel Fe_3O_4@UiO-66 theranostic agent was synthesized by in situ growth of UiO-66 MOF shell on Fe_3O_4 core. – The new composites can be applied as nanocarrier and contrast agent for MR imaging. – They revealed good biocompatibility and low toxicity in cytotoxicity tests. – In contrast, high cancer cell mortality, remarkable tumour size inhibition and significant darkening effect were obtained.	[328]
19	Cu(II)	BTC	$Cu_3(BTC)_2$ (HKUST-1)	Fe_3O_4, NIM	N/D	N/D	– Magnetic MOF nanocomposites were fabricated by incorporation of Fe_3O_4 nanorods with nanocrystals of HKUST-1. – An anticancer drug Nimesulide was loaded into pores. Adsorption in the range of 0.2 g of the drug/g of the composite was reported. – Complete drug delivery was observed after 11 days (physiological saline at 37 °C).	[329]
20	Gd(III)	BDC	Gd-BDC	MTX, Gd(III),	PNIPAM-co-PNAOSco-PFMA-MTX, GRGDS-NH_2	- FITZ-HSA (*in vitro*)	– A single theranostic device was synthesized by using a Gd-BDC MOF nanoparticles, PFMA, GRGDS-NH_2 and MTX. – New nanomaterials were biocompatible, had cancer cell targeting, bimodal imaging and disease treatment properties (see Fig. 25).	[127]
21	Zn(II)	OXA prodrug	N/D	OXA, PYRO	DOPA, PYRO,	- CT26, HT29, MC38 (*in vitro and in vivo*)	– NCP-enabled combination therapy for metastatic colorectal cancer was developed. – A new therapy combined oxaliplatin chemotherapy, pyrolipid-based PDT and PD-L1 checkpoint blockade cancer therapy. – NCP@pyrolipid carried high amounts of drugs. – New materials showed prolonged blood circulation and favourable tumour accumulation after administration. – CT26 and HT29 mouse models were studied and the new materials show inhibition of tumour growth.	[208]
22	Fe(III)	BDC	Fe-MIL-101	ART, DOX	N/D	SKOV3, A549, HeLa, BABL-3 T3,HUVEC (*in vitro*)	– The Fe-MIL-101 was more effective against SKOV3 cells than typical anticancer drugs. – The MOF was less effective against normal BABL-3 T3 cells. – Fe-MIL-101 was shown as non-toxic anti-angiogenic agent restricting ovarian tumour growth.	[330]

(*continued on next page*)

Table 14 (*continued*)

Select instances on the application of multifunctional MOFs in drug delivery and imaging.
MOFs as multifunctional systems

No.	Metal	Linker	MOF	Drug loaded (active substance)	Surface modification	Tested cell lines and *in vivo* models	Key findings (information)	Refs
23	Fe(III)	BTC	MIL-100(Fe)	DOX, $NaYF_4$:Yb(III)/Er (III), Fe	(FITC)-AS1411-NH_2, fluor-escein isothiocyanate (FITC)	- HEK 293, MCF-7 (*in vitro*)	– A novel multifintional nanocarrier composed of a MOF shell and up-conversion luminescent nanoparticles core was synthesized. – The material possessed high porosity and was nontoxic. – The DOX loading and release were studied in PBS at two different pH values. – The pH-sensitive drug release was observed.	[331]
24	Gd(III)	BDC	Gd-MOF	Gd(III), AuNP,	PAA	N/D	– The integration of GdMOF nanoparticles with gold nanoparticles for the preparation of a MRI/CT bimodal imaging agent was reported. – New hybrid GdMOF/Au composites were very stable. They were prepared by using poly(acrylic acid) as a bridge. – MRI and CT imaging showed high longitudinal relaxivity in MRI and excellent CT imaging performance of new MOF materials (see Fig. 26). – Dual-modal imaging contrast agent, Gd-PAA-Au nanocomposite was obtained and was more effective than the clinically used MRI contrast agent Magnevist®.	[125]
25	Fe(III)	BTC	MIL-100(Fe), PB	PB, ARS	PVP	- HeLa (*in vitro* and *in vivo*)	– A novel core–shell PB@MIL-100(Fe) dual MOF nanoparticles were obtained. – The artemisinin (a traditional Chinese anticancer medicine) with a high loading content of 848.4 mg/g was released from the d-MOFs. – *In vivo* photothermal therapy and chemotherapy were carried out and effective tumour ablation in an animal tumour model was observed. – Histological studies revealed that the drug delivery system had no obvious effect on the major organs of mice.	[332]
26	Eu(III), Gd(III)	$(N(C_4H_9)_4)_3[Mo(CN)_8]$	$Eu_{0.33}(III)Gd_{0.34}(III)/[Mo(CN)^8]^{3-}$	Eu(III), Gd(III), Chitosan	Chitosan	- Capan-1, HCT-116, HUVECs, fibroblasts (*in vitro*)	– A group of new bi-functional materials for MRI and optical imaging, based on $Ln_{0.333}(III)Gd_x(III)/[Mo(CN)_8]^{3-}$ was obtained.	[333]
27	Tb(III), Gd(III)	$(N(C_4H_9)_4)_3[Mo(CN)_8]$	$Tb_{0.33}(III)Gd_{0.35}(III)/[Mo(CN)_8]^{3-}$	Tb(III), Gd(III), Chitosan	Chitosan	- Capan-1, HCT-116, HUVECs, fibroblasts (*in vitro*)	– The materials showed better or similar effectiveness to the commercial contrast agents Omniscan® and Gd-DTPA®. – The toxicity tests showed that material was nontoxic. – High stability in aqueous solutions was observed.	

(*continued on next page*)

Table 14 (*continued*)

Select instances on the application of multifunctional MOFs in drug delivery and imaging.
MOFs as multifunctional systems

No.	Metal	Linker	MOF	Drug loaded (active substance)	Surface modification	Tested cell lines and *in vivo* models	Key findings (information)	Refs
28	Gd(III)	$(PPY)_2Ir(H_2DCPPY)]PF_6$	*f* -CPPs	Gd(III)	$(PPY)_2Ir(H_2DCPPY)]PF_6$	- HeLa (*in vitro*)	– The magneto-phosphorescent d-f nanoparticles were synthesized. – Magnetic Gd(III) ions were used as metallic nodes. – Water soluble nanoparticles were obtained by polyvinylpyrolidone modification, having red phosphorescence, moderate longitudinal relaxivity and low cytotoxicity. – The materials could be effectively taken up by living cells.	[334]
29	Zn(II)	Bisphosphonic acids containing CIS	NCP-1	CIS, siRNA	DOPA, PEG, DOPC, CHOL, siRNA	- SKOV-3, A2780/CIS, (*in vitro*),- CT-26, SKOV-3, A2780/CIS (*in vivo*)	– NCP particles allowed to incorporate multiple therapeutic modalities into a single vehicle. – The novel self-assembled core − shell nanoparticles combined two therapies: the chemotherapy of cisplatin or cisplatin and gemcitabine and the gene therapy of siRNA into a single platform. – A highly modular synthesis allowed for the optimized loading of different drugs. – A novel built-in endosomal escape mechanism was reported.	[335]
30	Zn(II)	Bisphosphonic acids containing CIS, GEM-MP	NCP-2	CIS, GEM-MP, siRNA (si*ERCC-1*, si*BCl-2*, and si*survivin*)				
31	Eu(III)	GMP	GMP/Eu	OVA, CpG	CpG, FITC	- RAW264.7 (*in vitro*)- B16-OVA (*in vivo*)	– Maximal antigen (OVA) encapsulating efficiency was about 55% (w/w). – PH depending release profiles of antigens (lower pH faster release) were reported. – About 60% of antigens were released at pH = 5.0 within 48 hrs. – In contrast, antigens were minimally released at pH = 7.4, indicating pH-dependent antigen release behavior. – A structure degradation was confirmed. – The ability of MOF-OVA to carry CpG was next assessed. – CpG were commonly used as immunostimulatory molecules and co-delivered APCs with antigens to improve immune response. – CpG alone cannot efficiently stimulate APCs, while pH-responsive MOF-OVA@CpG indeed induced greater production of TNF-α. – Successful inhibition of tumor growth was also achieved by this co-delivery systems due to the increased infiltration of tumor-killing immunocyte *in vivo*.	[220]

(*continued on next page*)

Table 14 (*continued*)

Select instances on the application of multifunctional MOFs in drug delivery and imaging.
MOFs as multifunctional systems

No.	Metal	Linker	MOF	Drug loaded (active substance)	Surface modification	Tested cell lines and *in vivo* models	Key findings (information)	Refs
32	Gd(III)	OPEA	$[Gd(OPE)\text{-}(NO_3)(H_2O)_2]\cdot H_2O$ (NCP-1)	OPEA, Gd(III)	N/D	- HEK 293 T, H1299 (*in vitro*)	– NCP-1 could mark it as a potential bimodal MRI/ optical imaging probe. – Langmuir surface area was equal to 293 m^2/g. – OPEA showed strong blue emission (λ = 445 nm) on 330 nm excitation and intense cyan emission (λ = 463 nm, λ = 390 nm) in solid state. – The presence of a large number of Gd(III) centers in NCP-1 resulted in enhanced transverse relaxivity of water and showed to be a potential negative contrast agent. – NCP-1 has been explored for sensing of nitroaromatic derivatives like: nitromethane, o-nitrophenol and nitrobenzene (see Fig. 27).	[121]
33	Hf(IV)	H4TBC	TBC-Hf	INCB24360 analogue (IDOi), TBC	N/D	- CT26, MC38, B16F10 (*in vitro*)- CT26, MC38, (*in vivo*)	– Encapsulating an INCB24360 analogue, 4-amino-N-(3-chloro-4-fluorophenyl)-N′-hydroxy-1,2,5-oxadiazole-3-carboximidamide (IDOi) into the TBC-Hf (1048 m2/g) channels to afford IDOi@TBC (loading was determined to be 4.7%)-Hf for the co-delivery of IDOi with photosensitizer. – IDOi was slowly leached from TBC-Hf, reaching 83.3% release after incubation in HBSS for 24 h.. – nMOF with large channels for highly efficient PDT, was simultaneously loaded with IDO inhibitor into its channels to achieve a combination of PDT and checkpoint blockade immunotherapy. – Successful inhibition of tumor growth (*in vitro* and *in vivo*) was also achieved by this co-delivery systems. Abscopal effect was observed in mice receiving treatment with PDT of IDOi@TBC-Hf. PDT treatment and IDOi immunotherapy synergize with each other and effectively generate systemic antitumor immunity.	[336]

four times greater IBU loading than that of silica MCM-41, showing the promise of MOFs for IBU storage. Bei and coworkers [339] used molecular simulations to investigate adsorption and diffusion behaviors of IBU in three bio-MOFs (bio-MOF-1, bio-MOF-11, bio-MOF-100) and UMCM-1. Using canonical Monte Carlo, grand canonical Monte Carlo (GCMC) simulations, and molecular dynamics (MD) simulations, they showed the loading and self-diffusion coefficients of IBU are proportional to the porosity of materials. They also revealed that IBU molecules are preferably adsorbed around the metal ions clusters of MOFs. Snurr's group [340] used GCMC simulations to screen a series of bio-compatible MOFs as carrier systems of IBU. They first validated their simulation results with the available experimental data of IBU uptake in MIL-53(Fe), MIL-100(Fe), and MIL-101(Cr), and then applied their computational methodology to predict IBU uptake of three bio-compatible MOFs having non-toxic metals, MOF-74(Mg), CD-MOF1, and BioMOF-100. Their simulation results showed that BioMOF-100 has a very high IBU capacity, six times higher than the value reported for mesoporous silicas. This high uptake was attributed to the presence of DMA cations in the pores which provide attractive interactions with the IBU molecules. Calero's group [341] used molecular simulation to predict molecular adsorption and enantioselectivity in MOFs. HMOF-1, which has a chiral structure, was found to separate racemic mixtures of IBU and the non-chiral structures of MIL-47 and MIL-53 were found to separate scalemic mixtures of IBU. Erucar and Keskin [342] used molecular simulations to investigate storage and release of IBU, in addition to two cosmetic molecules, caffeine (lipo-reducer) and urea (hydrating agent) in bio-compatible MOFs. After validating the accuracy of their molecular simulations with the experimentally available data for IBU, caffeine, and urea uptakes of MOFs, they examined 24 different biocompatible MOFs and predicted their uptakes for the same guest molecules. Bio-MOF-100 and MOF-74 material series were identified as promising candidates for drug/cosmetic molecule storage by outperforming widely studied MIL-53(Fe), MIL-100(Fe), MIL-101(Cr), zeolites, and mesoporous silica (MCM-41). MD simulations considering flexibility of MOFs showed the slow diffusion of drug molecules in MOFs' pores as desired.

As can be seen from this literature review, early computational studies generally focused on adsorption and diffusion of IBU in MOFs. Molecular simulations were recently performed to examine multi-storage and delivery of anti-cancer drugs in a series of MOFs since developing combination therapy requires the knowledge of simultaneous adsorption and diffusion of these drugs in the MOFs. Erucar and Keskin [343] studied 10 different MOF-74 materials having various physical and chemical properties for efficient storage and delivery of two anticancer drug molecules, methotrexate (MTX) and 5-fluorouracil (5-FU) using molecular simulations. They showed that at low fugacity, MTX adsorption is favored over 5-FU since MTX has stronger interactions with the MOFs whereas 5-FU adsorption is favored over MTX due to the entropic effects at high fugacity. MD simulations revealed that both drug molecules diffuse slowly making MOF-74 materials strong alternatives to traditional porous materials for delivery of these drugs. Froudakis' group [344] reported a multiscale computational study to examine microscopic behavior of the anti-cancer drug gemcitabine (GEM) stored in IRMOF-74-III and the functionalized OH-IRMOF-74-III. The maximum loading of GEM was computed to be three-fold greater than in lipid-coated mesoporous silica nanoparticles, highlighting the ability of the biocompatible MOFs as a promising encapsulator for GEM delivery. Interaction energy between GEM and both MOFs were examined and found to cause a slow delivery of the GEM. The same group also reported high GEM loading in a modified IRMOF-16 and used GCMC simulations to report drug release in this functionalized MOF [345].

Combining experiments and simulations is highly important to get molecular-level insights into the drug storage and delivery mechanisms of MOFs. Soares and coworkers [346] synthesized three new MOFs, characterized these materials, and showed that these new MOFs can adsorb large amounts of 5-FU. Using GCMC simulations, they also discussed the molecular interactions between 5-FU molecule and materials and provided a structural description of drug packing within the frameworks. Wang and coworkers [347] synthesized two isostructural MOFs as 5-FU carriers. Comparison of their GCMC simulation results with the molecular level properties revealed that there is a relation between the void space of the MOFs and the drug loading capacity. Mei and coworkers [348] synthesized a MOF and tested it for the adsorption of 5-FU. The loading of 5-FU in the MOF was studied by GCMC simulations and the radial distribution function data showed that the main driving forces for the loading of 5-FU were hydrogen bonding interactions. Other than 5-FU, Bulsulfan release from drug-loaded MOF was also studied using GCMC simulations [349]. Molecular docking calculations were also used in the literature to understand the preferred conformation of 5-FU molecule in the MOFs [251] and to study preferential binding sites of Doxorubicin in MOFs [243].

Almost all of these molecular simulations concluded that MOFs can uptake significant amounts of different types of drug molecules and these drug molecules release slowly in MOFs, which underlines the potential of MOFs for drug storage and delivery. Due to the very large number of available MOFs, application of the molecular simulations not only for a few MOF materials but to screen very large number of MOFs will be very important to identify the most appropriate MOFs among many prior to extensive experimental efforts. It seems that the number of new MOFs will likely rise quicker than our ability to theoretically foresee their performances for biomedical applications. New computational algorithms, improved molecular simulations techniques, and increased computational powers will be required to solve this issue. Therefore, it is expected to see a strong collaboration and knowledge transfer between chemistry, material science, computer science, biology, medicine, and engineering to fasten the research in the biomedical area of MOFs.

7. Summary and outlook

The extensive research on MOF materials and their biomedical application as drug carriers, contrast agents, biosensors or even theranostic particles, reflects the huge scientific and technological potential of this field. However, it is still an early-stage research, since no studies so far have reached the clinical trials.

MOF particles demonstrate numerous advantages that make them ideal candidates for drug carriers, particularly when compared to widely known materials such as inorganic materials (zeolites or mesoporous silica) or organic polymers. The diversity and

flexibility of routes for their modification, methods of functionalization, stabilization and synthesis of composites open an opportunity to design the chemical composition and structure of new MOFs to the required needs. It is then of no surprise, that the biomedical interest in these materials has been growing explosively in the last few years, predominantly in the anti-cancer research. In the simplest scenario, MOFs provide an additional vehicle to develop drug carriers that are passive, non-toxic and metabolizable. The more advanced approach involves synthesis of BIOMOFs with endogenous active components incorporated in the structure. The obtained pro-drugs release their active compounds simultaneously with the degradation of the whole structure. The drug release can be controlled through: i) modulation of the interactions between matrix material and the drug molecules, ii) modulation of the pore size that influences the drug diffusion efficiency, and iii) regulation of MOF degradation kinetics. Furthermore, MOF materials have one of the highest capacities for diagnostic and therapeutic particles loading, with the release of active compounds being controlled and gradual thus avoiding the burst effect and numerous side effects. The highly modular nature of the MOF materials synthesis also makes it possible to adjust the loading and release of different drugs and diagnostic agents in the same carrier. Biodegradability, required in the majority of biomedical applications, may be achieved by selecting appropriate metals and ligands, and through a series of surface modifications. Surface properties of hybrid nanoparticles can be optimized to obtain some beneficial properties such as targeting the appropriate cells, stealth properties, bio-adhesion, as well as changes in the drug release kinetics and stability of the carrier to obtain its prolonged circulation in the blood.

Moreover, MOF materials offer specific properties to be used as contrast agents in magnetic resonance imaging (MRI), optical imaging and X-ray computer tomography (CT). Thus, the effectiveness of the applied treatment can be monitored in real time. MOF materials also proved to be a promising platform for biosensing. Their unique properties allowed for highly specific and sensitive detection of small particles, ions or physico-chemical parameters. The future research direction should focus on tailored synthesis of MOF nanoparticles and fabricating the next generation of porous MOF-based sensors with enhanced sensitivity and selectivity.

Despite many significant advantages in the field, there are still some unanswered questions and critical challenges, associated with the use of MOF materials in the biomedical field. One of the most important issues to resolve is the mechanism and kinetics of MOF degradation (with or without drug loading), especially biodegradation since the process is typically MOF-specific. It should be taken into account that conditions in the human body and target tissues (the complexity of the matrix), such as pH, temperature or the presence of other active molecules, may affect the MOF degradation. Despite satisfactory drug delivery kinetics the burst effect has still been often observed. Thus, it is important to propose comprehensive encapsulation procedure for a given MOF/drug system to get the optimal delivery conditions. Finally, the synthesis of MOF nanoparticles and the appropriate modification of their surface are time-consuming processes that have been tested only for a few selected MOF structures. Therefore, reproduction of these methods to other MOF materials will require the intensive and extensive research in the near future. There is also lack of studies in the literature comparing administration procedures for different MOFs. It will be required in order to establish the most appropriate processing conditions. Also the general toxicity procedure is necessary for MOF based materials. Moreover, the studies on MOF should focus on the further development of *in vitro* and *in vivo* analyses, and thus increase their stability and efficacy and reduce toxicity in the organism. Pharmacokinetic studies on absorption, distribution, metabolism, and excretion (ADME) mechanisms *in vivo* are also of great importance. Obtained complex results will answer the question about the real and actual effectiveness of MOF as drugs, drug delivery and theranostic agents, leading in the future to intense preclinical and clinical studies.

In the presented review, the authors aimed to comprehensively describe the current state of knowledge in the subject of MOF application as biomaterials, especially in anti-cancer therapies. Overall, MOF structures can be advantageous and promising drug carriers, contrast agents or biosensors, supporting the anti-cancer therapies. In short-time perspective, it can be expected that research on the anti-cancer properties and toxicity of MOF, especially *in vivo*, will be continued and developed. There is also a great need for the standardization and validation of tests and testing methods. The promising perspective is to create even more advanced, tailored and sophisticated systems, e.g. through developing the concept of multivariate MTV-MOF materials, composite materials, multi-coatings and multiple functionalization. This will result in extending MOF functionality and range of potential applications. The obtained novel systems will be less toxic, even more multi-tasking, capable of simultaneous combined treatment using various treatment methods and/or of the multimodal imaging and biosensing. Furthermore, the development of surface engineering methods will allow improving the stability and biocompatibility of the systems. Another feature, that should be intensively exploited in MOF materials designed for anti-cancer therapy is their responsiveness to external factors, including pH, temperature, presence of specific ions or active compounds etc. However, in the case of anti-cancer treatment, the most important and desired feature is the highly selective drug delivery by the introduction of ligands targeting the tumour cells. All the scientific efforts will undoubtedly lead to creating more programmable, sophisticated and effective MOF-based systems for biomedical applications. To summarize, it is clear that MOF based anti-cancer treatments are still under development; however MOF materials have already shown remarkable and unique properties that should be useful at every stage of cancer therapy, and hence MOF-based technologies are expected to have a bright future in cancer medicine.

Declaration of Competing Interest

The authors declare that they have no known competing financial interests or personal relationships that could have appeared to influence the work reported in this paper.

Acknowledgments

The authors thank prof. Patricia Horcajada (IMDEA Energy, Madrid, Spain) for the review of manuscript and valuable suggestions considering the application of MOFs in medicine. We gratefully acknowledge financial support by the Polish National Science Centre (NCN) grant OPUS 9 no. 2015/17/B/ST5/01446.

References

[1] Hoskins B, Robson R. Infinite polymeric frameworks consisting of three dimensionally linked rod-like segments. J Am Chem Soc 1989;111:5962–4.
[2] Bieniek A, Terzyk AP, Wiśniewski M. Terminologia i nomenklatura sieci metalo-organicznych. Artykuł dyskusyjny. Przem Chem 2015;12:2203–7.
[3] Batten SR, Champness NR, Chen XM, Garcia-Martinez J, Kitagawa S, Öhrström L, et al. Terminology of metal–organic frameworks and coordination polymers (IUPAC Recommendations 2013). Pure Appl Chem 2013;85:1715–24.
[4] Butova VVE, Soldatov MA, Guda AA, Lomachenko KA, Lamberti C. Metal-organic frameworks: structure, properties, methods of synthesis and characterization. Russ Chem Rev 2016;85:280.
[5] Horike S, Kiatagawa S. Design of Porous Coordination Polymers/Metal–Organic Frameworks: Past, Present and Future. In Metal-Organic Frameworks: Applications from Catalysis to Gas Storage; 2011, p. 3–4.
[6] Kondo A, Kojima N, Kajiro H, Noguchi H, Hattori Y, Okino F, et al. Gas Adsorption Mechanism and Kinetics of an Elastic Layer-Structured Metal-Organic Framework. J Phys Chem C 2012;116:4157–62.
[7] Kondo A, Kajiro H, Noguchi H, Carlucci L, Proserpio DM, Ciani G, et al. Super flexibility of a 2D Cu-based porous coordination framework on gas adsorption in comparison with a 3D framework of identical composition: Framework dimensionality-dependent gas adsorptivities. J Am Chem Soc 2011;133:10512–22.
[8] Kondo A, Chinen A, Kajiro H, Nakagawa T, Kato K, Takata M, et al. Metal-Ion-Dependent Gas Sorptivity of Elastic Layer Structured MOFs. Chem Eur J 2009;15:7549–53.
[9] Stylianou KC, Imaz I, Maspoch D. Nanoscale Metal-Organic Frameworks. Metal-Organic Framework Materials 2014:19–37.
[10] Kanoh H, Kondo A, Noguchi H, Kajiro H, Tohdoh A, Hattori Y, et al. Elastic layer-structured metal organic frameworks (ELMs). J Colloid Interf Sci 2009;334:1–7.
[11] Banerjee D, Wang H, Deibert BJ, Li J. Alkaline Earth Metal Based Metal–Organic Frameworks: Synthesis, Properties, and Applications. In The Chemistry of Metal-Organic Frameworks: Synthesis, Characterization, and Applications The chemistry of metal-organic frameworks; 2016, p. 73–103.
[12] Furukawa H, Cordova KE, O'Keeffe M, Yaghi OM. The Chemistry and Applications of Metal-Organic Frameworks. Sci 2013;341:974 [1230444-1-12].
[13] Vagin S, Ott AK, Rieger B. Paddle-Wheel Zinc Carboxylate Clusters as Building Units for Metal-Organic Frameworks. Chem Ing Tech 2007;79:767–80.
[14] Florczak P, Janiszewska E, Kędzierska K, Kowalak S. Materiały MOF, nowa rodzina sit molekularnych o niezwykłych właściwościach i możliwościach zastosowań. Wiad Chem 2011;65:434–60.
[15] Ferey G. Metal-organic frameworks: the young child of the porous solids family. In Studies in surface science and catalysis, vol. 170. Elsevier 2007, p. 66–84.
[16] Howarth AJ, Liu Y, Li P, Li Z, Wang TC, Hupp JT, et al. Chemical, thermal and mechanical stabilities of metal–organic frameworks. Nat Rev Mater 2016;1:15018.
[17] Kreno LE, Leong K, Farha OK, Allendorf M, Van Duyne RP, Hupp JT. Metal-Organic Framework Materials as Chemical Sensors. Chem Rev 2012;112:1105–25.
[18] Huxford RC, Della Rocca J, Lin W. Metal-organic frameworks as potential drug carriers. Curr Opin Chem Biol 2010;14:262–8.
[19] Bennett TD, Cheetham AK. Amorphous metal–organic frameworks. Acc Chem Res 2014;47:1555–62.
[20] Dey C, Kundu T, Biswal BP, Mallick A, Banerjee R. Crystalline metal-organic frameworks (MOFs): synthesis, structure and function. Acta Cryst 2014;B70:3–10.
[21] Morozan A, Jaouen F. Metal organic frameworks for electrochemical applications. Energy Environ Sci 2012;5:9269–90.
[22] Alshammari A, Jiang Z, Cordova KE. Metal Organic Frameworks as Emerging Photocatalysts. Semicond Photocatal Mater Mech Appl 2016:301–41.
[23] Horcajada P, Serre C, Gref R, Couvreur P. Porous Metal–Organic Frameworks as New Drug Carriers. In Comprehensive Biomaterials; 2011, p. 559–73.
[24] Karagiaridi O, Bury W, Sarjeant AA, Hupp JT, Farha OK. Synthesis and characterization of functionalized metal-organic frameworks. J Vis Exp 2014;91:e52094.
[25] Cheng Y, Kondo A, Noguchi H, Kajiro H, Urita K, Ohba T, et al. Reversible structural change of Cu-MOF on exposure to water and its CO_2 adsorptivity. Langmuir 2009;25:4510–3.
[26] Kajiro H, Kondo A, Kaneko K, Kanoh H. Flexible two-dimensional square-grid coordination polymers: Structures and functions. Int J Mol Sci 2010;11:3803–45.
[27] Mueller U, Schubert M, Teich F, Puetter H, Schierle-Arndta K, Pastré J. Metal–organic frameworks – prospective industrial applications. J Mater Chem 2006;16:626–36.
[28] Li D, Kaneko K. Hydrogen bond-regulated microporous nature of copper complex-assembled microcrystals. Chem Phys Letters 2001;335:50–6.
[29] Sarkisov L, Martin RL, Haranczyk M, Smit B. On the flexibility of metal–organic frameworks. J Am Chem Soc 2014;136:2228–31.
[30] Czaja AU, Trukhan N, Müller U. Industrial applications of metal–organic frameworks. Chem Soc Rev 2009;38:1284–93.
[31] Cheng Y, Kajiro H, Noguchi H, Kondo A, Ohba T, Hattori Y, et al. Tuning of gate opening of an elastic layered structure MOF in CO_2 sorption with a trace of alcohol molecules. Langmuir 2011;27:6905–9.
[32] Ryder MR, Tan J-C. Nanoporous metal organic framework materials for smart applications. Mater Sci Technol 2014;30:1598–612.
[33] Anonim BASF. Metal Organic Frameworks (MOFs): Innovative Fuel Systems for Natural Gas Vehicles (NGVs). Chem Soc Rev 2014;43:6173–4.
[34] Li J-R, Kuppler RJ, Zhou H-C. Selective gas adsorption and separation in metal–organic frameworks. Chem Soc Rev 2009;38:1477–504.
[35] Mason JA, Veenstra M, Long JR. Evaluating metal–organic frameworks for natural gas storage. Chem Sci 2014;5:32–51.
[36] Peng Y, Krungleviciute V, Eryazici I, Hupp JT, Farha OK, Yildirim T. Methane storage in metal–organic frameworks: current records, surprise findings, and challenges. J Am Chem Soc 2013;135:11887–94.
[37] Li J-R, Sculley J, Zhou H-C. Metal–organic frameworks for separations. Chem Rev 2012;112:869–932.
[38] Horcajada P, Serre C, Vallet-Regí M, Sebban M, Taulelle F, Férey G. Metal–organic frameworks as efficient materials for drug delivery. Angew Chem Int Ed Engl 2006;45:5974–8.
[39] Lee J, Farha OK, Roberts J, Scheidt KA, Nguyen ST, Hupp JT. Metal–organic framework materials as catalysts. Chem Soc Rev 2009;38:1450–9.
[40] So MC, Wiederrecht GP, Mondloch JE, Hupp JT, Farha OK. Metal–organic framework materials for light-harvesting and energy transfer. Chem Commun 2015;51:3501–10.
[41] Wang J-L, Wang C, Lin W. Metal–organic frameworks for light harvesting and photocatalysis. ACS Catal 2012;2:2630–40.
[42] Kondo A, Noguchi H, Ohnishi S, Kajiro H, Tohdoh A, Hattori Y, et al. Novel expansion/shrinkage modulation of 2D layered MOF triggered by clathrate formation with CO_2 molecules. Nano Lett 2006;6:2581–4.
[43] Kondo A, Noguchi H, Kajiro H, Carlucci L, Mercandelli P, Proserpio DM, et al. Coordination symmetry-dependent structure restoration function of one-dimensional MOFs by molecular respiration. J Phys Chem B 2006;110:25565–7.
[44] Tan LL, Li H, Qiu YC, Chen DX, Wang X, Pan RY, et al. Stimuli-responsive metal–organic frameworks gated by pillar [5] arene supramolecular switches. Chem Sci 2015;6:1640–4.
[45] Keskin S, Kızılel S. Biomedical applications of metal organic frameworks. Ind Eng Chem Res 2011;50:1799–812.
[46] McKinlay AC, Morris RE, Horcajada P, Férey G, Gref R, Couvreur P, et al. BioMOFs: metal–organic frameworks for biological and medical applications. Angew Chem Int Ed 2010;49:6260–6.
[47] Imaz I, Rubio-Martínez M, An J, Sole-Font I, Rosi NL, Maspoch D. Metal–biomolecule frameworks (MBioFs). Chem Commun 2011;47:7287–302.
[48] Imaz I, Rubio-Martínez M, García-Fernández L, García F, Ruiz-Molina D, Hernando J, et al. Coordination polymer particles as potential drug delivery systems. Chem Commun 2010;46:4737–9.

[49] Novio F, Simmchen J, Vázquez-Mera N, Amorín-Ferré L, Ruiz-Molina D. Coordination polymer nanoparticles in medicine. Coord Chem Rev 2013;257:2839–47.
[50] Liu D, Lu K, Poon C, Lin W. Metal-organic frameworks as sensory materials and imaging agents. Inorg Chem 2013;53:1916–24.
[51] Cai W, Chu CC, Liu G, Wáng YXJ. Metal-Organic Framework – Based Nanomedicine Platforms for Drug Delivery and Molecular Imaging. Small 2015;11:4806–22.
[52] Horcajada P, Gref R, Baati T, Allan PK, Maurin G, Couvreur P, et al. Metal–organic frameworks in biomedicine. Chem Rev 2011;112:1232–68.
[53] Sun CY, Qin C, Wang XL, Su ZM. Metal-organic frameworks as potential drug delivery systems. Expert Opin Drug Deliv 2013;10:89–101.
[54] Miller SE, Teplensky MH, Moghadam PZ, Fairen-Jimenez D. Metal-organic frameworks as biosensors for luminescence-based detection and imaging. Interface Focus 2016;6:20160027.
[55] McKinlay AC, Allan PK, Renouf CL, Duncan MJ, Wheatley PS, Warrender SJ, et al. Multirate delivery of multiple therapeutic agents from metal-organic frameworks. APL Mater 2014;2:124108.
[56] He C, Liu D, Lin W. Nanomedicine applications of hybrid nanomaterials built from metal-ligand coordination bonds: nanoscale metal-organic frameworks and nanoscale coordination polymers. Chem Rev 2015;115:11079–108.
[57] Della Rocca J, Liu D, Lin W. Nanoscale metal-organic frameworks for biomedical imaging and drug delivery. Acc Chem Res 2011;44:957–68.
[58] Horcajada P, Serre C, Férey G, Couvreur P, Gref R. Des nanovecteurs hybrides pour la restitution retard de médicaments antitumouraux et antiviraux. Méd Sci 2010;26:761–7.
[59] Horcajada P, Chalati T, Serre C, Gillet B, Sebrie C, Baati T, et al. Porous metal-organic-framework nanoscale carriers as a potential platform for drug delivery and imaging. Nature Mater 2010;9:172–8.
[60] Wyszogrodzka AG, Dorożyński AP. Metal-Organic Frameworks: A New Class of Mesoporous Materials and Potential Possibilities of Their Use in Pharmaceutical Technology. Polim Med 2015;45:81–93.
[61] Liu R, Yu T, Shi Z, Wang Z. The preparation of metal–organic frameworks and their biomedical application. Int J Nanomedicine 2016;11:1187.
[62] Ibrahim M, Sabouni R, Husseini GA. Anti-Cancer Drug Delivery Using Metal Organic Frameworks (MOFs). Curr Med Chem 2017;24:193–214.
[63] He C, Lin W. Hybrid nanoparticles for cancer imaging and therapy. In Nanotechnology-Based Precision Tools for the Detection and Treatment of Cancer; 2015, p. 173–92.
[64] André V, Quaresma S. Bio-Inspired Metal-Organic Frameworks in the Pharmaceutical World: A Brief Review. Metal-Organic Frameworks 2016:135–56.
[65] Tamames-Tabar C, García-Márquez A, Blanco-Prieto MJ, Serre C, Horcajada P. MOFs in Pharmaceutical Technology. Bio- Bioinspir Nanomater 2014:83–112.
[66] Allendorf MD, Leong K, Zarkesh RA. Linkers with optical functionality. In The Chemistry of Metal-Organic Frameworks: Synthesis, Characterization, and Applications The chemistry of metal-organic frameworks; 2016, p. 480–87.
[67] Beetz M, Zimpel A, Wuttke S. Nanoparticles. In The Chemistry of Metal-Organic Frameworks: Synthesis, Characterization, and Applications The chemistry of metal-organic frameworks; 2016, p. 493–16.
[68] Beg S, Rahman M, Jain A, Saini S, Midoux P, Pichon C, et al. Nanoporous metal organic frameworks as hybrid polymer–metal composites for drug delivery and biomedical applications. Drug Discov Today 2016;00(00):1–13.
[69] Horcajada P, Serre C, McKinlayAC, Morris RE. Biomedical Applications of Metal-Organic Frameworks. In Metal-Organic Frameworks: Applications from Catalysis to Gas Storage; 2011, p. 215–44.
[70] Rocca JD, Lin W. Metal-Organic Frameworks for Biomedical Imaging. In Metal-Organic Frameworks: Applications from Catalysis to Gas Storage; 2011, p. 251–64.
[71] Salouti M, Ahangari A. Nanoparticle based drug delivery systems for treatment of infectious diseases. In Application of Nanotechnology in Drug Delivery; 2014, p. 155–92.
[72] Wilczewska AZ, Niemirowicz K, Markiewicz KH, Car H. Nanoparticles as drug delivery systems. Pharmacol Rep 2012;64:1020–37.
[73] Orellana-Tavra C, Baxter EF, Tian T, Bennett TD, Slater NK, Cheetham AK, et al. Amorphous metal–organic frameworks for drug delivery. Chem Commun 2015;51:13878–81.
[74] Brazel CS, Huang X. The Cost of Optimal Drug Delivery: Reducing and Preventing the Burst Effect in Matrix Systems. In Carrier-Based Drug Delivery; 2004, p. 267–82.
[75] Bansal P, Bharadwaj LM, Deep A, Rohilla SK, Salar RK. Metal Organic Frameworks: New Smart Material for Biological Application. Biotechnol Prosp Appl 2013:183–95.
[76] Rojas S, Devic T, Horcajada P. Metal organic frameworks based on bioactive components. J Mater Chem B 2017;5(14):2560–73.
[77] Horcajada P, Serre C, Maurin G, Ramsahye NA, Balas F, Vallet-Regi M, et al. Flexible porous metal-organic frameworks for a controlled drug delivery. J Am Chem Soc 2008;130:6774–80.
[78] Xiao B, Wheatley PS, Zhao X, Fletcher AJ, Fox S, Rossi AG, et al. High-capacity hydrogen and nitric oxide adsorption and storage in a metal-organic framework. J Am Chem Soc 2007;129:1203–9.
[79] Diring S, Wang DO, Kim C, Kondo M, Chen Y, Kitagawa S, et al. Localized cell stimulation by nitric oxide using a photoactive porous coordination polymer platform. Nature Commun 2013;4..
[80] Taylor-Pashow KM, Rocca JD, Xie Z, Tran S, Lin W. Postsynthetic modifications of Iron-Carboxylate nanoscale Metal-Organic frameworks for imaging and drug delivery. J Am Chem Soc 2009;131:14261–3.
[81] Zhuang J, Kuo CH, Chou LY, Liu DY, Weerapana E, Tsung CK. Optimized metal-organic-framework nanospheres for drug delivery: evaluation of small-molecule encapsulation. ACS Nano 2014;8:2812–9.
[82] Miller SR, Heurtaux D, Baati T, Horcajada P, Grenèche JM, Serre C. Biodegradable therapeutic MOFs for the delivery of bioactive molecules. Chem Commun 2010;46:4526–8.
[83] Kim Y, Nam HJ, Jung D-Y. Three-dimensional iron glutarate with five- and six-coordinated iron(II)-oxygen networks. Chem Lett 2009;38:72–3.
[84] Rieter WJ, Pott KM, Taylor KML, Lin W. Nanoscale coordination polymers for platinum based anticancer drug delivery. J Am Chem Soc 2008;130:11584–5.
[85] Ferrer P, da Silva I, Rubio-Zuazo J, Castro GR. Synthesis and crystal structure of the novel metal organic framework $Zn(C_3H_5NO_2S)_2$. Powder Diffr 2014;29:366–70.
[86] Fujita D, Fujita M. Fitting Proteins into Metal Organic Frameworks. ACS Cent Sci 2015;1:352–3.
[87] Fernandez D, Vega D, Goeta A. Alendronate zwitterions bind to calcium cations arranged in columns. Acta Crystallogr C 2003;59:543–5.
[88] Wang K, Geng Z, Yin Y, Ma X, Wang Z. Morphology effect on the luminescent property and antibacterial activity of coordination polymer particles with identical crystal structures. Cryst Eng Comm 2011;13:5100–4.
[89] Li W, Jin L, Zhu N, Hou X, Deng F, Sun H. Structure of Colloidal Bismuth Subcitrate (CBS) in Dilute HCl: Unique Assembly of Bismuth Citrate Dinuclear Units ($[Bi(cit)_2Bi]^{2-}$). J Am Chem Soc 2003;125:12408–9.
[90] Rood JA, Noll BC, Henderson KW. Synthesis, Structural Characterization, Gas Sorption and Guest-Exchange Studies of the Lightweight, Porous Metal-Organic Framework α-$[Mg_3(O_2CH)_6]$. Inorg Chem 2006;45:5521–8.
[91] Ingleson MJ, Barrio JP, Bacsa J, Dickinson C, Park H, Rosseinsky MJ. Generation of a solid Brønsted acid site in a chiral framework. Chem Commun 2008;11:1287–9.
[92] Rabone J, Yue Y-F, Chong SY, Stylianou KC, Bacsa J, Bradshaw D, et al. An Adaptable Peptide-Based Porous Material. Science 2010;329:1053–7.
[93] Serre C, Millange F, Surblé S, Férey G. A route to the synthesis of trivalent transition-metal porous carboxylates with trimeric secondary building units. Angew Chem Int Ed 2004;43:6285–9.
[94] Serre C, Surblé S, Mellot-Draznieks C, Filinchuk Y, Férey G. Evidence of flexibility in the nanoporous iron(III) carboxylate MIL-89. Dalton Trans 2008;40:5462–4.
[95] Jung WK, Koo HC, Kim KW, Shin S, Kim SH, Park YH. Antibacterial activity and mechanism of action of the silver ion in Staphylococcus aureus and Escherichia coli. Appl Environ Microbio 2008;74:2171–8.
[96] Berchel M, Le Gall T, Denis C, Le Hir S, Quentel F, Elléouet C, et al. A silver-based metal-organic framework material as a 'reservoir' of bactericidal metal ions.

New J Chem 2011;35:1000–3.
[97] Kirillov AM, Wieczorek SW, Lis A, da Silva M, Florek M, Krol J, et al. 1,3,5-triaza-7-phosphaadamantane-7-oxide (PTA = O): new diamondoid building block for design of three-dimensional metal-organic frameworks. Cryst Growth Des 2011;11:2711–6.
[98] Slenters TV, Sagué JL, Brunetto PS, Zuber S, Fleury A, Mirolo L, et al. Of chains and rings: synthetic strategies and theoretical investigations for tuning the structure of silver coordination compounds and their applications. Materials 2010;3:3407–29.
[99] Slenters TV, Hauser-Gerspach I, Daniels AU, Fromm KM. Silver coordination compounds as lightstable, nano-structured and anti-bacterial coatings for dental implant and restorative materials. J Mater Chem 2008;18:5359–62.
[100] An J, Gelb SJ, Rosi NL. Cation triggered drug release from a porous zinc-adeninate metal-organic framework. J Am Chem Soc 2009;131:8376–7.
[101] Su H, Sun F, Jia J, He H, Wang A, Zhu G. A highly porous medical metal-organic framework constructed from bioactive curcumin. Chem Commun 2015;51:5774–7.
[102] An J, Farha OK, Hupp JT, Pohl E, Yeh JI, Rosi NL. Metal-adeninate vertices for the construction of an exceptionally porous metal-organic framework. Nat Commun 2012;3:604–9.
[103] Taylor KM, Rieter WJ, Lin W. Manganese-based nanoscale metal-organic frameworks for magnetic resonance imaging. J Am Chem Soc 2008;130:14358–9.
[104] Liu D, Huxford RC, Lin W. Phosphorescent nanoscale coordination polymers as contrast agents for optical imaging. Angew Chem Int Ed 2011;123:3780–4.
[105] Lehr CM, Bouwstra JA, Schacht EH, Junginger HE. In vitro evaluation of mucoadhesive properties of chitosan and some other natural polymers. Int J Pharm 1992;78:43–8.
[106] Hidalgo T, Giménez-Marqués M, Bellido E, Avila J, Asensio MC, Salles F, et al. Chitosan-coated mesoporous MIL-100(Fe) nanoparticles as improved bio-compatible oral nanocarriers. Sci Rep 2017;7:43099.
[107] Huxford-Phillips RC, Russell SR, Liu D, Lin W. Lipid-coated nanoscale coordination polymers for targeted cisplatin delivery. RSC Adv 2013;3:14438–43.
[108] Wuttke S, Braig S, Preiß T, Zimpel A, Sicklinger J, Bellomo C, et al. MOF nanoparticles coated by lipid bilayers and their uptake by cancer cells. Chem Commun 2015;51:15752–5.
[109] He C, Lu K, Liu D, Lin W. Nanoscale metal-organic frameworks for the co-delivery of cisplatin and pooled siRNAs to enhance therapeutic efficacy in drug-resistant ovarian cancer cells. J Am Chem Soc 2014;136:5181–4.
[110] Morris W, Briley WE, Auyeung E, Cabezas MD, Mirkin CA. Nucleic acid–metal organic framework (MOF) nanoparticle conjugates. J Am Chem Soc 2014;136:7261–4.
[111] Park J, Jiang Q, Feng D, Mao L, Zhou HC. Size-Controlled Synthesis of Porphyrinic Metal-Organic Framework and Functionalization for Targeted Photodynamic Therapy. J Am Chem Soc 2016;138:3518–25.
[112] Chen L, Schechter B, Arnon R, Wilchek M. Tissue selective affinity targeting using the avidin–biotin system. Drug Dev Res 2000;50:258–71.
[113] Agostoni V, Horcajada P, Noiray M, Malanga M, Aykaç A, Jicsinszky L, et al. A "green" strategy to construct non-covalent, stable and bioactive coatings on porous MOF nanoparticles. Sci Rep 2015;5(1):1–7.
[114] Rieter WJ, Taylor KM, Lin W. Surface modification and functionalization of nanoscale metal-organic frameworks for controlled release and luminescence sensing. J Am Chem Soc 2007;129:9852–53.
[115] Gitanjali A, Brahmkhatri VP, Atreya HS. Nanomaterial based Magnetic Resonance Imaging of Cancer. J Indian Inst Sci 2014;94:423–54.
[116] Panczyk T, Konczak L, Zapotoczny S, Szabelski P, Nowakowska M. Molecular dynamics simulations of proton transverse relaxation times in suspensions of magnetic nanoparticles. J Colloid Interface Sci. 2015;437:187–96.
[117] Wang C, Volotskova O, Lu K, Ahmad M, Sun C, Xing L, et al. Synergistic Assembly of Heavy Metal Clusters and Luminescent Organic Bridging Ligands in Metal-Organic Frameworks for Highly Efficient X-ray Scintillation. J Am Chem Soc 2014;136:6171–4.
[118] Webster RM. Combination therapies in oncology. Nat Rev Drug Discov 2016;15:81–2.
[119] Rojas S, Wheatley PS, Quartapelle-Procopio E, Gil B, Marszalek B, Morris RE, et al. Metal–organic frameworks as potential multi-carriers of drugs. Cryst Eng Comm 2013;15:9364–7.
[120] He C, Lu J, Lin W. Hybrid nanoparticles for combination therapy of cancer. J Control Release 2015;219:224–36.
[121] Suresh VM, Chatterjee S, Modak R, Tiwari V, Patel AB, Kundu TK, et al. Oligo (p-phenyleneethynylene)-Derived Porous Luminescent Nanoscale Coordination Polymer of GdIII: Bimodal Imaging and Nitroaromatic Sensing. J Phys Chem C 2014;118:12241–9.
[122] Rieter WJ, Taylor KM, An H, Lin W, Lin W. Nanoscale metal-organic frameworks as potential multimodal contrast enhancing agents. J Am Chem Soc 2006;128:9024–5.
[123] Taylor KM, Jin A, Lin W. Surfactant-Assisted Synthesis of Nanoscale Gadolinium Metal-Organic Frameworks for Potential Multimodal Imaging. Angew Chem 2008;120:7836–9.
[124] Shin T-H, Choi J-S, Yun S, Kim I-S, Song H-T, Kim Y, et al. T_1 and T_2 Dual-Mode MRI Contrast Agent for Enhancing Accuracy by Engineered Nanomaterials. ACS Nano 2014:3393–401.
[125] Tian C, Zhu L, Lin F, Boyes SG. Poly (acrylic acid) Bridged Gadolinium Metal-Organic Framework–Gold Nanoparticle Composites as Contrast Agents for Computed Tomography and Magnetic Resonance Bimodal Imaging. ACS Appl Mater Interfaces 2015;7:17765–75.
[126] Wang C, Liu D, Lin W. Metal–organic frameworks as a tunable platform for designing functional molecular materials. J Am Chem Soc 2013;135:13222–34.
[127] Rowe MD, Thamm DH, Kraft SL, Boyes SG. Polymer-modified gadolinium metal-organic framework nanoparticles used as multifunctional nanomedicines for the targeted imaging and treatment of cancer. Biomacromolecules 2009;10:983–93.
[128] Smaldone RA, Forgan RS, Furukawa H, Gassensmith JJ, Slawin AM, Yaghi OM, et al. Metal–organic frameworks from edible natural products. Angew Chem Inter Ed 2010;49:8630–4.
[129] Baati T, Njim L, Neffati F, Kerkeni A, Bouttemi M, Gref R, et al. In depth analysis of the in vivo toxicity of nanoparticles of porous iron (III) metal–organic frameworks. Chem Sci 2013;4:1597–607.
[130] Wang XG, Dong ZY, Cheng H, Wan SS, Chen WH, Zou MZ, et al. A multifunctional metal–organic framework based tumour targeting drug delivery system for cancer therapy. Nanoscale 2015;7:16061–70.
[131] Au KM, Satterlee A, Min Y, Tian X, Kim YS, Caster JM, et al. Folate-targeted pH-responsive calcium zoledronate nanoscale metal-organic frameworks: Turning a bone antiresorptive agent into an anticancer therapeutic. Biomaterials 2016;82:178–93.
[132] Furukawa H, Müller U, Yaghi OM. "Heterogeneity within Order" in Metal-Organic Frameworks. Angew Chem Int Ed 2015;54:3417–30.
[133] Seki K. Design of an adsorbent with an ideal pore structure for methane adsorption using metal complexes. Chem Commun 2001;16:1496–7.
[134] Zhao B, Cheng P, Dai Y, Cheng C, Liao DZ, Yan SP, et al. A Nanotubular 3D Coordination Polymer Based on a 3d–4f Heterometallic Assembly. Angew Chem Int Ed 2003;42:934–6.
[135] Coudert FX. Responsive metal–organic frameworks and framework materials: under pressure, taking the heat, in the spotlight, with friends. Chem Mater 2015;27:1905–16.
[136] Nagarkar SS, Desai AV, Ghosh SK. Stimulus – Responsive Metal-Organic Frameworks. Chem Asian J 2014;9:2358–76.
[137] Tan QH, Wang YQ, Guo XY, Liu HT, Liu ZL. A gadolinium MOF acting as a multi-responsive and highly selective luminescent sensor for detecting o-, m-, and p-nitrophenol and Fe^{3+} ions in the aqueous phase. RSC Adv 2016;6:61725–31.
[138] Lin W, Hu Q, Yu J, Jiang K, Yang Y, Xiang S, et al. Low Cytotoxic Metal-Organic Frameworks as Temperature – Responsive Drug Carriers. ChemPlusChem 2016;81:804–10.
[139] Jasuja H, Walton KS. Effect of catenation and basicity of pillared ligands on the water stability of MOFs. Dalton Trans 2013;42:15421–6.
[140] Han SS, Mendoza-Cortez JL, Goddard III WA. Recent advances on simulation and theory of hydrogen storage in metal-organic frameworks and covalent organic frameworks. Chem Soc Rev 2009;38:1460–76.
[141] Barton J, Niemczyk A, Czaja K, Korach Ł, Kompozyty Sacher-Majewska B. biokompozyty i nanokompozyty polimerowe. Otrzymywanie, skład, właściwości i kierunki zastosowań. Chemik 2014;68:280–7.
[142] Campbell FC. Structural Composite Materials 2010:1–18.

[143] Zhu Q-L, Xu Q. Metal-Organic framework composites. Chem Soc Rev 2014;43:5468–512.
[144] Liu X-W, Sun T-J, Hu J-L, Wang S-D. Composites of metal–organic frameworks and carbon-based materials: preparations, functionalities and applications. J Mater Chem A 2016;4:3584–616.
[145] Ahmed I, Jhung SH. Composites of metal-organic frameworks: Preparation and applications in adsorption. Mater Today 2014;17:136–46.
[146] Choi KM, Jeong HM, Park JH, Zhang YB, Kang JK, Yaghi OM. Supercapacitors of nanocrystalline metal–organic frameworks. ACS Nano 2014;8(7):7451–7.
[147] de Oliveira CAF, da Silva FF, Jimenez GC, Neto JFDS, de Souza DMB, de Souza IA, et al. MOF@ activated carbon: a new material for adsorption of aldicarb in biological systems. Chem Commun 2013;49(58):6486–8.
[148] Yang SJ, Choi JY, Chae HK, Cho JH, Nahm KS, Park CR. Preparation and Enhanced Hydrostability and Hydrogen Storage Capacity of CNT@MOF-5 Hybrid Composite. Chem Mater 2009;21:1893–7.
[149] Wong AHH, Deng CX. Precision Medicine for Personalized Cancer Therapy. Int J Biol Sci 2015;11:1410.
[150] Stewart B, Wild CP, editors. World Cancer Report 2014, International Agency for Research on Cancer, WHO. 2014 [Online]. Available from: http://publications.iarc.fr/Non-Series-Publications/World-Cancer-Reports/World-Cancer-Report-2014725845 [accessed: 2nd November 2016].
[151] Thakor AS, Gambhir SS. Nanooncology: the future of cancer diagnosis and therapy. CA Cancer J Clin 2013;63:395–418.
[152] Jiang ZX, Zhang ZY. Targeting PTPs with small molecule inhibitors in cancer treatment. Cancer Metastasis Rev 2008;27:263–72.
[153] Scott AM, Wolchok JD, Old LJ. Antibody therapy of cancer. Nat Rev Cancer 2012;12:278–87.
[154] Shewach DS, Kuchta RD. Introduction to cancer chemotherapeutics. Chem Rev 2009;109:2859–61.
[155] Husain SR, Han J, Au P, Shannon K, Puri RK. Gene therapy for cancer: regulatory considerations for approval. Cancer Gene Ther 2015;22:554–63.
[156] Palakurthi S. Challenges in SN38 drug delivery: current success and future directions. Expert Opin Drug Deliv 2015;12:1911–21.
[157] Wallin A, Svanvik J, Holmlund B, Ferreud L, Sun XF. Anticancer effect of SN-38 on colon cancer cell lines with different metastatic potential. Oncol Rep 2008;19:1493–8.
[158] Maurya DK, Ayuzawa R, Doi C, Troyer D, Tamura M. Topoisomerase I inhibitor SN-38 effectively attenuates growth of human non-small cell lung cancer cell lines in vitro and in vivo. J Environ Pathol Toxicol Oncol 2011;30:1–10.
[159] Liu D, Chen Z. The effect of curcumin on breast cancer cells. J Breast Cancer 2013;16:133–7.
[160] Vallianou NG, Evangelopoulos A, Schizas N, Kazazis C. Potential anticancer properties and mechanisms of action of curcumin. Anticancer Res 2015;35:645–51.
[161] Perrone D, Ardito F, Giannatempo G, Dioguardi M, Troiano G, Lo Russo L, et al. Biological and therapeutic activities, and anticancer properties of curcumin (Review). Exp Ther Med 2015;10:1615–23.
[162] Wilken R, Veena MS, Wang MB, Srivatsan ES. Curcumin: A review of anti-cancer properties and therapeutic activity in head and neck squamous cell carcinoma. Mol Cancer 2011;10:12.
[163] Weiss A, Berndsen RH, Dubois M, Müller C, Schibli R, Griffioen AW, et al. In vivo anti-tumour activity of the organometallic ruthenium (ii)-arene complex [Ru(η^6-p-cymene)Cl_2(pta)](RAPTA-C) in human ovarian and colorectal carcinomas. Chem Sci 2014;5:4742–8.
[164] Sharkey EM, O'Neill HB, Kavarana MJ, Wang H, Creighton DJ, Sentz DL, et al. Pharmacokinetics and antitumour properties in tumour-bearing mice of an enediol analogue inhibitor of glyoxalase I. Cancer Chemoth Pharm 2000;46:156–66.
[165] Hamilton DS, Kavarana MJ, Sharkey EM, Eiseman JL, Creighton DJ. A new method for rapidly generating inhibitors of glyoxalase I inside tumour cells using S-(N-aryl-N-hydroxycarbamoyl) ethylsulfoxides. J Med Chem 1999;42:1823–7.
[166] Wang Z, Lei L, Cai XJ, Chen LY, Yuan M, Yang G, et al. A preliminary study of pamidronic acid downregulation of angiogenic factors igF-1/PecaM-1 expression in circulating level in bone metastatic breast cancer patients. Onco Targets Ther 2016;9:3147–52.
[167] Zhao X, Hu X. Dosing of zoledronic acid with its anti-tumour effects in breast cancer. J Bone Oncol 2015;4:98–101.
[168] Steinman RA, Brufsky AM, Oesterreich S. Zoledronic acid effectiveness against breast cancer metastases-a role for estrogen in the microenvironment? Breast Cancer Res 2012;14:213.
[169] Zhu X, Gu J, Wang Y, Li B, Li Y, Zhao W, et al. Inherent anchorages in UiO-66 nanoparticles for efficient capture of alendronate and its mediated release. Chem Commun 2014;50:8779–82.
[170] Verma S, Singh A, Mishra A. Gallic acid: molecular rival of cancer. Environ Toxicol Pharmacol 2013;35:473–85.
[171] Subramanian AP, Jaganathan SK, Mandal M, Supriyanto E, Muhamad II. Gallic acid induced apoptotic events in HCT-15 colon cancer cells. World J Gastroenterol 2016;22:3952–61.
[172] Zhao B, Hu M. Gallic acid reduces cell viability, proliferation, invasion and angiogenesis in human cervical cancer cells. Oncol Lett 2013;6:1749–55.
[173] Liu Z, Li D, Yu L, Niu F. Gallic acid as a cancer-selective agent induces apoptosis in pancreatic cancer cells. Chemotherapy 2012;58:185–94.
[174] Brown WA, Farmer KC, Skinner SA, Malcontenti-Wilson C, Misajon A, O'brien PE. 5-Aminosalicylic acid and olsalazine inhibit tumour growth in a rodent model of colorectal cancer. Dig Dis Sci 2000;45:1578–84.
[175] Méndez-Lucio O, Tran J, Medina-Franco JL, Meurice N, Muller M. Toward drug repurposing in epigenetics: olsalazine as a hypomethylating compound active in a cellular context. ChemMedChem 2014;9:560–5.
[176] Wagner CR, Ballato G, Akanni AO, McIntee EJ, Larson RS, Chang SL, et al. Potent growth inhibitory activity of zidovudine on cultured human breast cancer cells and rat mammary tumours. Cancer Res 1997;57:2341–5.
[177] Falchetti A, Franchi A, Bordi C, Mavilia C, Masi L, Cioppi F, et al. Azidothymidine induces apoptosis and inhibits cell growth and telomerase activity of human parathyroid cancer cells in culture. J Bone Miner Res 2005;20:410–8.
[178] Brown T, Sigurdson E, Rogatko A, Broccoli D. Telomerase inhibition using azidothymidine in the HT-29 colon cancer cell line. Ann Surg Oncol. 2003;10:910–5.
[179] Zhang ZM, Duan X, Yao S, Wang Z, Lin Z, Li YG, et al. Cation-mediated optical resolution and anticancer activity of chiral polyoxometalates built from entirely achiral building blocks. Chem Sci 2016;7:4220–9.
[180] Lu W, Jiaren ZBL. Anticancer polyoxometalates. Prog Chem 2013;25:1131–41.
[181] Davoodnia A, Allameh S, Fazli S, Tavakoli-Hoseini N. One-pot synthesis of 2-amino-3-cyano-4-arylsubstituted tetrahydrobenzo [b] pyrans catalysed by silica gel-supported polyphosphoric acid (PPA-SiO_2) as an efficient and reusable catalyst. Chem Pap 2011;65:714–20.
[182] Lopatina OA, Mezentzeva MV, Suetina IA, Isaeva EI, Gushina EA, Baklanova OV, et al. Polyoxometalates (POMs) cytotoxic and antiviral effect on human cells in vitro. J Nanomed Nanotechnol 2015;6:4. https://doi.org/10.4172/2157-7439.S1.022.
[183] Li XH, Li JJ, Zhang HW, Sun P, Zhang YL, Cai SH, et al. Nimesulide inhibits tumour growth in mice implanted hepatoma: overexpression of Bax over Bcl-2. Acta Pharmacol Sin 2003;24:1045–50.
[184] Zhong B, Cai X, Chennamaneni S, Yi X, Liu L, Pink JJ, et al. From COX-2 inhibitor nimesulide to potent anti-cancer agent: synthesis, in vitro, in vivo and pharmacokinetic evaluation. Eur J Med Chem 2012;47:432–44.
[185] Jakubowska-Mućka A, Sieńko J, Switaj T, Gołab J, Lasek W. Antitumour effects of sulindac in ovarian cell cultures. Ginekol Pol 2011;82:195–9.
[186] Crespo-Ortiz MP, Wei MQ. Antitumour activity of artemisinin and its derivatives: from a well-known antimalarial agent to a potential anticancer drug. J Biomed Biotechnol 2012;2012:247597.
[187] Michaelis M, Kleinschmidt MC, Barth S, Rothweiler F, Geiler J, Breitling R, et al. Anti-cancer effects of artesunate in a panel of chemoresistant neuroblastoma cell lines. Biochem Pharmacol 2010;79:130–6.
[188] Ilamathi M, Santhosh S, Sivaramakrishnan V. Artesunate as an Anti-Cancer Agent Targets Stat-3 and Favorably Suppresses Hepatocellular Carcinoma. Curr Top Med Chem 2016;16:2453–63.
[189] Li X, Zhou Y, Liu Y, Zhang X, Chen T, Chen K, et al. Preclinical Efficacy and Safety Assessment of Artemisinin-Chemotherapeutic Agent Conjugates for Ovarian Cancer. EBioMedicine 2016;14:44–54.
[190] Das AK. Anticancer effect of antimalarial artemisinin compounds. Ann Med Health Sci Res 2015;5:93–102.
[191] Firestone GL, Sundar SN. Anticancer activities of artemisinin and its bioactive derivatives. Expert Rev Mol Med 2009;11:e32.
[192] Sun RW, Zhang M, Li D, Li M, Wong AS. Enhanced anti-cancer activities of a gold (III) pyrrolidinedithiocarbamato complex incorporated in a biodegradable metal-organic framework. J Inorg Biochem 2016;163:1–7.

[193] Sun RW, Zhang M, Li D, Zhang ZF, Cai H, Li M, et al. Dinuclear Gold (I) Pyrrolidinedithiocarbamato Complex: Cytotoxic and Antimigratory Activities on Cancer Cells and the Use of Metal-Organic Framework. Chemistry–A Eur J 2015;21:18534–8.
[194] Lee ZW, Teo XY, Tay EY, Tan CH, Hagen T, Moore PK, et al. Utilizing hydrogen sulfide as a novel anticancer agent by targeting cancer glycolysis and pH imbalance. Br J Pharmacol 2014;171:4322–36.
[195] Zhang L, Qi Q, Yang J, Sun D, Li C, Xue Y, et al. An anticancer role of hydrogen sulfide in human gastric cancer cells. Oxid Med Cell Longev 2015;2015:636410.
[196] Huerta S. Nitric oxide for cancer therapy. Future Sci OA. 2015;1:FSO44.
[197] Hickok JR, Thomas DD. Nitric oxide and cancer therapy: the emperor has NO clothes. Curr Pharm Des 2010;16:381–91.
[198] Sinha BK, Kumar A, Bhattacharjee S, Espey MG, Mason RP. Effect of nitric oxide on the anticancer activity of the topoisomerase-active drugs etoposide and adriamycin in human melanoma cells. J Pharmacol Exp Ther 2013;347:607–14.
[199] Sinha BK. Nitric Oxide: Friend or Foe in Cancer Chemotherapy and Drug Resistance: A Perspective. J Cancer Sci Ther 2016;8:244–51.
[200] Liu J, Yang Y, Zhu W, Yi X, Dong Z, Xu X, et al. Nanoscale metal-organic frameworks for combined photodynamic & radiation therapy in cancer treatment. Biomaterials 2016;97:1–9.
[201] Lu K, He C, Lin W. Nanoscale metal-organic framework for highly effective photodynamic therapy of resistant head and neck cancer. J Am Chem Soc 2014;136:16712–5.
[202] Pushpan SK, Venkatraman S, Anand VG, Sankar J, Parmeswaran D, Ganesan S, et al. Porphyrins in photodynamic therapy-a search for ideal photosensitizers. Curr Med Chem Anticancer Agents 2002;2:187–207.
[203] Lu K, He C, Lin W. A Chlorin-Based Nanoscale Metal-Organic Framework for Photodynamic Therapy of Colon Cancers. J Am Chem Soc 2015;137:7600–3.
[204] Wawrzyńska M, Kałas W, Biały D, Zioło E, Arkowski J, Mazurek W, et al. In vitro photodynamic therapy with chlorin e6 leads to apoptosis of human vascular smooth muscle cells. Arch Immunol Ther Exp (Warsz) 2010;58:67–75.
[205] Mari C, Pierroz V, Ferrari S, Gasser G. Combination of Ru (II) complexes and light: new frontiers in cancer therapy. Chem Sci 2015;6:2660–86.
[206] Zhang W, Li B, Ma H, Zhang L, Guan Y, Zhang Y, et al. Combining Ruthenium (II) Complexes with Metal-Organic Frameworks to Realize Effective Two-Photon Absorption for Singlet Oxygen Generation. ACS Appl Mater Interfaces 2016;8:21465–71.
[207] Anikeeva N, Sykulev Y, Delikatny EJ, Popov AV. Core-based lipid nanoparticles as a nanoplatform for delivery of near-infrared fluorescent imaging agents. Am J Nucl Med Mol Imaging 2014;4:507–24.
[208] He C, Duan X, Guo N, Chan C, Poon C, Weichselbaum RR, et al. Core-shell nanoscale coordination polymers combine chemotherapy and photodynamic therapy to potentiate checkpoint blockade cancer immunotherapy. Nat Commun 2016;7(12499):1–12.
[209] He C, Liu D, Lin W. Self-assembled core–shell nanoparticles for combined chemotherapy and photodynamic therapy of resistant head and neck cancers. ACS Nano 2015;9:991–1003.
[210] Lovell JF, Jin CS, Huynh E, Jin H, Kim C, Rubinstein JL, et al. Porphysome nanovesicles generated by porphyrin bilayers for use as multimodal biophotonic contrast agents. Nat Mater 2011;10:324–32.
[211] Li M, Li L, Zhan C, Kohane DS. Core-Shell Nanostars for Multimodal Therapy and Imaging. Theranostics 2016;6:2306–13.
[212] Espinosa A, Silva AK, Sánchez-Iglesias A, Grzelczak M, Péchoux C, Desboeufs K, et al. Photothermal Therapy: Cancer cell internalization of gold nanostars impacts their photothermal efficiency in vitro and in vivo: Toward a plasmonic thermal fingerprint in tumoral environment. Adv Healthc Mater 2016;5:1040–8.
[213] Hoffman HA, Chakrabarti L, Dumont MF, Sandler AD, Fernandes R. Prussian blue nanoparticles for laser-induced photothermal therapy of tumours. RSC Adv 2014;4:29729–34.
[214] Cano-Mejia J, Burga RA, Sweeney EE, Fisher JP, Bollard CM, Sandler AD, et al. Prussian blue nanoparticle-based photothermal therapy combined with checkpoint inhibition for photothermal immunotherapy of neuroblastoma. Nanomedicine 2016;13:771–81.
[215] Gu S, Hu Z, Ngamcherdtrakul W, Castro DJ, Morry J, Reda MM, et al. Therapeutic siRNA for drug-resistant HER2-positive breast cancer. Oncotarget 2016;7:14727–41.
[216] Young SW, Stenzel M, Yang JL. Nanoparticle-siRNA: A potential cancer therapy? Crit Rev Onco Hematol 2016;98:159–69.
[217] Devi GR. siRNA-based approaches in cancer therapy. Cancer gene ther 2006;13:819–29.
[218] Cho-Chung YS. DNA drug design for cancer therapy. Curr Pharm Des 2005;11:2811–23.
[219] Hurley LH. DNA and its associated processes as targets for cancer therapy. Nat Rev Cancer 2002;2:188–200.
[220] Duan F, Feng X, Yang X, Sun W, Jin Y, Liu H, et al. A simple and powerful co-delivery system based on pH-responsive metal-organic frameworks for enhanced cancer immunotherapy. Biomaterials 2017;122:23–33.
[221] Jeanbart L, Ballester M, de Titta A, Corthésy P, Romero P, Hubbell JA, et al. Enhancing efficacy of anticancer vaccines by targeted delivery to tumor-draining lymph nodes. Cancer Immunol Res 2014;2:436–47.
[222] Gerweck LE, Seetharaman K. Cellular pH gradient in tumor versus normal tissue: potential exploitation for the treatment of cancer. Cancer Res 1996;56:1194–8.
[223] Monti M, Brandt L, Ikomi-Kumm J, Olsson H. Microcalorimetric investigation of cell metabolism in tumour cells from patients with non-Hodgkin lymphoma (NHL). Scand J Haematol 1986;36:353–7.
[224] Karnebogen M, Singer D, Kallerhoff M, Ringert RH. Microcalorimetric investigations on isolated tumorous and non-tumorous tissue samples. Thermochim Acta 1993;229:147–55.
[225] Eales KL, Hollinshead KER, Tennant DA. Hypoxia and metabolic adaptation of cancer cells. Oncogenesis 2016;5:e190.
[226] López-Lázaro M. Dual role of hydrogen peroxide in cancer: possible relevance to cancer chemoprevention and therapy. Cancer Lett 2007;252:1–8.
[227] Lu Y, Yan B. A ratiometric fluorescent pH sensor based on nanoscale metal–organic frameworks (MOFs) modified by europium (III) complexes. Chem Commun 2014;50:13323–6.
[228] Cui Y, Song R, Yu J, Liu M, Wang Z, Wu C, et al. Dual Emitting MOF Dye Composite for Ratiometric Temperature Sensing. Adv Mater 2015;27:1420–5.
[229] An J, Shade CM, Chengelis-Czegan DA, Petoud S, Rosi NL. Zinc-adeninate metal− organic framework for aqueous encapsulation and sensitization of near-infrared and visible emitting lanthanide cations. J Am Chem Soc 2011;133:1220–3.
[230] Bhardwaj SK, Sharma AL, Bhardwaj N, Kukkar M, Gill AA, Kim KH, et al. TCNQ-doped Cu-metal organic framework as a novel conductometric immunosensing platform for the quantification of prostate cancer antigen. Sens Actuators B: Chemical 2017;240:10–7.
[231] Zhang SY, Shi W, Cheng P, Zaworotko MJ. A Mixed-Crystal Lanthanide Zeolite-like Metal-Organic Framework as a Fluorescent Indicator for Lysophosphatidic Acid, a Cancer Biomarker. J Am Chem Soc 2015;137:12203–6.
[232] Liu F, Xu H. Development of a novel polystyrene/metal-organic framework-199 electrospun nanofiber adsorbent for thin film microextraction of aldehydes in human urine. Talanta 2017;162:261–7.
[233] Liu D, Poon C, Lu K, He C, Lin W. Self-assembled nanoscale coordination polymers with trigger release properties for effective anticancer therapy. Nat Commun 2014;5:4182.
[234] Huxford RC, Dekrafft KE, Boyle WS, Liu D, Lin W. Lipid-Coated Nanoscale Coordination Polymers for Targeted Delivery of Antifolates to Cancer Cells. Chem Sci. 2012;3:198–204.
[235] Xing L, Cao YY, Che SA. Synthesis of core-shell coordination polymer nanoparticles (CPNs) for pH-responsive controlled drug release. Chem Commun 2012;48:5995–7.
[236] Liu D, Kramer SA, Huxford-Phillips RC, Wang S, Della Rocca J, Lin W. Coercing bisphosphonates to kill cancer cells with nanoscale coordination Q2 polymers. Chem Commun 2012;48:2668–70.
[237] Wang KB, Ma XY, Shao DL, Geng ZR, Zhang ZY, Wang ZL. Coordination-Induced Assembly of Coordination Polymer Submicrospheres: Promising Antibacterial and in vitro Anticancer Activities. Cryst Growth Des 2012;12:3786–91.
[238] Chacón AM, Fuentes AB, Partida AZ. Synthesis and Characterization of a Gallic Acid Metal Organic Framework for Antitumoural Therapy. Biosaia: Revista de los másteres de Biotecnología Sanitaria y Biotecnología Ambiental, Industrial y. Alimentaria 2016;5.
[239] Levine DJ, Runčevski T, Kapelewski MT, Keitz BK, Oktawiec J, Reed DA, et al. Olsalazine-Based Metal-Organic Frameworks as Biocompatible Platforms for H_2 Adsorption and Drug Delivery. J Am Chem Soc 2016;138:10143–50.

[240] Ren F, Yang B, Cai J, Jiang Y, Xu J, Wang S. Toxic effect of zinc nanoscale metal-organic frameworks on rat pheochromocytoma (PC12) cells in vitro. J Hazard Mater 2014;271:283–91.
[241] Bůžek D, Zelenka J, Ulbrich P, Ruml T, Křížová I, Lang J, et al. Nanoscaled porphyrinic metal–organic frameworks: photosensitizer delivery systems for photodynamic therapy. J Mater Chem B 2017;5:1815–21.
[242] Lian HY, Hu M, Liu CH, Yamauchi Y, Wu KC. Highly biocompatible, hollow coordination polymer nanoparticles as cisplatin carriers for efficient intracellular drug delivery. Chem Commun 2012;48:5151–3.
[243] Vasconcelos IB, da Silva TG, Militao GCG, Soares TA, Rodrigues NM, Rodrigues MO, et al. Cytotoxicity and slow release of the anti-cancer drug doxorubicin from ZIF-8. RSC Adv 2012;2:9437–42.
[244] Rodriguez-Ruiz V, Maksimenko A, Anand R, Monti S, Agostoni V, Couvreur P, et al. Efficient "green" encapsulation of a highly hydrophilic anticancer drug in metal-organic framework nanoparticles. J Drug Target 2015;23:759–67.
[245] Kundu T, Mitra S, Patra P, Goswami A, Díaz Díaz D, Banerjee R. Mechanical Downsizing of a Gadolinium(III)-based Metal-Organic Framework for Anticancer Drug Delivery. Chemistry 2014;20:10514–8.
[246] Anand R, Borghi F, Manoli F, Manet I, Agostoni V, Reschiglian P, et al. Host-Guest Interactions in Fe(III)-Trimesate MOF Nanoparticles Loaded with Doxorubicin. J Phys Chem B 2014;118:8532–9.
[247] Sun CY, Qin C, Wang CG, Su ZM, Wang S, Wang XL, et al. Chiral Nanoporous Metal-Organic Frameworks with High Porosity as Materials for Drug Delivery. Adv Mater 2011;23:5629–32.
[248] Zhao D, Tan S, Yuan D, Lu W, Rezenom YH, Jiang H, et al. Surface Functionalization of Porous Coordination Nanocages Via Click Chemistry and Their Application in Drug Delivery. Adv Mater 2011;23:90–3.
[249] Sun CY, Qin C, Wang XL, Yang GS, Shao KZ, Lan YQ, et al. Zeolitic imidazolate framework-8 as efficient pH-sensitive drug delivery vehicle. Dalton Trans 2012;41:6906–9.
[250] Wang Y, Yang J, Liu YY, Ma JF. Controllable Syntheses of Porous Metal-Organic Frameworks: Encapsulation of Ln(III) Cations for Tunable Luminescence and Small Drug Molecules for Efficient Delivery. Chemistry 2013;19:14591–9.
[251] Liu JQ, Wu J, Jia ZB, Chen HL, Li QL, Sakiyama H, et al. Two isoreticular metal-organic frameworks with $CdSO_4$-like topology: selective gas sorption and drug delivery. Dalton Trans 2014;43:17265–73.
[252] Qin JS, Du DY, Li WL, Zhang JP, Li SL, Su ZM, et al. N-rich zeolite-like metal-organic framework with sodalite topology: high CO_2 uptake, selective gas adsorption and efficient drug delivery. Chem Sci 2012;3:2114–8.
[253] Lucena FR, de Araújo LC, Rodrigues Mdo D, da Silva TG, Pereira VR, Militão GC, et al. Induction of cancer cell death by apoptosis and slow release of 5-fluoracil from metal-organic frameworks Cu-BTC. Biomed Pharmacother 2013;67:707–13.
[254] McKinlay AC, Xiao B, Wragg DS, Wheatley PS, Megson IL, Morris RE. Exceptional behavior over the whole adsorption-storage-delivery cycle for NO in porous metal organic frameworks. J Am Chem Soc 2008;130:10440–4.
[255] McKinlay AC, Eubank JF, Wuttke S, Xiao B, Wheadey PS, Bazin P, et al. Nitric Oxide Adsorption and Delivery in Flexible MIL-88(Fe) Metal-Organic Frameworks. Chem Mater 2013;25:1592–9.
[256] Bloch ED, Queen WL, Chavan S, Wheatley PS, Zadrozny JM, Morris R, et al. Gradual release of strongly bound nitric oxide from $Fe_2(NO)_2$(dobdc). J Am Chem Soc 2015;137:3466–9.
[257] Koukaras EN, Montagnon T, Trikalitis P, Bikiaris D, Zdetsis AD, Froudakis GE. Toward Efficient Drug Delivery through Suitably Prepared Metal-Organic Frameworks: A First-Principles Study. J Phys Chem C 2014;118:8885–90.
[258] Lin W, Hu Q, Jiang K, Yang Y, Yang Y, Cui Y, et al. A porphyrin-based metal-organic framework as a pH-responsive drug carrier. J Solid State Chem 2016;237:307–12.
[259] Wu J, Xu JW, Liu WC, Yang SZ, Luo MM, Han YY, et al. Designed metal-organic framework based on metal–organic polyhedron: Drug delivery. Inorg Chem Commun 2016;71:32–4.
[260] Allan PK, Wheatley PS, Aldous D, Mohideen MI, Tang C, Hriljac JA, et al. Metal-organic frameworks for the storage and delivery of biologically active hydrogen sulfide. Dalton Trans 2012;41:4060–6.
[261] Ren H, Zhang L, An J, Wang T, Li L, Si X, et al. Polyacrylic acid@ zeolitic imidazolate framework-8 nanoparticles with ultrahigh drug loading capability for pH-sensitive drug release. Chem Commun 2014;50:1000–2.
[262] Chalati T, Horcajada P, Couvreur P, Serre C, Ben Yahia M, Maurin G, et al. Porous metal organic framework nanoparticles to address the challenges related to busulfan encapsulation. Nanomedicine 2011;6:1683–95.
[263] Procopio EQ, Rojas S, Padial NM, Galli S, Masciocchi N, Linares F, et al. Study of the incorporation and release of the non-conventional half-sandwich ruthenium (II) metallodrug RAPTA-C on a robust MOF. Chem Commun 2011;47:11751–3.
[264] Rojas S, Carmona FJ, Maldonado CR, Horcajada P, Hidalgo T, Serre C, et al. Nanoscaled Zinc Pyrazolate Metal-Organic Frameworks as Drug-Delivery Systems. Inorg Chem 2016;55:2650–63.
[265] Wang HN, Meng X, Wang XL, Yang GS, Su ZM. Auxiliary ligand induced structural allomorphism in nanotubular microporous metal–organic frameworks based on discrete magnesium clusters. Dalton Trans 2012;41:2231–3.
[266] Wang HN, Meng X, Yang GS, Wang XL, Shao KZ, Su ZM, et al. Stepwise assembly of metal-organic framework based on a metal-organic polyhedron precursor for drug delivery. Chem Commun 2011;47:7128–30.
[267] Agostoni V, Anand R, Monti S, Hall S, Maurin G, Horcajada P, et al. Impact of phosphorylation on the encapsulation of nucleoside analogues within porous iron (III) metal-organic framework MIL-100 (Fe) nanoparticles. J Mater Chem B 2013;1:4231–42.
[268] Agostoni V, Chalati T, Horcajada P, Willaime H, Anand R, Semiramoth N, et al. Towards an improved anti-HIV activity of nrti via metal-organic frameworks nanoparticles. Adv Healthc Mater 2013;2:1630–7.
[269] Filippousi M, Turner S, Leus K, Siafaka PI, Tseligka ED, Vandichel M, et al. Biocompatible Zr-based nanoscale MOFs coated with modified poly (ε-caprolactone) as anticancer drug carriers. Int J Pharm. 2016;509:208–18.
[270] Li S, Wang K, Shi Y, Cui Y, Chen B, He B, et al. Novel biological functions of ZIF-NP as a delivery vehicle: high pulmonary accumulation, favorable bio-compatibility, and improved therapeutic outcome. Adv Funct Mater 2016;26:2715–27.
[271] Sethi K, Sharma S, Roy I. Nanoscale iron carboxylate metal organic frameworks as drug carriers for magnetically aided intracellular delivery. RSC Adv 2016;6:76861–6.
[272] Zheng H, Zhang Y, Liu L, Wan W, Guo P, Nyström AM, et al. One-pot Synthesis of Metal-Organic Frameworks with Encapsulated Target Molecules and Their Applications for Controlled Drug Delivery. J Am Chem Soc 2016;138:962–8.
[273] Zheng M, Liu S, Guan X, Xie Z. One-Step Synthesis of Nanoscale Zeolitic Imidazolate Frameworks with High Curcumin Loading for Treatment of Cervical Cancer. ACS Appl Mater Interfaces 2015;7:22181–7.
[274] Gao PF, Zheng LL, Liang LJ, Yang XX, Li YF, Huang CZ. A new type of pH-responsive coordination polymer sphere as a vehicle for targeted anticancer drug delivery and sustained release. J Mater Chem B 2013;1:3202–8.
[275] di Nunzio MR, Agostoni V, Cohen B, Gref R, Douhal A. A "ship in a bottle" strategy to load a hydrophilic anticancer drug in porous metal organic framework nanoparticles: efficient encapsulation, matrix stabilization, and photodelivery. J Med Chem 2014;57:411–20.
[276] Cheng H, Zhu JY, Li SY, Zeng JY, Lei Q, Chen KW, et al. An O_2 Self Sufficient Biomimetic Nanoplatform for Highly Specific and Efficient Photodynamic Therapy. Adv Funct Mater 2016;26:7847–60.
[277] Nguyen JG, Tanabe KK, Cohen SM. Postsynthetic diazeniumdiolate formation and NO release from MOFs. CrystEngComm 2010;12:2335–8.
[278] Tan LL, Li H, Zhou Y, Zhang Y, Feng X, Wang B, et al. Zn^{2+}-Triggered drug release from biocompatible zirconium mofs equipped with supramolecular gates. Small 2015;11:3807–13.
[279] Torad NL, Li YQ, Ishihara S, Ariga K, Kamachi Y, Lian HY, et al. MOF-derived Nanoporous Carbon as Intracellular Drug Delivery Carriers. Chem Lett 2014;43:717–9.

[280] Harding JL, Reynolds MM. Composite materials with embedded metal organic framework catalysts for nitric oxide release from bioavailable S-nitrosothiols. J Mater Chem B 2014;2:2530–6.
[281] Taylor KM, Jin A, Lin W. Surfactant-assisted synthesis of nanoscale gadolinium metal-organic frameworks for potential multimodal imaging. Angew Chem Int Ed 2008;47:7722–5.
[282] Hatakeyama W, Sanchez TJ, Rowe MD, Serkova NJ, Liberatore MW, Boyes SG. Synthesis of Gadolinium Nanoscale Metal-Organic Framework with Hydrotropes: Manipulation of Particle Size and Magnetic Resonance Imaging Capability. ACS Appl Mater Interfaces 2011;3:1502–10.
[283] Rowe MD, Chang CC, Thamm DH, Kraft SL, Harmon Jr JF, Vogt AP, et al. Tuning the Magnetic Resonance Imaging Properties of Positive Contrast Agent Nanoparticles by Surface Modification with RAFT Polymers. Langmuir 2009;25:9487–99.
[284] Pereira GA, Peters JA, Paz FA, Rocha J, Geraldes CF. Evaluation of [Ln (H_2cmp)(H_2O)] metal organic framework materials for potential application as magnetic resonance imaging contrast agents. Inorg Chem 2010;49:2969–74.
[285] Yang H, Qin CY, Yu C, Lu Y, Zhang HW, Xue FF, et al. RGD-Conjugated Nanoscale Coordination Polymers for Targeted T_1- and T_2-weighted Magnetic Resonance Imaging of Tumours in vivo. Adv Funct Mater 2014;24:1738–47.
[286] Dekrafft KE, Xie Z, Cao G, Tran S, Ma L, Zhou OZ, et al. Iodinated nanoscale coordination polymers as potential contrast agents for computed tomography. Angew Chem Int Edit 2009;48:9901–4.
[287] Dekrafft KE, Boyle WS, Burk LM, Zhou OZ, Lin W. Zr- and Hf-based nanoscale metal-organic frameworks as contrast agents for computed tomography. J Mater Chem 2012;22:18139–44.
[288] Zhong SL, Xu R, Zhang LF, Qu WG, Gao GQ, Wu XL, et al. Terbium-based infinite coordination polymer hollow microspheres: preparation and white-light emission. J Mater Chem 2011;21:16574–80.
[289] Oh M, Mirkin CA. Chemically tailorable colloidal particles from infinite coordination polymers. Nature 2005;438:651–4.
[290] Nishiyabu R, Aime C, Gondo R, Kaneko K, Kimizuka N. Selective inclusion of anionic quantum dots in coordination network shells of nucleotides and lanthanide ions. Chem Commun 2010;46:4333–5.
[291] Nishiyabu R, Aime C, Gondo R, Noguchi T, Kimizuka N. Confining Molecules within Aqueous Coordination Nanoparticles by Adaptive Molecular Self-Assembly. Angew Chem Int Ed 2009;48:9465–8.
[292] Nishiyabu R, Hashimoto N, Cho T, Watanabe K, Yasunaga T, Endo A, et al. Nanoparticles of Adaptive Supramolecular Networks Self-Assembled from Nucleotides and Lanthanide Ions. J Am Chem Soc 2009;131:2151–8.
[293] Aime C, Nishiyahu R, Gondo R, Kimizuka N. Switching On Luminescence in Nucleotide/Lanthanide Coordination Nanoparticles via Synergistic Interactions with a Cofactor Ligand. Chem Eur J 2010;16:3604–7.
[294] Aime C, Nishiyabu R, Gondo R, Kaneko K, Kimizuka N. Controlled self-assembly of nucleotide-lanthanide complexes: specific formation of nanofibers from dimeric guanine nucleotides. Chem Commun 2008;48:6534–6.
[295] Zhang L, Qian X, Liu L, Shi Z, Li Y, Wang S, et al. Water-dispersed quantum dots of coordination polymers with strong photoluminescence. Chem Commun 2012;48:6166–8.
[296] Foucault-Collet A, Gogick KA, White KA, Villette S, Pallier A, Collet G, et al. Lanthanide near infrared imaging in living cells with Yb^{3+} nano metal organic frameworks. Proc Natl Acad Sci U S A. 2013;110:17199–204.
[297] He C, Lu K, Lin W. Nanoscale metal-organic frameworks for real-time intracellular pH sensing in live cells. J Am Chem Soc 2014;136:12253–6.
[298] Ma H, Li X, Yan T, Li Y, Zhang Y, Wu D, et al. Electrochemiluminescent immunosensing of prostate-specific antigen based on silver nanoparticles-doped Pb (II) metal-organic framework. Biosens Bioelectron 2016;79:379–85.
[299] Xu R, Wang Y, Duan X, Lu K, Micheroni D, Hu A, et al. Nanoscale Metal-Organic Frameworks for Ratiometric Oxygen Sensing in Live Cells. J Am Chem Soc 2016;138:2158–61.
[300] Dou Z, Yu J, Cui Y, Yang Y, Wang Z, Yang D, et al. Luminescent Metal-Organic Framework Films as Highly Sensitive and Fast-Response Oxygen Sensors. J Am Chem Soc 2014;136:5527–30.
[301] Wu Y, Han J, Xue P, Xu R, Kang Y. Nano metal–organic framework (NMOF)-based strategies for multiplexed microRNA detection in solution and living cancer cells. Nanoscale 2015;7:1753–9.
[302] Schmidt K, Podmore I. Current Challenges in Volatile Organic Compounds Analysis as Potential Biomarkers of Cancer. J Biomark 2015;2015:981458.
[303] Cui F, Deng Q, Sun L. Prussian blue modified metal-organic framework MIL-101(Fe) with intrinsic peroxidase-like catalytic activity as a colorimetric biosensing platform. RSC Adv 2015;5:98215–21.
[304] Cui Y, Xu H, Yue Y, Guo Z, Yu J, Chen Z, et al. A luminescent mixed-lanthanide metal–organic framework thermometer. J Am Chem Soc 2012;134:3979–82.
[305] Cadiau A, Brites CD, Costa PM, Ferreira RA, Rocha J, Carlos LD. Ratiometric nanothermometer based on an emissive Ln^{3+}-organic framework. ACS Nano 2013;7:7213–8.
[306] Wang Z, Ananias D, Carné-Sánchez A, Brites CD, Imaz I, Maspoch D, et al. Lanthanide-Organic Framework Nanothermometers Prepared by Spray-Drying. Adv Funct Mater 2015;25:2824–30.
[307] Xia T, Song T, Cui Y, Yang Y, Qian G. A dye encapsulated terbium-based metal-organic framework for ratiometric temperature sensing. Dalton Trans 2016;45:18689–95.
[308] Zhao D, Zhang J, Yue D, Lian X, Cui Y, Yang Y, et al. A highly sensitive near-infrared luminescent metal− organic framework thermometer in physiological range. Chem Commun 2016;52:8259–62.
[309] Lian X, Zhao D, Cui Y, Yang Y, Qian G. A near infrared luminescent metal–organic framework for temperature sensing in the physiological range. Chem Commun 2015;51:17676–9.
[310] Zhou Y, Yan B, Lei F. Postsynthetic lanthanide functionalization of nanosized metal–organic frameworks for highly sensitive ratiometric luminescent thermometry. Chem Commun 2014;50:15235–8.
[311] Han YH, Tian CB, Li QH, Du SW. Highly chemical and thermally stable luminescent Eu_xTb_{1-x} MOF materials for broad-range pH and temperature sensors. J Mater Chem C 2014;2:8065–70.
[312] Rao X, Song T, Gao J, Cui Y, Yang Y, Wu C, et al. A highly sensitive mixed lanthanide metal–organic framework self-calibrated luminescent thermometer. J Am Chem Soc 2013;135:15559–64.
[313] Wei Y, Sa R, Li Q, Wu K. Highly stable and sensitive LnMOF ratiometric thermometers constructed with mixed ligands. Dalton Trans 2015;44:3067–74.
[314] Cui Y, Zou W, Song R, Yu J, Zhang W, Yang Y, et al. A ratiometric and colorimetric luminescent thermometer over a wide temperature range based on a lanthanide coordination polymer. Chem Commun 2014;50:719–21.
[315] Florea A, Guo Z, Cristea C, Bessueille F, Vocanson F, Goutaland F, et al. Anticancer drug detection using a highly sensitive molecularly imprinted electrochemical sensor based on an electropolymerized microporous metal organic framework. Talanta 2015;138:71–6.
[316] Wu PY, Wang J, He C, Zhang XL, Wang YT, Liu T, et al. Luminescent Metal-Organic Frameworks for Selectively Sensing Nitric Oxide in an Aqueous Solution and in Living Cells. Adv Funct Mater 2012;22:1698–703.
[317] Poon C, He C, Liu D, Lu K, Lin W. Self-assembled nanoscale coordination polymers carrying oxaliplatin and gemcitabine for synergistic combination therapy of pancreatic cancer. J Controlled Release 2015;201:90–9.
[318] He L, Wang TT, An JP, Li XM, Zhang LY, Li L, et al. Carbon nanodots@zeolitic imidazolate framework-8 nanoparticles for simultaneous pHresponsive drug delivery and fluorescence imaging. Cryst Eng Comm 2014;16:3259–63.
[319] Li R, Ren X, Zhao J, Feng X, Jiang X, Fan X, et al. Polyoxometallates trapped in a zeolitic imidazolate framework leading to high uptake and selectivity of bioactive molecules. J Mater Chem A 2014;2:2168–73.
[320] Liu DM, He CB, Poon C, Lin WB. Theranostic nanoscale coordination polymers for magnetic resonance imaging and bisphosphonate delivery. J Mater Chem B 2014;2:8249–55.
[321] He C, Liu D, Lin W. Self-assembled nanoscale coordination polymers carrying siRNAs and cisplatin for effective treatment of resistant ovarian cancer. Biomaterials 2015;36:124–33.

[322] Chowdhuri AR, Bhattacharya D, Sahu SK. Magnetic nanoscale metal organic frameworks for potential targeted anticancer drug delivery, imaging and as an MRI contrast agent. Dalton Trans 2016;45:2963–73.
[323] Bian R, Wang T, Zhang L, Li L, Wang C. A combination of tri-modal cancer imaging and in vivo drug delivery by metal–organic framework based composite nanoparticles. Biomater Sci 2015;3:1270–8.
[324] Mocniak KA, Kubajewska I, Spillane DE, Williams GR, Morris RE. Incorporation of cisplatin into the metal–organic frameworks UiO66-NH 2 and UiO66–encapsulation vs. conjugation. RSC Adv 2015;5:83648–56.
[325] Corber SR, Tang R, Achilefu S. Cisplatin-based metal organic framework nanoparticles for targeted drug delivery and tumour imaging. Abstr Pap Am Chem S 2014;247:10–1.
[326] Zhang L, Lei J, Ma F, Ling P, Liu J, Ju H. A porphyrin photosensitized metal–organic framework for cancer cell apoptosis and caspase responsive theranostics. Chem Commun 2015;51:10831–4.
[327] Chowdhuri AR, Singh T, Ghosh SK, Sahu SK. Carbon Dots Embedded Magnetic Nanoparticles@ Chitosan@ Metal Organic Framework as a Nanoprobe for pH Sensitive Targeted Anticancer Drug Delivery. ACS Appl Mater Interfaces 2016;8:16573–83.
[328] Zhao HX, Zou Q, Sun SK, Yu C, Zhang X, Li RJ, et al. Theranostic metal–organic framework core–shell composites for magnetic resonance imaging and drug delivery. Chem Sci 2016;7:5294–301.
[329] Ke F, Yuan YP, Qiu LG, Shen YH, Xie AJ, Zhu JF, et al. Facile fabrication of magnetic metal − organic framework nanocomposites for potential targeted drug delivery. J Mater Chem 2011;21:3843–8.
[330] Wang J, Chen D, Li B, He J, Duan D, Shao D, et al. Fe-MIL-101 exhibits selective cytotoxicity and inhibition of angiogenesis in ovarian cancer cells via downregulation of MMP. Sci Rep 2016;26126:1–13.
[331] Deng K, Hou Z, Li X, Li C, Zhang Y, Deng X, et al. Aptamer-mediated up-conversion core/MOF shell nanocomposites for targeted drug delivery and cell imaging. Sci Rep 2015;5:1–7.
[332] Wang D, Zhou J, Chen R, Shi R, Zhao G, Xia G, et al. Controllable synthesis of dual-MOFs nanostructures for pH-responsive artemisinin delivery, magnetic resonance and optical dual-model imaging-guided chemo/photothermal combinational cancer therapy. Biomaterials 2016;100:27–40.
[333] Chelebaeva E, Larionova J, Guari Y, Ferreira RAS, Carlos LD, Trifonov AA, et al. Nanoscale coordination polymers exhibiting luminescence properties and NMR relaxivity. Nanoscale 2011;3:1200–10.
[334] Zhou ZG, Li DR, Yang H, Zhu YC, Yang SP. Synthesis of d-f coordination polymer nanoparticles and their application in phosphorescence and magnetic resonance imaging. Dalton Trans 2011;40:11941–4.
[335] He C, Poon C, Chan C, Yamada SD, Lin W. Nanoscale coordination polymers codeliver chemotherapeutics and siRNAs to eradicate tumors of cisplatin-resistant ovarian cancer. J Am Chem Soc 2016;138:6010–9.
[336] Lu K, He C, Guo N, Chan C, Ni K, Weichselbaum RR, et al. Chlorin-Based Nanoscale Metal-Organic Framework Systemically Rejects Colorectal Cancers via Synergistic Photodynamic Therapy and Checkpoint Blockade Immunotherapy. J Am Chem Soc 2016;138:12502–10.
[337] Kotzabasaki M, Froudakis GE. Review of computer simulations on anti-cancer drug delivery in MOFs. Inorg Chem Front 2018;6:1255–72.
[338] Babarao R, Jiang J. Unraveling the Energetics and Dynamics of Ibuprofen in Mesoporous Metal-Organic Frameworks. J Phys Chem C 2009;113:18287–91.
[339] Bei L, Yuanhui L, Zhi L, Guangjin C. Molecular Simulation of Drug Adsorption and Diffusion in Bio-MOFs. Acta Chim. Sinica 2014;72:942–8.
[340] Bernini MC, Fairen-Jimenez D, Pasinetti M, Ramirez-Pastor AJ, Snurr RQ. Screening of Bio-Compatible Metal-Organic Frameworks as Potential Drug Carriers Using Monte Carlo Simulations. J Mater Chem B 2014;2:766–74.
[341] Bueno-Perez R, Martin-Calvo A, Gomez-Alvarez P, Gutierrez-Sevillano JJ, Merkling PJ, Vlugt TJH, et al. Enantioselective Adsorption of Ibuprofen and Lysine in Metal-Organic Frameworks. Chem Commun 2014;50:10849–52.
[342] Erucar I, Keskin S. Efficient storage of drug and cosmetic molecules in bio-compatible MOFs: A molecular simulation study. Ind Eng Chem Res 2016;55(7):1929–39.
[343] Erucar I, Keskin S. Computational Investigation of Metal Organic Frameworks for Storage and Delivery of Anticancer Drugs. J Mater Chem B 2017;5:7342–51.
[344] Kotzabasaki M, Galdadas I, Tylianakis E, Klontzas E, Cournia Z, Froudakis GE. Multiscale simulations reveal IRMOF-74-III as a potent drug carrier for gemcitabine delivery. J Mater Chem B 2017;5:3277–82.
[345] Kotzabasaki M, Tylianakis E, Klontzas E, Froudakis GE. OH-functionalization strategy in Metal-Organic Frameworks for drug delivery. Chem Phys Lett 2017;685:114–8.
[346] Liu JQ, Li XF, Gu CY, da Silva JC, Barros AL, Alves-Jr S, et al. A combined experimental and computational study of novel nanocage-based metal–organic frameworks for drug delivery. Dalton Trans 2015;44(44):19370–82.
[347] Wang J, Jin J, Li F, Li B, Liu J, Jin J, et al. Combined experimental and theoretical insight into the drug delivery of nanoporous metal–organic frameworks. RSC Adv 2015;104:85606–12.
[348] Li F, Li B, Wang C, Zeng Y, Liu J, Gu CY, et al. Encapsulation of pharmaceutical ingredient linker in metal–organic framework: combined experimental and theoretical insight into the drug delivery. RSC Adv 2016;53:47959–65.
[349] Ma DY, Li Z, Xiao JX, Deng R, Lin PF, Chen RQ, et al. Hydrostable and nitryl/methyl-functionalized metal–organic framework for drug delivery and highly selective CO_2 adsorption. Inorg Chem 2015;54(14):6719–26.

Adam Bieniek is currently a research and teaching assistant working at NCU at Faculty of Chemistry. He received his BS degree and Ms degree from Faculty of Chemistry, Nicolaus Copernicus University in Toruń in 2011 and 2013, respectively. He was PhD candidate at NCU in 2013-2016. He is a member of Physicochemistry of Carbon Materials Research Group. His research is focused on design, synthesis and properties of metal-organic frameworks, as well as their application in biomedical field.

Artur Piotr Terzyk is a Professor and the leader of Physicochemistry of Carbon Materials Research Group working at the Nicolaus Copernicus University in Toruń, Poland (pcm.umk.pl). He graduated in 1991, and received PhD in Physical Chemistry in 1996. In 1995 he received Foundation for Polish Science award. His habilitation (2006) was awarded by the Prime Minister of Poland. His papers have been cited more than 3000 times. His scientific interests are: adsorption, nanomaterials, wetting, calorimetry, molecular simulations and medical nanochemistry. He is awarded by Shihan Kenneth Funakoshi (FSKA) by a nidan black belt in Shotokan karate. He is a great fan of Joy Division and cold/new wave music.

Marek Wiśniewski is a professor at the Nicolaus Copernicus University in Toruń, Poland. He is the member of Chair of Materials Chemistry, Adsorption and Catalysis, and Physicochemistry of Carbon Materials Research Group. He has published more than 80 papers in reputed journals. Currently, his research is focused on design, synthesis and properties of novel, bioinspired and functional nanomaterials, as well as their emerging applications in diverse fields.

Katarzyna Roszek is currently working as a university professor at Department of Biochemistry, Faculty of Biological and Veterinary Sciences, Nicolaus Copernicus University in Torun, Poland. In 2006 she obtained her PhD in biological sciences from the Institute of General and Molecular Biology, NCU in Torun, working in the field of enzymology. She is the author of over 50 refereed publications, 2 book chapters, and over 40 conference presentations. Currently, her research interest is focused on cytotoxicity issues and biomedical applications of nanomaterials and biomaterials, adult stem cells, and nucleotide signalling in the extracellular environment.

Piotr Kowalczyk is a senior lecturer in physics at the Murdoch University. He obtained his PhD degree from Chiba University in 2004. Prior to joining Murdoch University, he worked as an assistance professor in the Institute of Physical Chemistry of the Polish Academy of Sciences in Warsaw (Poland), Postdoctoral Research Fellow in Chemical Engineering, the University of Queensland (Australia), Research Fellow in Applied Physics, the Royal Melbourne Institute of Technology (Australia), and Senior Research Fellow at the Department of Chemistry of Curtin University (Australia). He has co-authored 144 refereed journal articles, 9 books chapters and co-edited one book. Currently, his research is focused on the synthesis, characterization, and molecular modelling of carbon-based nanomaterials for emerging biomedical applications. In 2018, he was highlighted by The Australian as the Australia's research leader in the field of Dispersion Chemistry (The Stars of 2018).

Lev Sarkisov is Professor in Chemical Engineering at the University of Manchester and a visiting Professor in the School of Engineering at the University of Edinburgh. He received his PhD degree in Chemical Engineering from the University of Massachusetts-Amherst, USA, in 2001. Prior to joining the University of Manchester, he was Professor in Molecular Thermodynamics at the University of Edinburgh and held research posts at Northwestern and Yale universities. His research interests include theory of adsorption in porous materials, multiscale process engineering, and novel computational methods in application to chemical engineering problems.

Seda Keskin is a full professor at the Chemical and Biological Engineering Department of Koc University, Istanbul, Turkey. She received her PhD from Georgia Institute of Technology, School of Chemical and Biomolecular Engineering in 2009. Her main research area is molecular modeling of new generation nanoporous materials, specifically metal organic frameworks, for energy applications such as gas storage and separation. She is the author of 120 published papers which received more than 6000 citations to date.

Katsumi Kaneko is a distinguished professor at Research Initiative for Supra-Materials, Shinshu University. He was a professor at Graduate School of Science, Chiba University before moving to Shinshu University in 2010. He graduated the master program of Physical Chemistry of the University of Tokyo in 1971 and later he obtained Doctor of Science from the University of Tokyo. He developed "nanospace molecular science" in Chiba University. His current interest is on "in-pore nanomaterials science", challenging new innovation in Adsorption and Nanomaterials fields. He was in charge of president of International Adsorption Society from 2004 to 2007. He is a recipient of Charles Petinos Award of American Carbon Society. He is a fellow of Royal Society of Chemistry, International Adsorption Society, and Chemical Society of Japan.